Monomethyl Pt complexes coordinated to hemilabile facially coordinating ligands in aqueous solution: Aerobic oxidation and C-O coupling to form methanol.

Jason Dean Prantner

A dissertation

submitted in partial fulfillment of the

requirements for the degree of

Doctor of Philosophy

University of Washington

2014

Reading Committee:

Karen I. Goldberg, Chair

D. Michael Heinekey

Julia A. Kovacs

Program Authorized to Offer Degree:

Chemistry

University of Washington

Abstract

Monomethyl Pt complexes coordinated to hemilabile facially coordinating ligands in aqueous solution: Aerobic oxidation and C-O coupling to form methanol.

Jason Dean Prantner

Chair of the Supervisory Committee:

Professor Karen I. Goldberg

Department of Chemistry

Oxidation of monomethyl Pt^{II} to monomethyl Pt^{IV} followed by reductive elimination of methanol are key consecutive steps in homogenous catalytic oxidation of methane to methanol. The development of a catalytic system that uses water as the solvent and molecular oxygen as the oxidant, both of which are inexpensive and non-toxic, would be a major advancement. Facially coordinating ligands containing a hemilabile arm have been shown to enhance aerobic oxidation of monomethyl Pt^{II} to Pt^{IV} without restricting reductive elimination of the methanol from the monomethyl Pt^{IV} product. A major focus of this thesis was the study of the reactivity of methyl platinum when coordinated to the tridentate ligand bis(3,5-dimethylpyrazol-1-yl)-acetate (NNO, **1**). In water, the dimethyl $NNOPt^{II}$ complex (**5**) undergoes protonlysis to generate methane and monomethyl $NNOPt^{II}$ complex (**6**) while the monomethyl $NNOPt^{II}$ product is stable up to 100 °C. In both cases the reaction is shown to be highly pH

dependent with protonlysis of the monomethyl $NNOPt^{II}$ occurring at room temperature at pH < 4. The reaction of monomethyl $NNOPt^{II}$ (**6**) with molecular oxygen produced monomethyl $NNOPt^{IV}$ (**10**) with concurrent coordination of the hemilabile carboxylate arm in NNO. In addition to oxidation, a rare oxidative methyl transfer reaction was observed producing dimethyl $NNOPt^{IV}$ (**11**) with an equivalent of demethylated $NNOPt^{II}$ (**7**). Studies of the reaction show that higher pH and temperature favored oxidative methyl transfer over oxidation. A mechanism is proposed in which the reaction of **6** with O_2 produces a hydroperoxide monomethyl $NNOPt^{IV}$ intermediate ($\mathbf{I_1}$) that can then react with a second equivalent of **6** resulting in two equivalents of the oxidized monomethyl Pt^{IV} product **10**. Isomerization of $\mathbf{I_1}$ to $\mathbf{I_2}$ moves the Pt-CH_3 group trans to a good leaving group, the carboxylate arm of NNO. In this position, the platinum bound methyl group is more susceptible to removal by S_N2 attack of **6** forming the dimethyl $NNOPt^{IV}$ product (**11**) with an equivalent of **7**.

Reductive elimination from the monomethyl Pt^{IV} product of oxidation (**10**) generating methanol and **7** was also observed. Interestingly, at high [**7**] the decomposition of **10** was found to be first-order in **10** and **7**. A mechanism is proposed in which reductive elimination is faster from a dinuclear monomethyl $NNOPt^{II}/NNOPt^{IV}$ intermediate ($\mathbf{I_3}$) formed from **7** and **10**.

A novel facially coordinating ligand was synthesized in which the hemilabile arm contains an anionic N from a sulfonyl amidate group (NNN, **15**). Three different NNN variants were synthesized with a different substituent (R) bound to the hemilabile arm (R = H: (bis(3,5-dimethylpyrazol-1-yl)-N-benzenesulfonylacetamide (**18**), R = CH_3: Bis(3,5-dimethylpyrazol-1-yl)-N-toluenesulfonylacetamide (**16**), R = Cl: Bis(3,5-dimethylpyrazol-1-yl)-N-p-chlorobenzenesulfonylacetamide (**20**)). The substituents were chosen based on their Hammett para parameter (CH_3: -0.17, H: 0.00, Cl: 0.23) which should in turn effect the electron density at the sulfonyl amidate N. In general, the NNNPt system performed similarly to the NNOPt system in terms of: protonlysis of dimethyl $NNNPt^{II}$ in water, aerobic

oxidation of monomethyl NNNPt^{II} to monomethyl NNNPt^{IV} and reductive elimination of methanol from monomethyl NNNPt^{IV}.

Table of Contents

List of Figures

List of Tables

Acknowledgements

Thank you Karen for your patience while allowing me to develop during the course of my studies. I owe a special thanks to Luc for his generosity and compassion in helping me get started in experimental chemistry. My sisters Alisa and Kara and my great friend Ehren were always encouraging. My mom Lorraine was a critical support throughout the entire process. I am most grateful to my wife Gretchen for helping me to better understand what I was going through. My life has got easier and more rewarding every day since we met. Watching our kids Max and Harriet grow up during this process has been a tremendous joy. Thank you to all the faculty, staff and students that I encountered here at the University of Washington for creating a challenging and supportive community.

Chapter 1 : Introduction

Important materials used in modern life like plastics, adhesives and paints are typically produced from petroleum based feedstocks.[1] Problems with the use of petroleum include its volatile price and the concentration of petroleum in a few geographic locations.[2] A potentially lower cost and more geographically disperse hydrocarbon source like natural gas is an attractive alternatives to petroleum.[3] The main component of natural gas is methane (~80%)[4] which could be transformed into a variety of "functionalized" chemicals like alkenes, alcohols, amines, carbonyl-containing compounds, and others that could serve as feedstocks for high value materials.

The controlled catalytic functionalization of methane has proven to be difficult for a number of reasons.[5] The C(sp^3)-H bonds in methane are relatively inert towards heterolytic (BDE: 105 kcal/mol) or homolytic (pKa(est.): 48) cleavage.[6] Often the C-H bonds in the products of alkane functionalization are more reactive than the C-H bonds in the starting material. Specifically, in the conversion of methane to methanol the C-H bond in methanol, with a BDE of 96 kcal/mol, is smaller than the BDEs of the C-H bonds in methane. The weaker bonds in methanol can result in reduced yields due to over oxidation of methanol.[6] Also, terminally functionalized hydrocarbons are general preferred in industry but terminal C-H bonds are typically stronger than internal C-H bonds (General trend for BDEs of C-H bonds: $1^o > 2^o > 3^o$).[6,7] Finally, the system must meet the general requirements of an industrial scale synthetic method such as fast reaction rate, low energy consumption, and atom economy.[8]

The ideal functionalization of alkanes would involve breaking a strong 1^o C-H bond and be highly selective for the hydrocarbon starting material over the functionalized product. Homogeneous transition metal systems can display this type of selectivity.[9] Even through all of the challenges described above, transition metal homogeneous catalysis of the functionalization of alkanes is developing.[8] Catalytic partial oxidation of methane was first reported in 1972 by Shilov using Pt salts as

both the catalyst and the stoichiometric oxidant (Figure 1.1).[10] Research following this remarkable discovery focused on developing an understanding of the mechanism of the functionalization reaction and on the development of systems that employ more practical oxidants.[11,12]

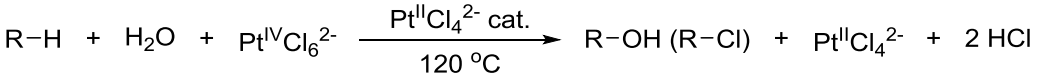

Figure 1.1. Homogeneous Platinum mediated catalysis of methane to methanol (chloromethane) using Pt^{IV} as the stoichiometric oxidant.[10]

Periana developed a Pt based system that converts methane to methyl bisulfate using inexpensive sulfuric acid as the oxidant.[12] This system was an impressive improvement over the Shilov system in terms of the conversion of methane to the oxidized product (yield of methyl bisulfate 70% based on methane), selectivity (> 90%) and stability (TON > 300).[12] Unfortunately, the system is inhibited by H_2O which is produced during the reaction. To keep the concentration of H_2O low the reaction is performed in fuming sulfuric acid complicating separation of the products.

A general cycle for the catalytic transformation of methane to a partially oxidized product using homogeneous platinum proposed by Shilov[10] consists of three key steps: C-H activation, oxidation and C-X coupling (Figure 1.2). During C-H activation, a C-H bond in the alkane substrate is broken and a Pt-C bond is formed. The resulting (alkyl)Pt^{II} containing species is oxidized to (alkyl)Pt^{IV} in the oxidation step. Finally, the functionalized product is released by reductive elimination resulting in regeneration of the platinum catalyst in the C-X coupling step. A similar mechanism was proposed to operate in the Periana system[12].

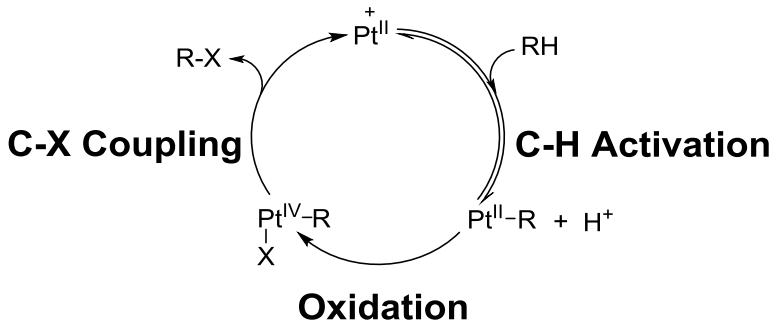

Figure 1.2. Proposed catalytic cycle for alkane functionalization.[10,12]

The oxidation step has attracted attention due to the impracticality of using Pt^{IV} as a stoichiometric oxidant in the Shilov system. The most promising oxidant for a commercially viable process, considering cost, availability and environmental impact is widely considered to be molecular oxygen/air.[13] Hindering the development of an oxygen-based process, however, has been an incomplete understanding of how the various platinum species that are involved in the reaction, e.g. methyl Pt^{II} complexes, react with oxygen.[14] Labelling studies performed by Labinger and Bercaw et al. found that the Pt^{IV}-CH_3 generated from the oxidation step occurs through electron transfer from Pt^{II}-CH_3 to the Pt^{IV} oxidant rather than methyl transfer from Pt^{II}-CH_3 to the available Pt^{IV} center (Figure 1.3).[15] Therefore it may be possible to use a variety of direct oxidants (including O_2) in place of Pt^{IV}. Sen and co-workers have developed a Wacker-type system in which the Pt oxidant was regenerated by a co-catalyst ($CuCl_2$) which was itself oxidized by O_2 thereby displacing Pt^{IV} as the stoichiometric oxidant.[16] Although interesting, the system was most effective with alkylsulfonates rather than hydrocarbons and even within this limited substrate scope, the catalyst turnover (< 60) was insufficient for practical application.

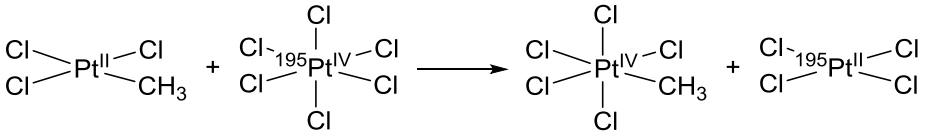

Figure 1.3. The methyl group remains associated with the same platinum center (unlabeled) during the oxidation of Pt^{II} to Pt^{IV}.[15]

Labinger, Bercaw and Goldberg found dioxygen could directly oxidize a dimethyl Pt^{II} species coordinated to bpy or diimine ligands (Figure 1.4a).[17] Aerobic oxidation did not occur when a platinum bound methyl was replaced with a chloro ligand (Figure 1.4b).[18] As a monomethyl Pt^{II} can be considered a model of the product of C-H activation of methane (Figure 1.2), oxidation of this species may be critical to catalytic performance. Studies of irreversible one-electron oxidation of a series of platinum compounds showed that the difficulty of oxidation of the platinum center increased when methyl ligands were replaced with chloro ligands (Figure 1.4c).[19] The N_2 ligand backbone can also effect the reactivity of the Pt^{II} center with O_2. Faster oxidation was observed when using diamine ligands rather than diimine ligands were used.[18] The greater electron density at the platinum center when ligated to the diamine rather than diimine ligands was suggested as the cause. Unsurprisingly, the combination of these findings suggests that increasing electron density at Pt^{II} enhances oxidation to Pt^{IV}.

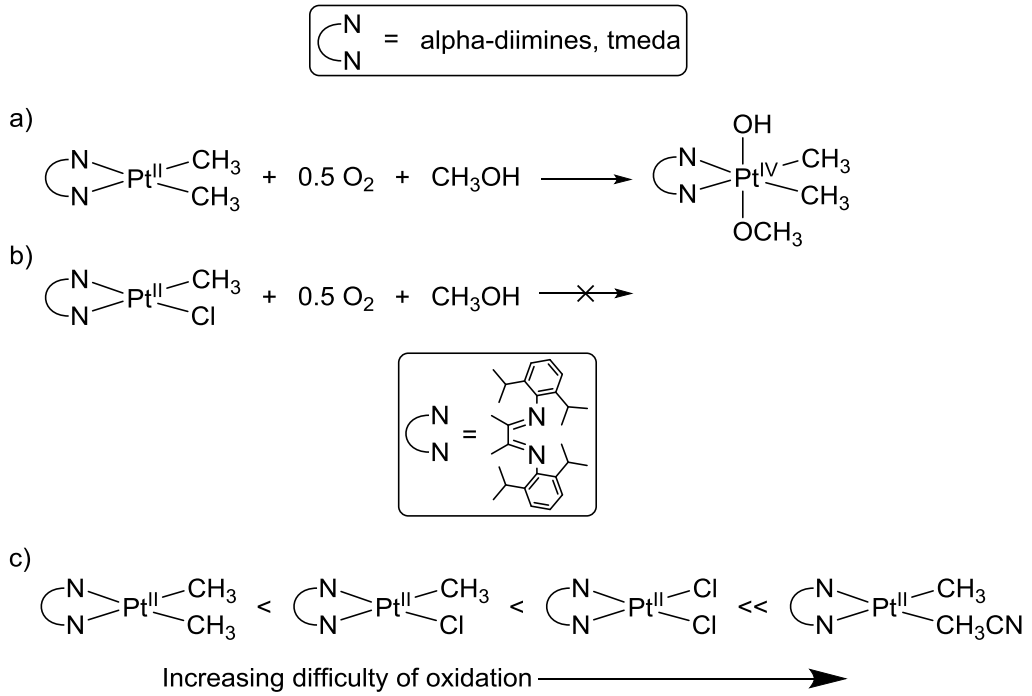

Figure 1.4. a) Aerobic oxidation of dimethyl platinum(II).[17] b) Aerobic oxidation does not occur with monomethyl platinum(II).[18] c) Increase in difficulty of oxidation upon substitution of platinum(II) bound methyl with chloro or solvent (CH_3CN). [19]

Based on this understanding, oxidation of Pt^{II} by dioxygen could be enhanced by including more electron donating ligands. Facially-coordinating ligands also appear to aid the transition of Pt^{II} to Pt^{IV}. Sarneski observed oxidation of Pt^{II} to Pt^{IV} by dioxygen occurred in the presence of the fac-coordinating *cis,cis*-1,3,5-triaminocyclohexane (tach) (Figure 1.5a) but no oxidation occurs when only the bidentate *cis*-1,3-diaminocyclohexane (dach) is available (Figure 1.5b).[20] Puddephat used this understanding to oxidize a dimethyl Pt^{II} bound to the facially coordinating ligand, 1,4,7-triazacyclononane (tacn) also using dioxygen (Figure 1.5c).[21]

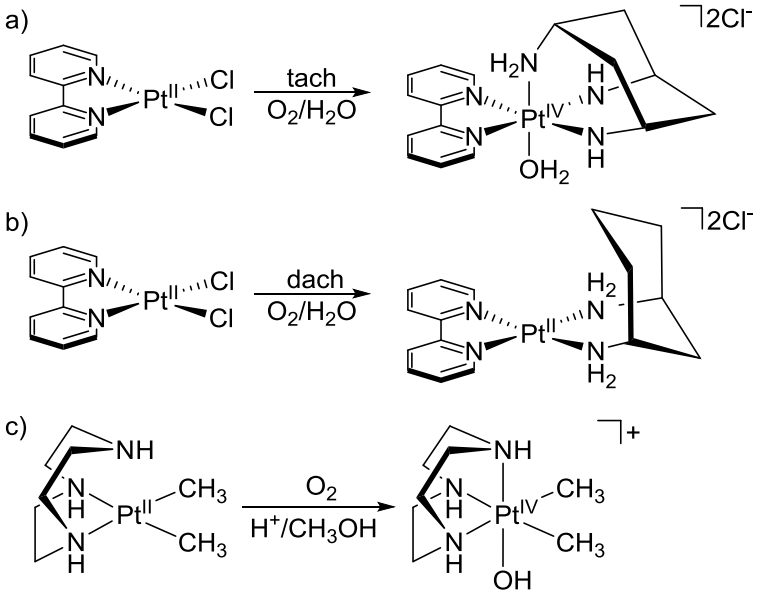

Figure 1.5. Aerobic oxidation of Pt^{II} to Pt^{IV} enhanced in the presence of a facially coordinating ligand. a) Aerobic oxidation of bpy Pt^{II} when bound to *cis, cis*-1,3,5-triaminocyclohexane (tach). b) No oxidation of bpy Pt^{II} when bound to *cis*-1, 3-diaminocyclohexane (dach).[20] c) Aerobic oxidation of a dimethyl Pt^{II} coordinated to the tridentate triamine, 1, 4, 7-triazacyclononane (tacn).[21]

To give a fuller understanding of how electron donating and facially coordinating ligands enhance aerobic oxidation the mechanism of oxidation should be considered. The aerobic oxidation of Pt^{II} is thought to occur through electrophilic attack of O_2.[15] Based on this mechanism, increased reactivity of Pt^{II} with O_2 may be the result of elevation of the HOMO on Pt due to donation of electron density into the filled d_z^2 orbital (Figure 1.6). This description is consistent with the greater ease of

oxidation of dimethyl Pt^{II} compared with dichloro Pt^{II} as well as diamine versus diimine shown above.[15,19] Wieghardt observed aerobic oxidation of Pt^{II} to Pt^{IV} when bound to a facially coordinating ligand tacn[22]. The reaction of Pt^{II} with O_2 was also proposed to occur through precoordination of the N from the unbound arm in tacn into the filled d_z^2 orbital (Figure 1.6). Both electron donating and facially coordinating ligands may be a beneficial feature in the design of a homogeneous alkane functionalization catalyst that uses O_2 as an oxidant.

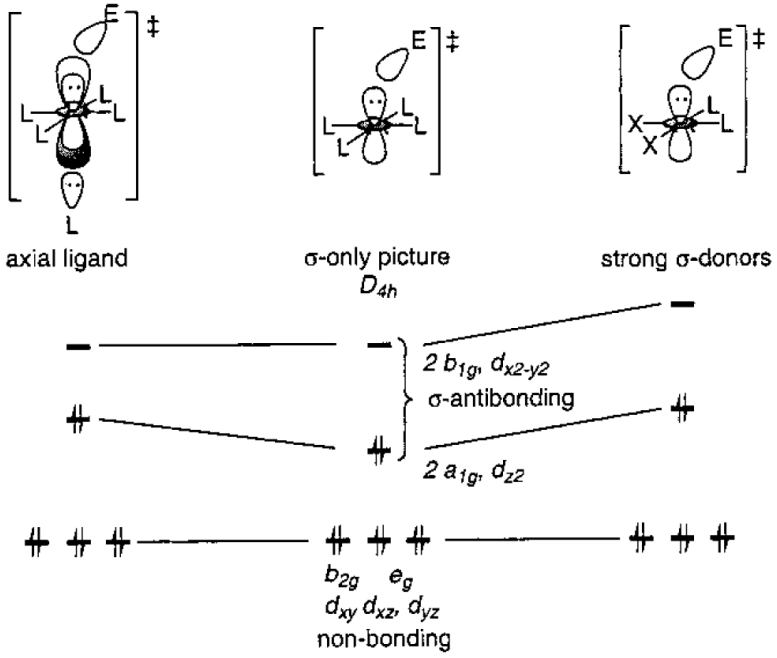

Figure 1.6. Qualitative MO diagram proposed by Labinger and Bercaw showing the electrophilic attack of O_2 (E) on the d_z^2 orbital on Pt^{II}.[18] Reactivity is enhanced by elevation of the energy of the HOMO due to electron donation into the filled orbital. Left: electron donation from an axially positioned ligand (L = solvent or free arm of facially coordinating ligand). Center: weakly electron donating equatorial ligands on Pt^{II}. Right: strongly electron donating equatorial bound ligands. Reprinted with permission from: Rostovtsev, V. V; Henling, L. M.; Labinger, J. A.; Bercaw, J. E. *Inorg. Chem.* **2002**, *41*, 3608. Copyright 2002 American Chemical Society.

Vedernikov used this facially coordinating ligand hypothesis in the design of the ligand dpms (di(2-pyridyl)methanesulfonate, Figure 1.7).[23] The dpms ligand chelates to a monomethyl Pt^{II} in a bidentate fashion. After the (dpms)Pt^{II} complex was exposed to O_2,[24] the dpms adopted a tridentate configuration in the oxidized monomethyl Pt^{IV} product. The Vedernikov system demonstrated facile

aerobic oxidation of monomethyl Pt^{II} which may potentially be exploited to replace the Pt^{IV} oxidant used in the Shilov system with dioxygen.

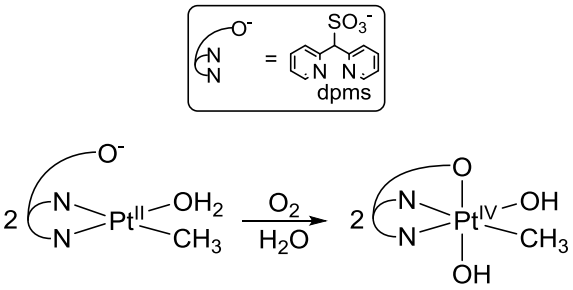

Figure 1.7. Aerobic oxidation of monomethyl Pt^{II} to Pt^{IV} with facially coordinating dpms with hemilabile arm.[24]

Returning to the Shilov cycle, following oxidation the C-X coupling step generates the functionalized product (Figure 1.2). Previous work in the Goldberg group outlined a pathway that involves ligand dissociation from a Pt^{IV} complex to generate a 5-coordinate intermediate prior to formation of the C-O bond (Figure 1.8).[25] This general reaction scheme has been proposed in a variety of carbon heteroatom bond forming reactions from Pt^{IV}.[26] Ligand dissociation preceding facile C-O coupling creates a potential conflict with ligand association (facial coordination) which aids aerobic oxidation from Pt^{II} to Pt^{IV}.

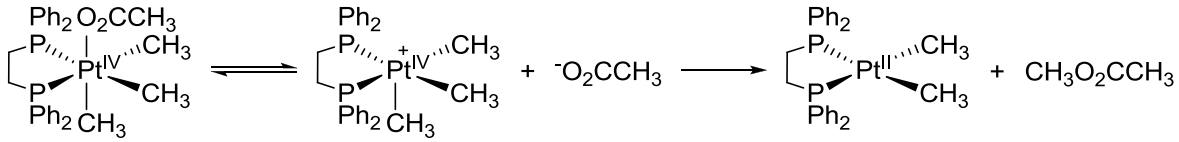

Figure 1.8. Formation of 5-coordinate intermediate during C-O coupling from Pt.[25]

Vedernikov balanced these seemingly conflicting requirements by incorporating the hemilabile sulfonate arm in the dpms system.[24] After room temperature aerobic oxidation of the monomethyl Pt^{II} to Pt^{IV}, increasing the temperature (75 °C) resulted in C-O coupling forming methanol (Figure 1.9). The

use of a facially coordinating ligand containing a hemilabile arm resulted in a system that is capable of performing aerobic oxidation and C-O coupling under mild conditions. Interestingly, while the facially coordinating ligand is sufficient to allow for oxidation of the monomethyl Pt^{II}, the product of C-O coupling $(dpms)Pt^{II}(OH)_2$ is stable to oxidation in air. Oxidation of $(dpms)Pt^{II}(OH)_2$ to $(dpms)Pt^{IV}(OH)_3$ would produce a species less likely to be competent for C-H activation and potentially inhibit catalysis. While the dpms system has found this potentially critical balance the Vedernikov group has not reported on C-H activation from the product of C-O coupling $(dpms)Pt^{II}(OH)_2$ or catalytic activity of the system as a whole.

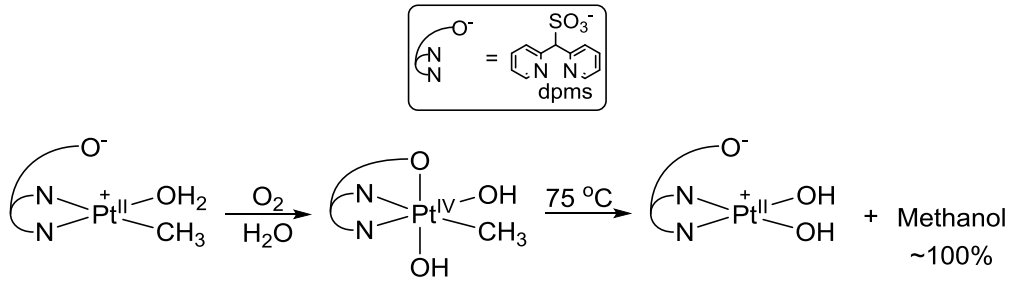

Figure 1.9. Oxidation with O_2 and methanol production in Vedernikov system.[24]

The sulfonate group in the dpms system plays a powerful role as a hemilabile ligand critical to both the oxidation and C-O coupling reactions.[24] However, the sulfonate moiety is a relatively weak base (pKa of methanesulfonic acid (H_2O) = -1.9 at 25 °C)[27] and thus control its lability with pH, through protonation of the O in SO_3 bound to Pt^{IV}, is unlikely. A stronger base functionality might allow for better control of the hemilability of the facially coordinating ligand through adjusting the pH. Herein, is described an aqueous platinum system with a facially coordinating NNO ligand containing a carboxylate hemilabile arm (NNO = bis(3,5-dimethylpyrazol-1-yl)-acetate (**1**), Figure 1.10).[28] The carboxylate group, which can be considered the conjugate base of a weak acid (pK_a of acetic acid (H_2O)

= 4.76 at 25 °C) should have a different pH profile than a sulfonate arm, the conjugate base of a strong acid.[29]

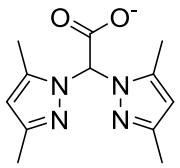

1

Figure 1.10. Facially coordinating NNO ligand containing a carboxylate hemilabile arm (NNO = bis(3,5-dimethylpyrazol-1-yl)-acetate (**1**))[28]

Chapter 2 focuses on the stability of aqueous dimethyl and monomethyl $NNOPt^{II}$ with a consideration for pH. In Chapter 3 the reactivity of aqueous monomethyl $NNOPt^{II}$ with dioxygen across a range of pH is examined. C-O coupling from the monomethyl $NNOPt^{IV}$ product of oxidation observed in both basic and acidic solutions is described in Chapter 4. Finally, Chapter 5 covers the synthesis of a novel anionic NNN ligand along with the reactivity of the NNNPt system in regards to stability in water, oxidation and C-O coupling.

---

[1] U.S. Department of Energy website, http://www.eia.gov/energyexplained/index.cfm?page=oil_use, 10/29/14.
[2] (a) U.S. Department of Energy website, http://www.eia.gov/dnav/pet/pet_pri_spt_s1_d.htm, 10/29/14. (b) U.S. Geological Survey website, http://energy.usgs.gov/OilGas/AssessmentsData/WorldPetroleumAssessment.aspx, 10/29/14.
[3] Central Intelligence Agency website, https://www.cia.gov/library/publications/the-world-factbook/rankorder/2253rank.html, 10/29/14.
[4] Danesh, Ali: PVT and Phase Behavior of Petroleum Reservoir Fluids, Elsevier, 1998.
[5] Lersch, M.; Tilset, M. *Chem. Rev.* **2005**, 105, 2471.
[6] (a) Blanksby, S.J.; Ellison, G.B. *Acc. Chem. Res.* **2003**, *36*, 255. (b) Smith, M.B.; March, J. *"March's Advanced Organic Chemistry"* John Wiley & Sons: Hoboken, 2007.
[7] Stahl, S.S.; Labinger, J.A.; Bercaw, J.E. *Angew. Chem. Int. Ed.* **1998**, 37, 2180.
[8] Periana, R.A.; et al. *J. Mol. Catal. A.* **2004**, 7.
[9] Crabtree, R.H. "*The Organometallic Chemistry of the Transition Metals*" John Wiley & Sons: Hoboken, 2005
[10] (a) Shilov, A. E.; Shulpin, G. B. *Russ. Chem. Rev.* **1987**, *56*, 442. (b) Shilov, A. E.; Shul'pin, G. B. *Activation and Catalytic Reactions of Saturated Hydrocarbons in the Presence of Metal Complexes*; Kluwer Academic Publishers: Boston, 2000.
[11] (a) Stahl, S. S.; Labinger, J. A.; Bercaw, J. E. *Angew. Chem. Int. Ed.* **1998**, *37*, 2180 (b) Labinger, J. A.; Bercaw, J. E. *Nature* **2002**, *417*, 507. (c) Fekl, U.; Goldberg, K. I. *Adv. Inorg. Chem.* **2003**, *54*, 259. (d) Lersch, M.; Tilset, M. *Chem. Rev.* **2005**, *105*, 2471. (e) Vedernikov, A. N. *Chem. Commun.* **2009**, *32*, 4781.

[12] (a) Periana, R. A.; Douglas, R. J.; Taube, D. J.; Gamble, S.; Taube, H.; Satoh, T.; Fujii, H. *Science* **1998**, *280*, 560. (b) Mironov, O. A.; Bischof, S. M.; Konnick, M. M.; Hashiguchi, B. G.; Ziatdinov, V. R.; Goddard, W. A.; Ahlquist, M.; Periana, R. A. *J. Am. Chem. Soc*. **2013**, *135*, 14644.
[13] Shi, Z.; Zhang, C.; Tang, C.; Jiao, N. *Chem. Soc. Rev.* **2012**, *41*, 3381.
[14] Boisvert, L.; Goldberg, K. I. *Acc. Chem. Res.* **2012**, *45*, 899 and references therein.
[15] Luinstra, G. A.; Wang, L.; Stahl, S. S.; Labinger, J. A.; Bercaw, J. E. *J. Orgmet. Chem.* **1995**, *540*, 75.
[16] Lin, M.; Shen, C.; Garcia-Zayas, E. A.; Sen, A. *J. Am. Chem. Soc.* **2001**, *123*, 1000.
[17] Rostovtsev, V. V.; Lasseter, T. L.; Goldberg, K. I.; Labinger, J. A.; Bercaw, J. E. *Organometallics* **1998**, *17*, 4530.
[18] Rostovtsev, V. V; Henling, L. M.; Labinger, J. A.; Bercaw, J. E. *Inorg. Chem.* **2002**, *41*, 3608.
[19] Scollard, J. D.; Day, M.; Labinger, J.A.; Bercaw, J. E. *Helv. Chim. Acta.* **2001**, *84*, 3247.
[20] Sarnski, J. E.; McPhail, A. T.; Onan, K. D.; Erickson, L. E.; Reilley, C. N. *J. Am. Chem. Soc.* **1977**, *99*, 7376.
[21] Prokopchuk, E. M.; Jenkins, H. A.; Puddephatt, R. J. *Organometallics* **1999**, *18*, 2861.
[22] Wieghardt, K.; Koppen, M.; Swiridoff, W; Weiss, J. *J. Chem. Soc., Dalton Trans.* **1983**, 1869.
[23] Fettinger, J. C.; Mohr, F.; Vedernikov, A. N. *J. Am. Chem. Soc.* **2004**, 1*26*, 11160.
[24] Binfield, S. A.; Zavalij, P. Y.; Khusnutdinova, J. A.; Vedernikov, A. N. *J. Am. Chem. Soc.* **2006**, *128*, 82.
[25] Williams, B. S.; Goldberg, K. I. *J. Am. Chem. Soc.* **2001**, *123*, 2576.
[26] Grice, K. A.; Scheuermann, M. L.; Goldberg, K. I. *Top Organomet Chem* **2011**, *35*, 1 and references therein.
[27] Patai, S.; Rappoport, Z.; Stirling, C. J. M. *The Chemistry of Sulphones and Sulphoxides* John Wiley & Sons: New York, 1988.
[28] Otero, A.; Fernández-Baeza, J.; Tejeda, J.; Antiñolo, A.; Carrillo-Hermosilla, F.; Díez-Barra, E.; Lara-Sánchez, A.; Fernández-López, M. *J. Chem. Soc., Dalton Trans*. **1999**, 3537.
[29] March, J.; Smith, M. B. *March's Advanced Organic Chemistry*, 6th ed.; John Wiley & Sons: Hoboken, 2007.

Chapter 2 : Synthesis of NNO platinum methyl compounds and their stability in water

Introduction

Using water as the solvent in the Shilov system offers the benefits of low cost and low toxicity when compared with traditional organic solvents.[1] Unfortunately, the Pt^{II}-CH_3 product from the C-H activation of methane is generally unstable in protic media.[2] Protonation of the methyl Pt complex results in breaking of the Pt-C bond liberating methane (Figure 2.1). Studies of protonolysis of (tmeda)$Pt^{II}(CH_3)Cl$ found a step-wise mechanism in which the Pt^{II} center is protonated forming the a Pt^{IV} hydrido. Reductive coupling of the methyl and hydrido then forms a methane σ adduct which can then liberate methane through exchange with the solvent.[3] A concerted mechanism that does not involve a methane σ adduct is suspected at Pt centers with lower electron density.[4]

Protonolysis of the Pt^{II}-CH_3 can prevent the methyl group, produced from C-H activation of methane, from being moved through the catalytic cycle. This reversibility of C-H activation of methane requires that for an oxidant to be useful in a Shilov type system the oxidation must be fast enough to capture the unstable Pt^{II}-CH_3 and convert it to Pt^{IV}-CH_3.[5] Due to the competition between oxidation and protonolysis, finding a replacement for the platinum(IV) oxidant used in the Shilov system may in part depend on the stability of the Pt^{II}-CH_3. This chapter describes the synthesis of NNO platinum(II) methyl species and their stability to protonlysis in neutral and acidic water. Select properties of the platinum products generated from protonlysis are also discussed.

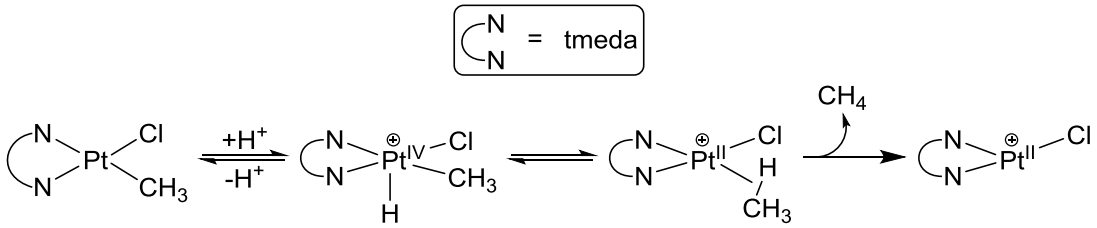

Figure 2.1. Proposed mechanism for the protonolysis of a Pt^{II}-CH_3 bond.[3]

Results and Discussion

Platination of NNO and KNNO.

The acid form of the NNO (bis(3,5-dimethylpyrazol-1-yl)-acetic acid (**2**)) was prepared using a previously reported method.[6] Combining **2** with $[Pt(CH_3)_2S(CH_3)_2]_2$ in THF gave a mixture of C_1 and C_s-symmetric NNO platinum(IV) dimethyl hydrido isomers κ^3-NNO$Pt(CH_3)_2H$ (**3**$_{ax}$ and **3**$_{eq}$, Figure 2.2). In the product mixture, the isomers were in a *ca.* 1:1 ratio but crystallization from CH_2Cl_2/pentane gives **3**$_{ax}$ almost exclusively by ^{1}H NMR spectroscopy. Complex **3**$_{ax}$ does not equilibrate to a mixture of isomers when left at room temperature in THF-d_8 after 72 h.

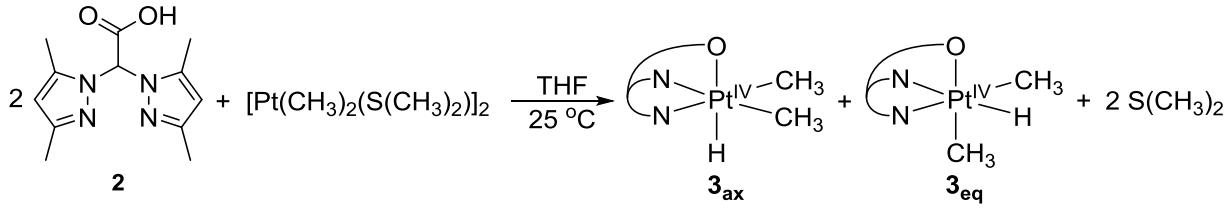

Figure 2.2. Reaction of NNO acid with dimethyl platinum(II) source.

The hydride in the C_s-symmetric isomer **3**$_{ax}$ was observed in the ^{1}H NMR spectrum (CD_2Cl_2) as a singlet at -23.74 ppm with ^{195}Pt satellites ($^1J_{Pt\text{-}H}$ = 1557 Hz). The up-field shift and large coupling constant are characteristic of Pt^{IV} hydrides.[7] The two chemically equivalent equatorial methyl groups bound to Pt were observed in the ^{1}H NMR spectrum as a singlet with a chemical shift of 1.10 ppm and ^{195}Pt satellites ($^2J_{Pt\text{-}H}$ = 69 Hz) consistent with reported Pt^{IV} methyls.[8] The four pyrazolyl bound methyl groups appeared as two singlets at 2.25 and 2.42 ppm consistent with a C_s symmetric complex.

The hydride in the C_1-symmetric isomer $\mathbf{3_{eq}}$ was observed in the ^{1}H NMR spectrum as a singlet at -21.83 ppm with Pt satellites ($^1J_{Pt\text{-}H}$ = 1461 Hz). The Pt-CH_3 groups in $\mathbf{3_{eq}}$ are not chemically equivalent with chemical shifts of 1.26 ppm ($^2J_{Pt\text{-}H}$ = 75 Hz) and 1.29 ppm ($^2J_{Pt\text{-}H}$ = 69 Hz) consistent with reported Pt^{IV}-hydride and Pt^{IV}-methyl complexes.[7,8] Also, the methyl groups on the pyrazole rings resolved into three separate peaks (2.28 (3H), 2.33 (3H), 2.44 (6H) ppm) due to lower symmetry in $\mathbf{3_{eq}}$.

The potassium salt of the NNO ligand (potassium bis(3,5-dimethylpyrazol-1-yl)-acetate (**4**)) formed cleanly from the addition of KH to a toluene solution of **2**. The Pt^{II} dimethyl complex K[κ^2-NNOPt$(CH_3)_2$] (**5**) was produced from the reaction of **4** with [$PtMe_2(SMe_2)]_2$ in toluene (Figure 2.3). Complex **5** was isolated and fully characterized by NMR spectroscopy, elemental analysis and X-ray crystallography (ORTEP in Figure 2.4). As expected, the NNO ligand is bidentate coordinating through the two pyrazolyls, while the carboxylate group is associated with the potassium counter ion rather than the platinum center.

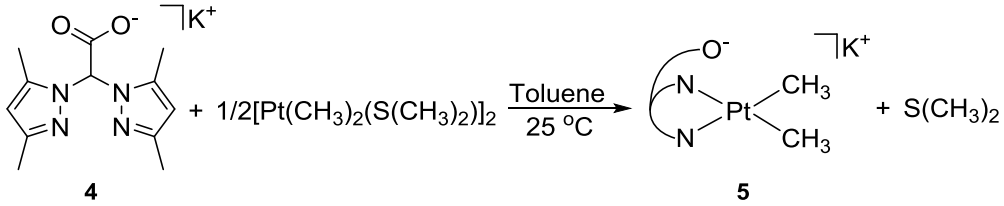

Figure 2.3. Reaction of NNO potassium salt with dimethyl platinum(II) source.

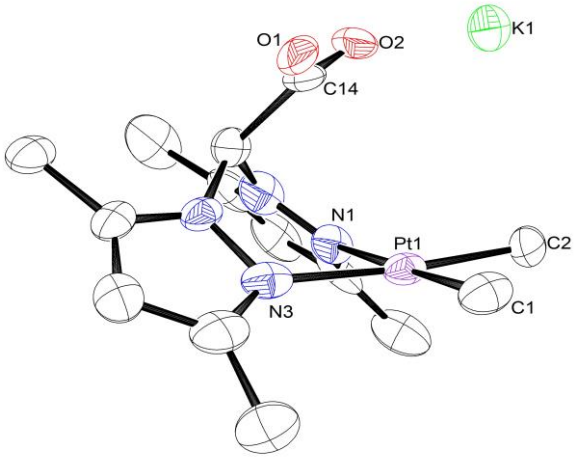

Figure 2.4. ORTEP of **5** ellipsoids at the 50% probability level. Hydrogen atoms are excluded for clarity. Selected bond distances (Å) and angles (°): Pt1-C1 = 2.032(13), Pt1-C2 = 2.041(15), Pt1-N1 = 2.104(11), Pt1-N3 = 2.118(13), C14-O1 = 1.20(2), C14-O2 = 1.27(2), C1-Pt1-C2 = 86.1(6), C1-Pt1-N1 = 178.9(5), C2-Pt1-N1 = 94.0(5), C2-Pt1-N3 = 175.0(5),N1-Pt1-N3 = 85.2(5), N3-Pt1-C1 = 94.7(5), O1-C14-O2 = 129.0(15)

Reactivity of NNO Platinum dimethyl compounds with H_2O

Dissolution of **5** in H_2O results in protonation of a platinum bound methyl group with release of methane, thereby producing the monomethyl Pt^{II} complex K[κ^2-NNOPt^{II}(CH_3)(OH)] (**6**, Figure 2.5). In the product mixture, **6** is observed by ^{1}H NMR spectroscopy with the Pt^{II}-CH_3 at 0.70 ppm and characteristic ^{195}Pt satellites ($^2J_{Pt\text{-}H}$ = 81 Hz), along with free methane (0.15 ppm). The methyl groups in NNO appear as four singlets (2.24, 2.27, 2.37, 2.39 ppm) consistent with C_1 symmetry. Similar protonolysis reactions with other nitrogen ligated platinum(II) dimethyl complexes have been reported in water and methanol.[2]

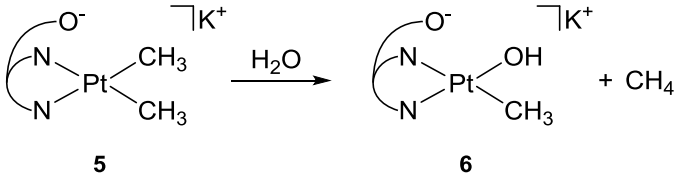

Figure 2.5. Protonolysis of Pt^{II}-CH_3 of **5** in H_2O.

When the protonolysis of **5** is performed in D_2O the signals for the Pt-CH_3 group of **6** and free methane are absent from the ^1H NMR spectrum. When the reaction is performed in a 1:1 H_2O:D_2O solution, the Pt-CH_3 group in **6** and free methane are observed as a mix of isotopologues (Pt-$CH_{3-n}D_n$ and $CH_{4-n}D_n$ respectively). This observation suggests that H/D scrambling into the Pt-CH_3 group of **5** occurs and is followed by the slower loss of methane to result in production of **6** (Figure 2.6). Following the findings of other related systems,[2] the mechanism for this reaction likely involves a methane σ-complex. A similar type of σ-complex has been implicated in the C-H activation step in the Shilov cycle.[9] No H/D scrambling was observed when the protio complex **6** was heated (60 °C) in D_2O.

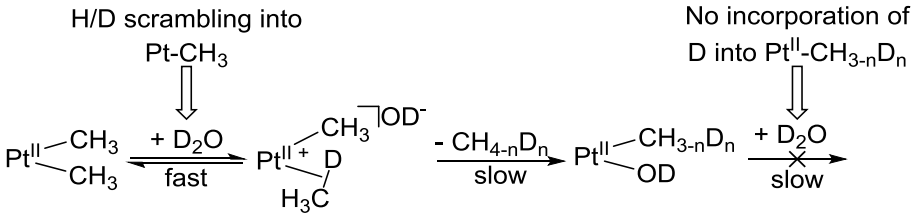

Figure 2.6. Proposed mechanism of H/D scrambling into Pt-CH_3 groups during protonolysis of 5 in D_2O.

The Pt-CH_3 of **6** is also susceptible to protonolysis but higher temperatures or a decrease in pH are required. Addition of HBF_4 (100 mM) to dilute H_2O solutions of **6** (2 mM) results in the production of methane and κ^2-NNOPt$^{II}L_2$ (7, L = OH^-/H_2O, Figure 2.7). The ^1H NMR spectrum of the products of protonolysis of **6** shows only the signals associated with the NNO ligand, shifted from the free ligand. The NNOPt product possesses a C_s-symmetry (rather than the C_1-symmetry of **6**) resulting in its identification as 7. Protonated complex 7 is also observed by ESI-MS at m/z of 478.4 (calcd. 478.11, Figure 2.14) matching the expected isotopic pattern. Lastly, a signal at 0.14 ppm is consistent with free methane.

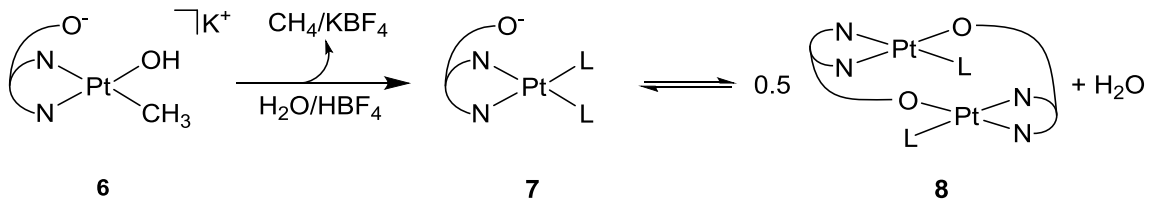

Figure 2.7. Protonolysis of Pt^{II}-CH_3 of **6** in acidic solution.

Studies of more concentrated solutions of 7 revealed its ability to form two different dimers depending on the pH of the solution. Under acidic conditions, heating a concentrated solution of **6** (40 mM) produced light yellow crystals that when examined by X-ray crystallography revealed a dimeric species**, 8,** wherein the carboxylate bridges to a second Pt^{II} center (Figure 2.7 and Figure 2.8). By ^1H NMR spectroscopy, the product solution contained both 7 and **8**. The signals for **8** were consistent with a C_2-symmetric compound; all four methyl groups in NNO are chemically inequivalent (2.50, 2.47, 2.39, 2.03 ppm).

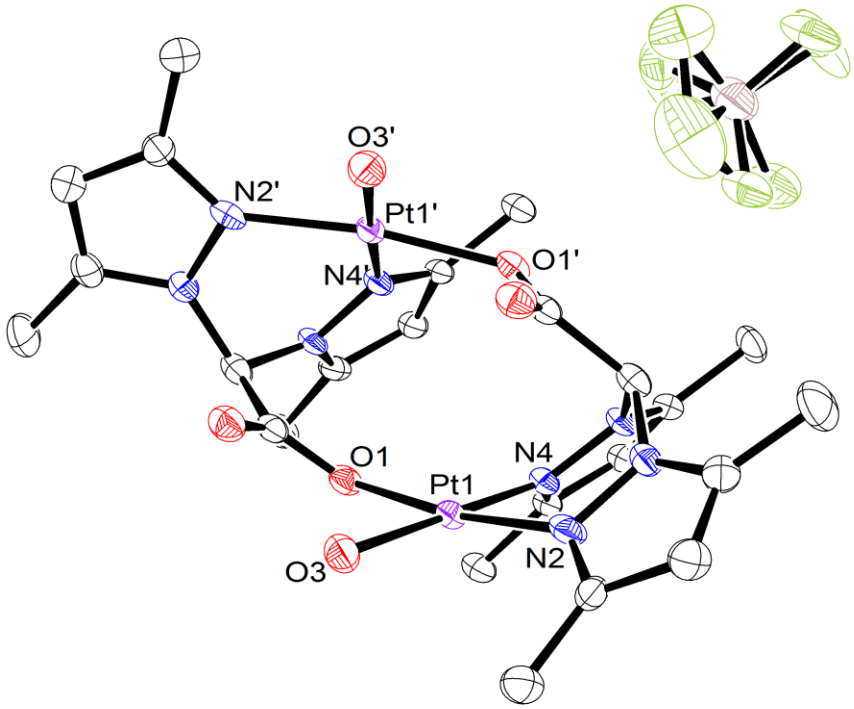

Figure 2.8. ORTEP of **8**. Displacement ellipsoids shown at the 50% probability level. Hydrogen atoms omitted for clarity. Selected bond distances (Å) and angles (°): Pt1-O1 = 2.022(4), Pt1-O3 = 2.039(4), Pt1-N2 = 1.98951), Pt1-N4 = 1.964(5), O1-Pt1-O3 = 90.18(18), N2-Pt1-O3 = 93.7(2), N4-Pt1-O1 = 87.94(19), N4-Pt1-N2 = 88.3(2).

Simultaneous observation of both 7 and **8** in solution prompted a temperature study to investigate the possibility of an equilibrium between 7 and **8**. The concentration of both 7 and **8** were followed by ^{1}H NMR spectroscopy from 60 – 100 °C. A Van't Hoff analysis (Figure 2.9) showed that the formation of **8** from 7 is entropically favored (ΔS = 3.0 ± 0.3 cal/(K•mol)) but enthalpically disfavored (ΔH = 7.3 ± 1.2 kcal/mol). The favorable entropy for this dimerization reaction can be explained by the generation of the two free water molecules that are liberated as two molecules of 7 are converted to **8**.

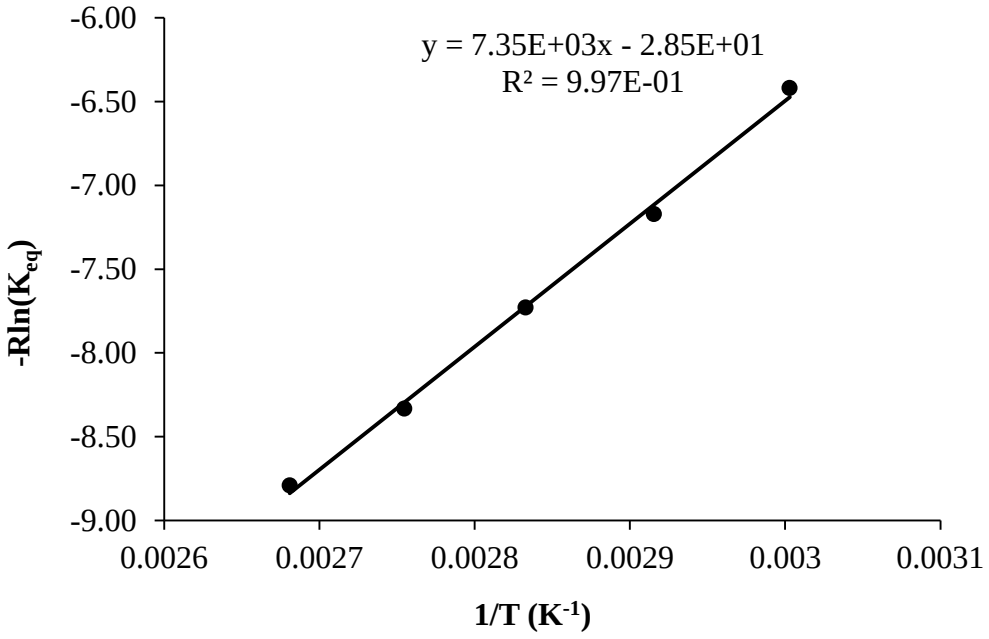

Figure 2.9. Van't Hoff plot for the formation of **8** from **7** in H_2O. [**7** + **8**] = 6 mM, [HBF_4] = 100 mM. The equilibrium between **7** and **8** was observed at T = 60, 70, 80, 90 and 100 °C.

The stability of **7** in alkaline solution was also studied. Addition of KOH (0.5 μL of 1M solution) to an H_2O solution of **7** (5.6 mM) giving a pH of 8 followed by heating at 100 ^oC resulted in the precipitation of light yellow crystals (Figure 2.10). X-ray diffraction analysis of the crystals (Figure 2.11) identified the product as a hydroxo bridged NNO platinum dimer (**9**). Both platinum centers in **9** possess a square-planar geometry. Interestingly, the conformation of **9** in the crystal has both

carboxylate arms on the same side above the plane containing platinum atoms and bridging hydroxides. This conformation may result from the stabilizing influence of a hydrogen bonding network consisting of the carboxylate arms and two water molecules.

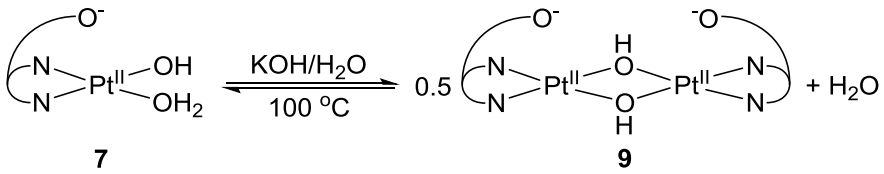

Figure 2.10. Monomer/dimer equilibrium in basic solution.

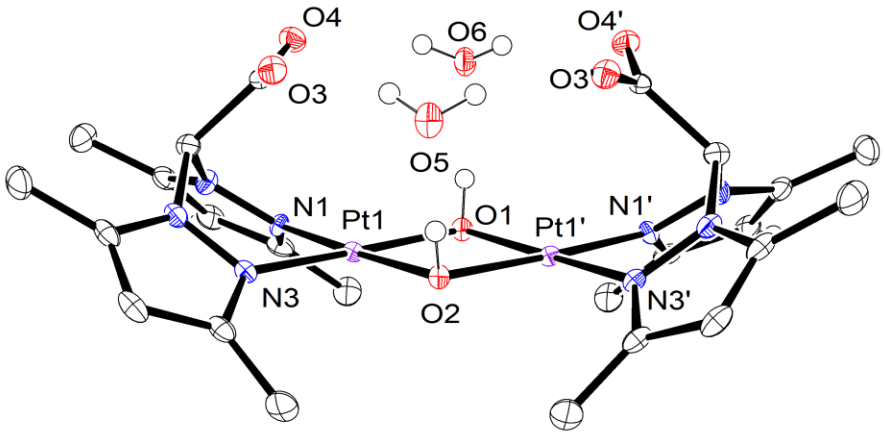

Figure 2.11. ORTEP of **9**. Displacement ellipsoids shown at the 50% probability level. Hydrogen atoms omitted for clarity. Selected bond distances (Å) and angles (deg): Pt1-N1 = 1.997(4), Pt1-N3 = 1.998(4), Pt1-O1 = 2.034(3), Pt1-O2 = 2.026(3), N1-Pt1-N3 = 88.73(17), N3-Pt1-O2 = 94.14(16), O2-Pt1-O1 = 81.56(15), N1-Pt1-O1 = 95.51(16), Pt1-O1-Pt1' = 98.2(2), Pt1-O2-Pt1' = 98.7(2).

When the formation of **9** from **7** was followed by ^{1}H NMR spectroscopy, signals associated with the NNO ligand in the monomer **7** (6.84, 6.13, 2.46, 2.34 ppm) decreased while signals attributed to **9** (6.69, 6.07, 2.41, 2.34 ppm) increased in intensity. Although there is a change in symmetry on conversion from **7** (C_s) to **9** (C_{2v}) in both cases the mirror plane between the pyrazolyl rings in the NNO ligand result in two signals for the pyrazolyl bound methyl groups. After converting 7 to **9** the mixture of aqueous and solid **9** in H_2O was left at room temperature for four days with no production of 7. This

may be due to the low solubility of **9** driving the equilibrium to **9**. Addition of a HBF_4 (pD = 1.5) to a mix of crystalline/aqueous **9** and heating at 100 °C results in slow dissolution of the solid and transformation to 7/**8** by ^1H NMR spectroscopy.

Similar to **5**, the Pt^{IV} dimethyl hydride **3** also loses methane upon reaction with water. Dissolving **3** in H_2O and heating at 50 °C results in slow production of methane and protonated complex **6**H^+ (Figure 2.12). Heating at higher temperatures (80 °C) for 24 hours results in complete conversion of **6**H^+ giving **7** and more methane. Under similar conditions (80 °C for 24 hrs) only 20% of **6** (from **5** see Figure 2.5) is lost to protonolysis. As **6**H^+ can be considered the product of protonation of **6** more rapid protonlysis of the Pt^{II}-CH_3 observed is to be expected.

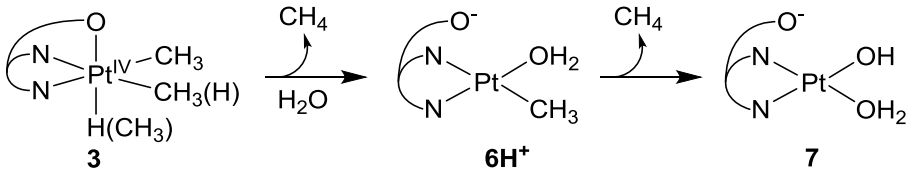

Figure 2.12. Reaction of **3** with H_2O.

Conclusions

Both the acid (**2**) and potassium salt (**4**) of the NNO ligand could be isolated. The product of the reaction of NNO with $[Pt(CH_3)_2S(CH_3)_2]_2$ is dependent on the protonation state of the NNO ligand. When $[Pt(CH_3)_2S(CH_3)_2]_2$ is treated with the NNO acid (**2**), a dimethylhydrido platinum(IV) complex (**3**) is formed. An octahedral coordination about the Pt^{IV} center is consistent with binding of the two pyrazolyls and the carboxylate arm in a *fac* arrangement about the metal center. When $[Pt(CH_3)_2S(CH_3)_2]_2$ was treated with the potassium salt of NNO (**4**), a dimethyl platinum(II) complex (**5**) is produced. The remaining sites in the square planar coordination of **5** are occupied by the two pyrazolyls; the carboxylate arm of the NNO ligand is associated with the counter cation potassium rather than platinum.

Both (NNO)$Pt^{IV}Me_2H$ (**3**) and $KNNOPt^{II}Me_2$ (**5**) are stable in organic solvents at room temperature. However, both complexes react with water to produce methane and monomethyl platinum(II) (**6**H^+ and **6** respectively). The deprotonated **6** is more thermally stable than **6**H^+ but both eventually lose a second equivalent of methane producing (NNO)$Pt(L)_2$ (**7**, L= H_2O, OH) at higher temperatures. Complex **7** can also be generated from **6** by decreasing the pH of the solution through addition of HBF_4. The NNO platinum product **7** can dimerize to two different pH dependent products. Under acidic conditions dimer **8** is formed through bridging NNO while the hydroxide bridged **9** is produced in alkaline solutions (Figure 2.13).

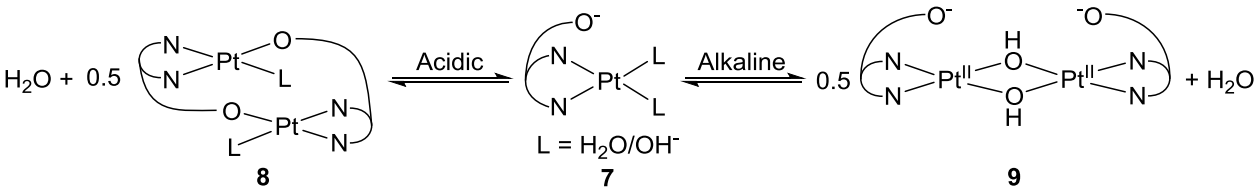

Figure 2.13. pH dependent dimerization of **7**.

As **6** can be considered the product of C-H activation of methane by **7** (see C-H activation, Figure 1.2), the stability of the Pt^{II}-CH_3 of **6** in solutions of varying alkalinity provides an opportunity to examine the reactivity of this system in regards to Shilov type catalytic functionalization of methane. The following chapter will explore the oxidation of the platinum center in **6** by dioxygen, a key step in aerobic methane to methanol catalysis. The "demethylated" NNO platinum species **7** is observed as a product of methyl transfer between two monomethyl Pt centers as well as a product of C-O coupling from monomethyl platinum(IV). Both of these reactions are examined in subsequent chapters. As pH dependent reactivity is an important focus in this work, most of the observed reactivity in the NNO system was analyzed across the pH spectrum. Whenever **7** is a product of these reactions, the dimers **8** or **9** are often observed, when the conditions (concentration and pH) support their formation.

Experimental

General Considerations

THF, diethyl ether, acetonitrile, and methylene chloride were dried by passage through activated alumina while hexane, benzene, and toluene were dried by passage through activated alumina and Q5 reactant columns under argon. THF-d_8 was vacuum transferred from sodium/benzophenone ketyl. H_2O, D_2O and HBF_4/H_2O were sparged with N_2 to remove dissolved O_2. All other reagents and gases were obtained from commercial vendors and used as received. NMR solvents were obtained from Cambridge Isotope Laboratories. ^{1}H NMR spectra were referenced to the residual protiated solvent signal or dioxane internal standard when appropriate. ^{13}C NMR spectra were referenced to dioxane as an internal standard. $[Pt(CH_3)_2(\mu\text{-}S(CH_3)_2)]_2$ was prepared from a previously reported method.[10] KH was obtained as a suspension in oil and was purified by washing with pentane. pH/pD measurements were obtained using a Hach company ISFET pH Stainless Steel NMR Tube Probe calibrated using phosphate buffered H_2O solutions of pH 4, 7 and 10 from EMD Millipore. Readings from pH meter when the probe was in D_2O solutions are reported as pD. Elemental analyses were performed by the CENTC Elemental Analysis Facility at the University of Rochester.

Bis(3,5-dimethylpyrazol-1-yl)-acetic acid (2). The following is a modification of previously reported methods.[6] A 500 mL 3-neck round-bottom flask was charged with bis(3,5-dimethyl-1-pyrazolyl)methane[6a] (4.47 g, 21.9 mmol) which was then dissolved in THF (250 mL). The colorless solution was cooled to *ca*. -78 °C. 2.6 M n-Butyllithium (8.42 mL, 21.9 mmol) in hexanes was added drop-wise. The resulting cloudy white mixture was stirred at -78 °C for 45 m. Dry CO_2 was bubbled through the mixture giving a clear colorless solution. The solution was allowed to slowly warm to room temperature with bubbling of CO_2 for 1 h. The solvent was removed under low pressure leaving a faint yellow solid. The solid was dissolved in H_2O (35 mL). 6M HCl was added until a pH of 7 was obtained. The solution was washed with Et_2O (2 x 150 mL), then 6M HCl was added to the aqueous solution until

a pH of 1 was reached resulting in a white precipitate (**2**) that was collected on a frit. **2** remaining in the filtrate was extracted with Et_2O (6 x 150 mL). The Et_2O was removed under vacuum giving a white solid. The solid was dissolved in THF and dried over Na_2SO_4 then the solvent was removed under low pressure to give a white solid. The white solid was crystallized from hot acetonitrile. Yield: 2.62 g (48%). ^{1}H NMR (300 MHz, $CDCl_3$, 298 K): δ 2.15 (s, 6H, CH_3), 2.21 (s, 6H, CH_3), 5.87 (s, 2H, H_{pz}), 6.80 (s, 1H, CH).

κ^3-NNOPt^{IV}(CH$_3$)$_2$H (3). A 100 mL round-bottom flask was charged with $[Pt(CH_3)_2(\mu\text{-}S(CH_3)_2)]_2$ (500 mg, 0.87 mmol) and **2** (433 mg, 1.74 mmol) to which 35 mL of dry THF was added. After 5 m the solution became cloudy and the mixture was stirred for 24 h. A white precipitate formed upon addition of 25 mL of pentane. The white solid collected contained a mix of complexes $\mathbf{3_{ax}}$ and $\mathbf{3_{eq}}$ (~5:1). Yield 68%. Crystallization from CH_2Cl_2 gives mainly complex $\mathbf{3_{ax}}$ (~91%). ^{1}H NMR spectral data for complex $\mathbf{3_{ax}}$ (300 MHz, CD_2Cl_2, 298 K): δ -23.74 (s, $^1J_{Pt\text{-}H}$ = 1557 Hz, 1H, Pt-H), 1.10 (s, $^2J_{Pt\text{-}H}$ = 69 Hz, 6H), 2.25 (s, 6H, CH_3), 2.42 (s, 6H, CH_3), 6.02 (s, 2H, H_{pz}), 6.44 (s, 1H, CH). ^{1}H NMR spectral data for complex $\mathbf{3_{eq}}$ (300 MHz, CD_2Cl_2, 298 K): δ -21.83 (s, $^1J_{Pt\text{-}H}$ = 1461 Hz, 1H), 1.26 (s, $^2J_{Pt\text{-}H}$ = 75 Hz, 3H, CH_{3ax}), 1.29 (s, $^2J_{Pt\text{-}H}$ = 69 Hz, 3H, CH_{3eq}), 2.28 (s, 3H, CH_3), 2.33 (s, 3H, CH_3), 2.44 (s, 6H, CH_3), 6.03 (s, 2H, H_{pz}), 6.42 (s, 1H, CH).

Potassium Bis(3,5-dimethylpyrazol-1-yl)-acetate (4). A 100 mL round-bottom flask was charged with **2** (0.5 g, 2.0 mmol) and 75 mL of air-free toluene. Then potassium hydride (*ca*. 1 mg, > 2 mmol) was added to the solution and vigorous bubbling was observed. After *ca*. 20 m the solid was separated by filtration and the solvent was removed *in vacuo* revealing a white solid. ^{1}H NMR (500 MHz, CD_3OD, 298 K): δ = 2.16 (s, 6H, CH_3), 2.24 (s, 6H, CH_3), 5.85 (s, 2H, H_{pz}), 6.63 (s, 1H, CH).

Potassium-κ^2-NNOPt^{II}(CH$_3$)$_2$ (5). A 100 mL round-bottom flask was charged with $[Pt(CH_3)_2(\mu\text{-}S(CH_3)_2)]_2$ (0.694 g, 1.21 mmol), **4** (0.692 g, 2.42 mmol) and 10 mL of toluene. The light yellow solution was stirred overnight giving a white precipitate. The precipitate was collected and washed with

toluene. Yield: 0.801 g (65%). Crystals suitable for X-ray diffraction (see below) were grown from methanol/diethyl ether at room temperature (~22 °C). ^{1}H NMR (300 MHz, THF-d_8, 298 K): δ 0.35 (s, $^{2}J_{Pt\text{-}H}$ = 88 Hz, 6H, Pt-CH_3), 2.19 (s, 6H, CH_3), 2.24 (s, 6H, CH_3), 5.78 (s, 2H, H_{pz}), 6.27 (s, 1H, CH). ^{1}H NMR (500 MHz, CD_2Cl_2, 298 K): δ 0.28 (s, 6H, Pt-CH_3), 2.22 (s, 6H, CH_3), 2.24 (s, 6H, CH_3), 5.86 (s, 2H, H_{pz}), 6.18 (s, 1H, CH). ^{13}C NMR (500 MHz, CD_2Cl_2, 298 K): δ -21.95 (s, $^{1}J_{Pt\text{-}C}$ = 829 Hz, Pt-CH_3), 11.91, 14.71, 69.17, 106.99, 140.70, 149.49, 168.84. Anal. Calcd for $KC_{14}H_{21}N_4O_2Pt$: C, 32.9; H, 4.1; N, 11.0. Found: C, 33.8; H, 4.1; N, 10.7.

Potassium- κ^2-NNOPt^{II}(CH$_3$)OH (6). A 50 mL round bottom flask was charged with complex **5** (0.225 g, 0.44 mmol) and N_2-sparged H_2O (*ca*. 5 mL). Bubbling was observed upon addition of H_2O. The solution was stirred for 24 h at 40 °C then filtered. The solvent was removed revealing a beige-colored solid. Yield: 0.195 g (87 %). ^{1}H NMR (300 MHz, D_2O, 298 K): δ 0.70 (s, $^{2}J_{Pt\text{-}H}$ = 81 Hz, 3H, CH_3), 2.24 (s, 3H, CH_3), 2.27 (s, 3H, CH_3), 2.37 (s, 3H, CH_3), 2.39 (s, 3H, CH_3), 6.05 (s, 1H, H_{pz}), 6.06 (s, 1H, H_{pz}), 6.45 (s, 1H, CH). ^{13}C NMR (500 MHz, D_2O, 298 K): δ -21.85 ($^{1}J_{Pt\text{-}C}$ = 757 Hz), 10.46, 10.99, 12.19, 13.89, 68.37, 106.85, 107.33, 142.31, 142.59, 150.75, 152.21, 169.84. Anal. Calcd for $KC_{13}H_{19}N_4O_3Pt$: C, 30.4; H, 3.7; N, 10.9. Found: C, 30.0; H, 3.59; N, 10.6.

κ^2-NNOPt^{II}(OH)$_2$ (7). Complex **6** (0.5 mg, 0.001 mmol) was dissolved in 0.5 mL N_2-sparged D_2O followed by addition of 50% HBF_4/H_2O (6 μL, 0.004 mmol) and 1,4 dioxane (0.1 μL, int. std.). The reaction mixture was then transferred to a Teflon cap sealed NMR tube and heated at 80 °C for 3 h. Yield: 97%. ^{1}H NMR (300 MHz, D_2O, 298 K): δ 2.33 (s, 6H, CH_3), 2.41 (s, 6H, CH_3), 6.07 (s, 2H, H_{pz}). ^{13}C NMR (500 MHz, D_2O, 298 K): δ 10.76, 12.48, 69.06, 107.91, 145.76, 153.41, 167.62. ESI-MS (HBF_4/H_2O) Calculated for $C_{12}H_{19}N_4O_4Pt$: m/z = 478.11. Found: m/z = 478.2. Experimentally determined and calculated isotopic patterns match (Figure 2.14).

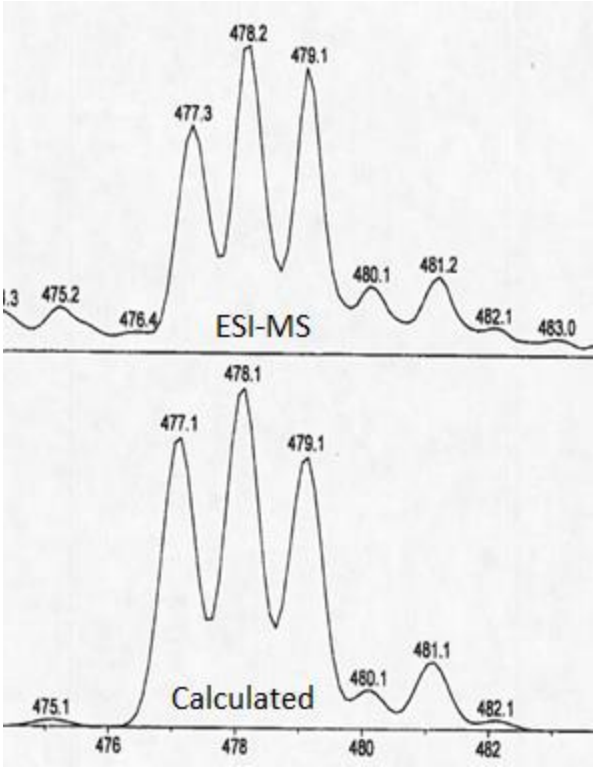

Figure 2.14. Experimentally determined and calculated isotopic pattern from ESI-MS analysis of **7**.

Carboxylate arm bridged dimer [κ^2-NNOPt^{II}(OH$_2$)]$_2$ (8). Complex **5** (100 mg, 0.195 mmol) was dissolved in 5 mL N_2-sparged H_2O and heated at 60 °C for 12 h. The solution was filtered, then transferred to a Teflon cap sealed NMR tube and excess 50% HBF_4/H_2O (1 mL, 7.97 mmol) was added. The solution was heated at 90 °C for 1 h producing a white solid. The white solid was dissolved in methanol. Crystals suitable for X-ray diffraction (see below) were grown from slow evaporation of the solution. ^{1}H NMR (500 MHz, D_2O, 298 K): δ 2.03 (s, 6H, CH_3), 2.39 (s, 6H, CH_3), 2.47 (s, 6H, CH_3), 2.50 (s, 6H, CH_3), 6.04 (s, 2H, H_{pz}), 6.19 (s, 2H, H_{pz}), 7.17 (s, 2H, CH).

Van't Hoff studies of equilibrium between 7 and 8. A Teflon cap sealed NMR tube was charged with an H_2O solution of **6** (6 mM) and HBF_4 (100 mM) with 1,4 dioxane (0.1 μL, int. std.). The sample was heated at 110 °C for 48 h until **6** was no longer detectable by ^{1}H NMR spectroscopy. The solution was placed in a 100 °C bath for 48 h then examined by ^{1}H NMR spectroscopy. The [**7**] and [**8**] were

determined using the integration of their respective methine signals in the NNO backbone (6.96 ppm and 7.24 ppm). This procedure was repeated at 90, 80, 70 and 60 °C.

Hydroxo bridged dimer [κ^2-NNOPt^{II}(OH)]$_2$ (9). A Teflon cap sealed NMR tube was charged with **6** (4.5 mg, 0.009 mmol), 1.0 M KOH (30 μL, 0.03 mmol), 1,4 dioxane (0.1 μL, int. std.) and D_2O (0.5 mL). The solution was heated at 100 °C for 3 h producing light yellow crystals suitable for X-ray diffraction (see below) which were washed in 0 °C H_2O. ^{1}H NMR (300 MHz, D_2O, 298 K): δ 2.35 (s, 12H, CH_3), 2.42 (s, 12H, CH_3), 6.07 (s, 4H, H_{pz}), 6.71 (s, 2H, CH).

Crystallographic characterization of compound 5

A small colorless block, measuring 0.17 x 0.15 x 0.07 mm^3 was mounted on a glass capillary with oil. Data was collected at -173^{o}C on a Bruker APEX II single crystal X-ray diffractometer, Mo-radiation. Crystal-to-detector distance was 40 mm and exposure time was 30 seconds per degree for all sets. The scan width was 0.5^o. Data collection was 99.8% complete to 25^o in ϑ. A total of 210790 (merged) reflections were collected covering the indices, h = -20 to 20, k = -33 to 33, l = -30 to 37. 26206 reflections were symmetry independent and the R_{int} = 0.1192 indicated that the data was slightly of less than average quality (0.07). Indexing and unit cell refinement indicated a primitive monoclinic lattice. The space group was found to be P 2_1/c (No.14). The data was integrated and scaled using SAINT, SADABS within the APEX2 software package by Bruker.[11]

Solution by direct methods (SHELXS, SIR97[12]) produced a complete heavy atom phasing model consistent with the proposed structure. The structure was completed by difference Fourier synthesis with SHELXL97.[13,14] Scattering factors are from Waasmair and Kirfel[15]. Hydrogen atoms were placed in geometrically idealized positions and constrained to ride on their parent atoms with C---H distances in the range 0.95-1.00 Angstrom. Isotropic thermal parameters U_{eq} were fixed such that they were 1.2 U_{eq} of their parent atom Ueq for CH's and 1.5 U_{eq} of their parent atom U_{eq} in case of methyl groups. All non-hydrogen atoms were refined anisotropically by full-matrix least-squares.

Table 2.1. Crystallographic data for **5**.

Parameter	**5**
Empirical formula	C100 H158 K6 N24 O16 Pt6
Formula weight	3357.64
Temperature	100(2) K
Wavelength	0.71073 Å
Crystal system	Monoclinic
Space group	P 1 21/c 1
Unit cell dimensions	a = 16.1160(4) Å α= 90°. b = 26.5699(6) Å β= 96.6080(10)°. c = 29.9824(6) Å γ = 90°.
Volume	12753.2(5) $Å^3$
Z	4
Density (calculated)	1.749 Mg/m^3
Absorption coefficient	6.817 mm^{-1}
F(000)	6544
Crystal size	0.17 x 0.15 x 0.07 mm^3
Theta range for data collection	1.92 to 26.48°.
Index ranges	-20<=h<=20, -33<=k<=33, -30<=l<=37
Reflections collected	210790
Independent reflections	26206 [R(int) = 0.1192]
Completeness to theta = 25.00°	99.8 %
Max. and min. transmission	0.6469 and 0.3903
Refinement method	Full-matrix least-squares on F^2
Data / restraints / parameters	26206 / 204 / 1450
Goodness-of-fit on F^2	1.070
Final R indices [I>2sigma(I)]	R1 = 0.0739, wR2 = 0.1429
R indices (all data)	R1 = 0.1457, wR2 = 0.1760
Largest diff. peak and hole	3.439 and -2.648 $e.Å^{-3}$

Crystallographic characterization of compound 8

A colorless prism, measuring 0.21 x 0.16 x 0.09 mm^3 was mounted on a glass capillary with oil. Data was collected at -173^oC on a Bruker APEX II single crystal X-ray diffractometer, Mo-radiation.

Crystal-to-detector distance was 40 mm and exposure time was 10 seconds per degree for all sets. The scan width was 0.5^o. Data collection was 99.1% complete to 25^o in ϑ. A total of 69123 (merged) reflections were collected covering the indices, h = -32 to 32, k = -11 to 11, l = -29 to 29. 5420 reflections were symmetry independent and the R_{int} = 0.0617 indicated that the data was good (average quality 0.07). Indexing and unit cell refinement indicated a C-centered monoclinic lattice. The space group was found to be C 2/c (No.15). The data was integrated and scaled using SAINT, SADABS within the APEX2 software package by Bruker.[11]

Solution by direct methods (SHELXS, SIR97[12]) produced a complete heavy atom phasing model consistent with the proposed structure. The structure was completed by difference Fourier synthesis with SHELXL97.[13,14] Scattering factors are from Waasmair and Kirfel[15]. Hydrogen atoms were placed in geometrically idealized positions and constrained to ride on their parent atoms with C---H distances in the range 0.95-1.00 Angstrom. Isotropic thermal parameters U_{eq} were fixed such that they were 1.2 U_{eq} of their parent atom Ueq for CH's and 1.5 U_{eq} of their parent atom U_{eq} in case of methyl groups. All non-hydrogen atoms were refined anisotropically by full-matrix least-squares. The dimer is 2^+ charged and accompanied by two BF_4^- anions which are bridged by water molecules. O_3 hydrogen bonds to O_1 of the symmetry related half of the dimer which has C_2 symmetry. The fluorines of BF_4^- are disordered at a ratio of 60% to 40%.

Table 2.2. Crystallographic data for **8**.

Parameter	**8**
Empirical formula	C24 H36 B2 F8 N8 O8 Pt2
Formula weight	1128.41

Temperature	100(2) K
Wavelength	0.71073 Å
Crystal system	Monoclinic
Space group	C 2/c
Unit cell dimensions	a = 22.9540(17) Å α= 90°. b = 8.2221(5) Å β= 113.264(7)°. c = 20.5433(16) Å γ = 90°.
Volume	3561.9(4) $Å^3$
Z	4
Density (calculated)	2.104 Mg/m^3
Absorption coefficient	7.944 mm^{-1}
F(000)	2152
Crystal size	0.21 x 0.16 x 0.09 mm^3
Theta range for data collection	2.16 to 30.63°.
Index ranges	-32<=h<=32, -11<=k<=11, -29<=l<=29
Reflections collected	69123
Independent reflections	5420 [R(int) = 0.0617]
Completeness to theta = 25.00°	99.1 %
Max. and min. transmission	0.5350 and 0.2862
Refinement method	Full-matrix least-squares on F^2
Data / restraints / parameters	5420 / 0 / 277
Goodness-of-fit on F^2	1.193
Final R indices [I>2sigma(I)]	R1 = 0.0391, wR2 = 0.0732
R indices (all data)	R1 = 0.0622, wR2 = 0.0887
Largest diff. peak and hole	3.554 and -3.227 $e.Å^{-3}$

Crystallographic characterization of compound 9

A colorless plate, measuring 0.16 x 0.15 x 0.02 mm^3 was mounted on a glass capillary with oil. Data was collected at -173^oC on a Bruker APEX II single crystal X-ray diffractometer, Mo-radiation.

Crystal-to-detector distance was 40 mm and exposure time was 10 seconds per degree for all sets. The scan width was 0.5°. Data collection was 100% complete to 25° in ϑ. A total of 25138 (merged) reflections were collected covering the indices, h = -18 to 29, k = -19 to 21, l = -11 to 11. 3961 reflections were symmetry independent and the R_{int} = 0.0386 indicated that the data was good (average quality 0.07). Indexing and unit cell refinement indicated an orthorhombic P lattice. The space group was found to be P n m a (No.62).

The data was integrated and scaled using SAINT, SADABS within the APEX2 software package by Bruker.[11] Solution by direct methods (SHELXS, SIR97[12]) produced a complete heavy atom phasing model consistent with the proposed structure. The structure was completed by difference Fourier synthesis with SHELXL97.[13,14] Scattering factors are from Waasmair and Kirfel[15]. Hydrogen atoms were placed in geometrically idealized positions and constrained to ride on their parent atoms with C---H distances in the range 0.95-1.00 Angstrom. Isotropic thermal parameters U_{eq} were fixed such that they were 1.2 U_{eq} of their parent atom Ueq for CH's and 1.5 U_{eq} of their parent atom U_{eq} in case of methyl groups. All non-hydrogen atoms were refined anisotropically by full-matrix least-squares. The dimer exhibits a closely linked network of the carboxyl oxygens, the two bridging hydroxys and two waters. The resulting dimer molecule thus is almost of C_{2v} (mm2) symmetry.

Table 2.3. Crystallographic data for **9**.

Parameter	**9**
Empirical formula	C24 H36 N8 O8 Pt2
Formula weight	954.79
Temperature	100(2) K
Wavelength	0.71073 Å
Crystal system	Orthorhombic
Space group	P n m a

Unit cell dimensions	a = 21.9819(4) Å b = 16.4596(3) Å c = 8.5220(2) Å
Volume	3083.37(11) $Å^3$
Z	4
Density (calculated)	2.057 Mg/m^3
Absorption coefficient	9.122 mm^{-1}
F(000)	1824
Crystal size	0.16 x 0.15 x 0.02 mm^3
Theta range for data collection	1.85 to 28.29°.
Index ranges	-18<=h<=29, -19<=k<=21, -11<=l<=11
Reflections collected	25138
Independent reflections	3961 [R(int) = 0.0386]
Completeness to theta = 25.00°	100.0 %
Max. and min. transmission	0.8386 and 0.3231
Refinement method	Full-matrix least-squares on F^2
Data / restraints / parameters	3961 / 0 / 200
Goodness-of-fit on F^2	1.000
Final R indices [I>2sigma(I)]	R1 = 0.0286, wR2 = 0.0741
R indices (all data)	R1 = 0.0359, wR2 = 0.0800
Largest diff. peak and hole	2.116 and -1.098 $e.Å^{-3}$

[1] RSC Green Chemistry No. 20 Alternative Solvents for Green Chemistry: 2Nd Edition By Francesca M Kerton and Ray Marriott # FM Kerton and R Marriott 2013 Published by the Royal Society of Chemistry, www.rsc.org.

[2] (a) Lersch, M.; Tilset, M. *Chem. Rev.* **2005**, *105*, 2471. (b) Fettinger, J. C.; Mohr, F.; Vedernikov, A. N. *J. Am. Chem. Soc.* **2004**, 1*26*, 11160. (c) Stahl, S. S.; Labinger, J. A.; Bercaw, J. E. *J. Am. Chem. Soc.* **1996**, *118*, 5961. (d) Derrick W. Lucey, D. W.; Helfer, D. S.; Atwood, J. D. *Organometallics* **2003,** *22,* 826.

[3] Chen, G. S.; Lin. B.; Labinger, J. A.; Bercaw, J. E. *Organometallics* **2010**, *29*, 4354.

[4] Chen, G. S.; Lin. B.; Labinger, J. A.; Bercaw, J. E. *J. Am. Chem. Soc.* **2008**, *130* (52), 17654.

[5] Weinberg, D. R.; Labinger, J. A.; Bercaw, J.E. *Organometallics* **2007,** *26,* 167.

[6] (a) Otero, A. J.; Fernandez-Baeza, J.; Tejada, J.; Antinolo, A.; Carrillo-Hermosilla, F.; Diez-Barra, E.; Lara-Sanchez, A.; Fernandez-Lopez, M.; Lanfranchi, M.; Pellinghelli, M. A. *J. Chem. Soc., Dalton Trans*., **1999**, 3537. (b) Field, L. D.; Messerle, B. A.; Rehr, M.; Soler, L. P.; Hambley, T. W. *Organometallics* **2003,** *22*, 2387. (c) Otero, A.; Fernández-Baeza, J.; Tejeda, J.; Antiñolo, A.; Carrillo-Hermosilla, F.; Díez-Barra, E.; Lara-Sánchez, A.; Fernández-López, M. *J. Chem. Soc., Dalton Trans*. **2000**, 2367.

[7] (a) Wick, D.D.; Goldberg, K.I. *J. Am. Chem. Soc*. **1997,** *119,* 10235. (b) Vedernikov, A.N.; Fettinger, J.C.; Mohr, F. *J. Am. Chem. Soc.*, **2004**, 126 (36), 11160. (c) Prokopchuk, E.M.; Puddephatt, R.J. *Organometallics* **2003,** *22*, 787. (d) Puddephatt, R. J. *Coor. Chem. Rev.* **2001**, 521.

[8] Holtcamp, M.W.; Henling, L.M.; Day, M.W.; Labinger, J.A.; Bercaw, J.E. *lnorganica Chimica Acta* **1998**, 270, 467.
[9] (a) Shilov, A. E.; Shulpin, G. B. *Russ. Chem. Rev.* **1987**, *56*, 442. (b) Shilov, A. E.; Shul'pin, G. B. *Activation and Catalytic Reactions of Saturated Hydrocarbons in the Presence of Metal Complexes*; Kluwer Academic Publishers: Boston, 2000.
[10] Scott, J. D.; Puddephatt, R. J. *Organometallics* **1983**, *2*,1643.
[11] Bruker (**2007**) APEX2 (Version 2.1-4), SAINT (version 7.34A), SADABS (version 2007/4), BrukerAXS Inc, Madison, Wisconsin, USA.
[12] (a) Altomare, A.; Burla, C.; Camalli M.; Cascarano L.; Giacovazzo C.; Guagliardi A.; Moliterni A.G.G.; Polidori G.; Spagna R. J. *Appl. Cryst.* **1999**, *32*, 115. (b) Altomare, A.; Cascarano, G.; Giacovazzo, C.; Guagliardi, A., *J. Appl. Cryst.* **1993**, *26*, 343.
[13] Sheldrick, G. M. SHELXL-97: Program for the Refinement of Crystal Structures 1997 University of Gottingen, Germany.
[14] Mackay, S.; Edwards, C.; Henderson, A.; Gilmore, C.; Stewart, N.; Shankland, K.; Donald, A.; *MaXus: a computer program for the solution and refinement of crystal structures from diffraction data*. University of Glasgow, Scotland, 1997.
[15] Waasmaier, D.; Kirfel, A. *Acta Crystallogr. A.* **1995**, *51*, 416.

Chapter 3 : Aerobic oxidation of monomethyl platinum(II) to monomethyl platinum(IV) in competition with methyl group transfer to form dimethyl platinum(IV)

Introduction

Pt^{II}-CH_3 complexes, generated from methane, are key proposed intermediates in both the Shilov methane oxidation system[1] and in the Catalytica Pt methane oxidation system (Figure 1.2).[2] In both systems, it is proposed that Pt^{II}-CH_3 species are oxidized to form Pt^{IV}-CH_3 species using Pt^{IV} as the oxidant. Ideally, oxygen could replace Pt^{IV} as the oxidant and this concept has inspired investigations of the reactions of Pt^{II}-CH_3 complexes with molecular oxygen.[3,4] In studies of model Pt^{II} complexes with bpy and diimine ligands, Labinger, Bercaw, and Goldberg were able to demonstrate oxidation of dimethyl Pt^{II} to dimethyl Pt^{IV} complexes in methanol using molecular oxygen (Figure 1.4a).[3b] However, subsequent work by Labinger and Bercaw showed that monomethyl Pt^{II} complexes, the type of species that would be generated by activation of methane at a Pt^{II} center, were significantly more difficult to oxidize (Figure 1.4 b and c).[3c] Vedernikov addressed this challenge by incorporating a facially coordinating ligand that promoted aerobic oxidation of the monomethyl Pt^{II} to monomethyl Pt^{IV} (Figure 1.9).[4b]

Herein, we describe aqueous aerobic oxidation of a monomethyl Pt^{II} system with a facially coordinating ligand that incorporates a hemilabile carboxylate arm (**1**, Figure 1.10). In addition to direct oxidation to form a monomethyl Pt^{IV} complex, a rare competitive oxidative methyl transfer reaction to form a dimethyl Pt^{IV} complex was observed. Further, it was demonstrated that the oxidation reaction conditions can be modified to favor one Pt^{IV} product over the other.

Results and Discussion

Dissolution of isolated monomethyl Pt^{II} complexes **6** (4 mM) in D_2O resulted in a significantly alkaline solution (pD = 10). This is attributed to a small degree of protonation of **6,** presumably at the hydroxide position, to generate **6**D^+ and KOD as (Figure 3.1). A pK_a value of 8.5 (0.2) was measured for **6**D^+ (Figure 3.2). Complex **6**/**6**D^+ was stable in D_2O under anaerobic conditions at room temperature.

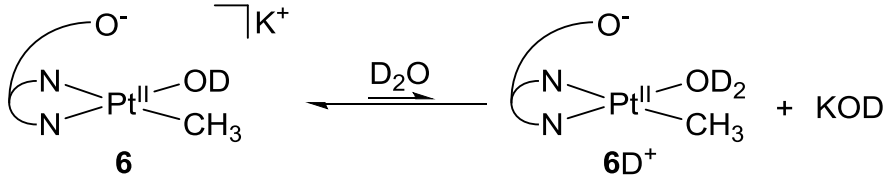

Figure 3.1. Production of KOD from **6** in D_2O.

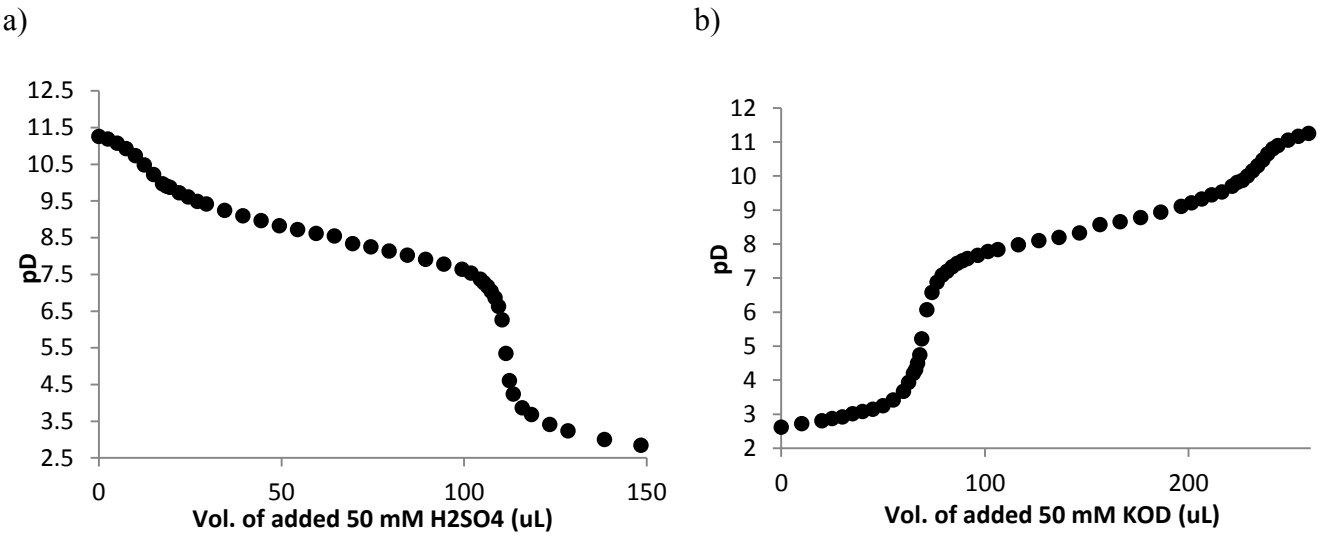

Figure 3.2. a) Titration of **6** with 50mM H_2SO_4. b) Titration of **6**D^+ with 50 mM KOD.

Upon exposure to air, a slow reaction (5% conversion of **6** after 3 hours) was observed by ^1H NMR spectroscopy. Under higher O_2 pressure (8.2 atm), evidence of reaction of **6** with O_2 was observed by ^1H NMR spectroscopy within minutes at room temperature. The reaction slowed considerably over time with full conversion of **6** (95%) requiring approximately 2 weeks (Table 3.1: Entry 1). The

expected product based on previously reported aerobic oxidations of Pt^{II} monomethyl and dimethyl complexes,[3,4] κ^3-NNO$Pt^{IV}(CH_3)(OH)_2$ (**10**), was identified as the major product of the reaction (89%, Figure 3.3). Complex **10** exhibits a Pt^{IV}-CH_3 signal in the ^{1}H NMR spectrum at 2.48 ppm ($^2J_{Pt\text{-}H}$ = 72.4 Hz). Four singlets corresponding to the methyl groups on the pyrazolyl of NNO (2.53, 2.50, 2.42 and 2.41 ppm) are indicative of a C_1-symmetric structure (Figure 3.3). During the reaction of **6** with O_2 the pD of the solution increased from 10 – 12. The increase in alkalinity is consistent with the stoichiometric production of KOD with each equivalent of **10** that is generated.

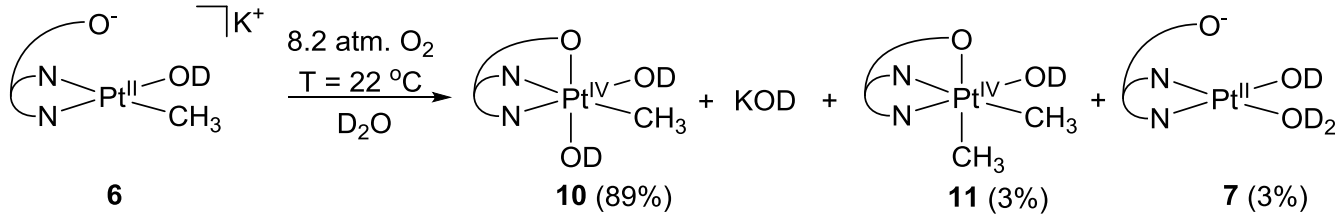

Figure 3.3. Reaction of **6** with dioxygen.

An independent synthesis of complex **10** was achieved by oxidation of **6** with H_2O_2. The ^{1}H NMR spectrum of the product of the H_2O_2 reaction was identical to **10** produced during the reaction of **6** with O_2. Crystals of **10** grown from slow evaporation of H_2O were used for characterization of **10** by X-ray diffraction (Figure 3.4). Octahedral coordination about the platinum center was confirmed with the carboxylate arm of the NNO ligand attached to the metal (Pt-O bond distance of 2.0706(12) Å). The Pt-CH_3 group resides trans to one of the pyrazolyls of NNO ligand consistent with the C_1-symmetry noted in the solution characterization. The two hydroxide ligands are inequivalent with one trans to the coordinated carboxylate having a shorter Pt-OH bond length (1.9587(12) Å) relative to the Pt-OH bond observed for the hydroxide trans to a pyrazolyl moiety (1.9806(12) Å).

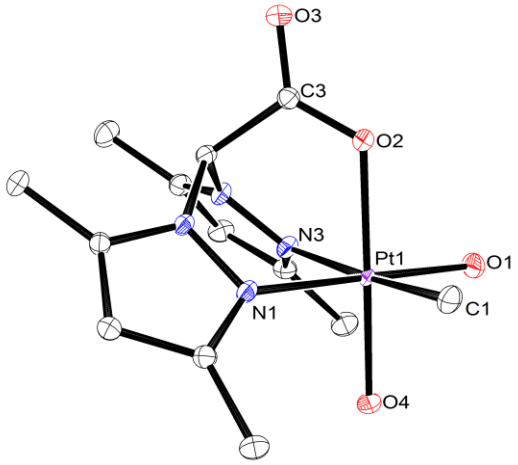

Figure 3.4. ORTEP of **10**. Displacement ellipsoids at the 50% probability level. Hydrogen atoms are excluded for clarity. Selected bond distances (Å) and angles (°): Pt1-C1 = 2.0301(16), Pt1-O1 = 1.9806(12), Pt1-O2 = 2.0706(12), Pt1-O4 = 1.9587(12), Pt1-N1 = 2.0353(13), Pt1-N3 = 2.1759(13), O2-C3 = 1.2268(19), O3-C3 = 1.2894(18), N3-Pt1-O1 = 92.20(5), C1-Pt1-N1 = 93.55(6), C1-Pt1-O1 = 89.02(6), C1-Pt1-O2 = 90.00(6), O4-Pt1-C1 = 91.39(6), O2-C3-O3 = 124.88(15), N1-N3-Pt1 = 85.30(5).

Along with **10**, the aqueous reaction of **6** and dioxygen produced two minor Pt species that were observed by ^{1}H NMR spectroscopy. These minor products, identified as κ^3-NNOPt^{IV}(CH$_3$)$_2$(OD) (**11**) (3%) and κ^2-NNOPt^{II}(OD)(D$_2$O) (**7**) (3%), were confirmed by independent synthesis. The dimethyl Pt^{IV} **11** was prepared by the addition of MeI to **6**. Complex **11** is distinguished by singlets for two inequivalent Pt^{IV}-CH$_3$ groups (2.01 and 1.75 ppm, 1:1 ratio) with ^{195}Pt satellites (77.1 and 69.8 Hz, respectively). The solid-state structure of **11** was determined by X-ray crystallography (Figure 3.5). An octahedral geometry about the platinum(IV) with coordination of the carboxylate group is evident. The two platinum-bound methyl groups, one trans to the carboxylate arm and the other trans to a pyrazolyl from the NNO ligand have similar Pt-C bond lengths (2.0310(18) and 2.0368(18) Å, respectively).

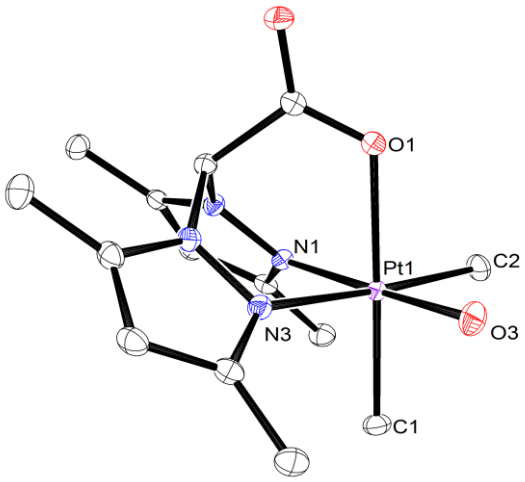

Figure 3.5. ORTEP of **11**. Displacement ellipsoids at the 50% probability level. Hydrogen atoms are excluded for clarity. Selected bond distances (Å) and angles (°): Pt1-C1 = 2.0310(18), Pt1-C2 = 2.0368(18), Pt1-O1 = 2.1766(13), Pt1-O3 = 1.9828(13), Pt1-N1 = 2.0488(14), Pt1-N3 = 2.1597(15), O1-C14 = 1.278(2), O2-C14 = 1.231(2), N3-Pt1-O3 = 89.90(6), O1-Pt1-O3 = 90.00(6), O1-Pt1-C2 = 90.91(7), O2-C14-O1 = 125.87(17), O3-Pt1-C2 = 89.51(7), C1-Pt1-C2 = 91.24(8), C2-Pt1-N1 = 93.70(7).

The second minor product, identified as κ^2-NNOPt^{II}(OD)(D_2O) (**7**), notably has no Pt-CH_3 groups. The identical yields of **7** (3%) and **11** (3%) are likely a consequence of the methyl transfer as for each dimethyl complex **11** produced an equivalent of "demethylated" NNOPt must be formed. Complex **7** was observed in the ^{1}H NMR spectrum by a singlet at 6.07 ppm for the two aromatic hydrogens and two singlets at 2.41 and 2.33 ppm for the four pyrazolyl bound methyl groups suggesting a C_s-symmetric species. Independent synthesis of **7** was performed by the addition of excess HBF_4 to a solution of **5** resulting in protonolysis of the remaining Pt-CH_3 group as methane (Figure 2.7). The ^{1}H NMR signals of independently synthesized **7** matched those attributed to the product from the reaction of **6** with O_2.

There have only been a small number of reported aerobic oxidations of monomethyl or dimethyl Pt^{II} species to produce their corresponding monomethyl or dimethyl Pt^{IV} respectively, and mechanistic understanding of this reaction class is still emerging.[3,4] Notably, previous studies by Labinger, Bercaw

and coworkers determined that the oxidation of $L_2Pt^{II}(CH_3)_2$ (L_2 = α-diimine) with oxygen in methanol to form $L_2Pt^{IV}Me_2(OH)(OCH_3)$ was first-order in both $[O_2]$ and $[L_2Pt^{II}(CH_3)_2]$ but zero order in $[H^+]$ (Figure 3.6).[3cb] Furthermore, a Pt^{IV} hydroperoxide intermediate was observed which can then react with the Pt^{II} dimethyl starting material to form two equivalents of the dimethyl hydroxide product (k_3, Figure 3.6). A slower competitive disproportionation of the hydroperoxide complex to form the same hydroxide product was also proposed (k_2, Figure 3.6).

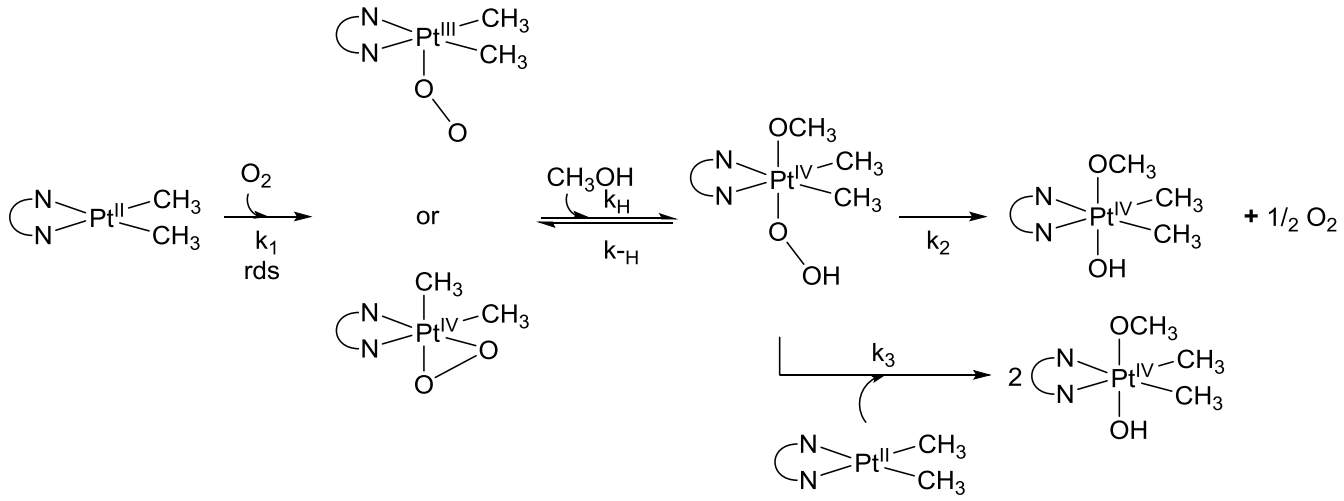

Figure 3.6. Mechanism for the aerobic oxidation of $L_2Pt^{II}(CH_3)_2$ determined by Labinger and Bercaw.[3c]

In buffered alkaline solutions (pD = 11, Table 3.1: Entries 6 and 7), the reaction of **6** with O_2 showed first-order kinetic behavior with respect to [**6**] (Figure 3.7). The reaction was also found to be first-order in $[O_2]$; k_{obs} increased from 8.0 (0.1) x 10^{-5} s^{-1} at 4.1 atm of O_2 to 1.6 (0.2) x 10^{-4} s^{-1} at 8.2 atm of O_2. There was no significant change in the product distribution with the change in oxygen pressure. With a significantly lower pressure of O_2 (2.1 atm), a slightly higher yield of **10** (71%) and lower yield of **11**, **7** and **8** (14, 7 and 6% respectively) was noted. An oxidation reaction that is first-order in monomethyl Pt^{II} and O_2 is consistent with the mechanism determined by Labinger and Bercaw (Figure 3.6).

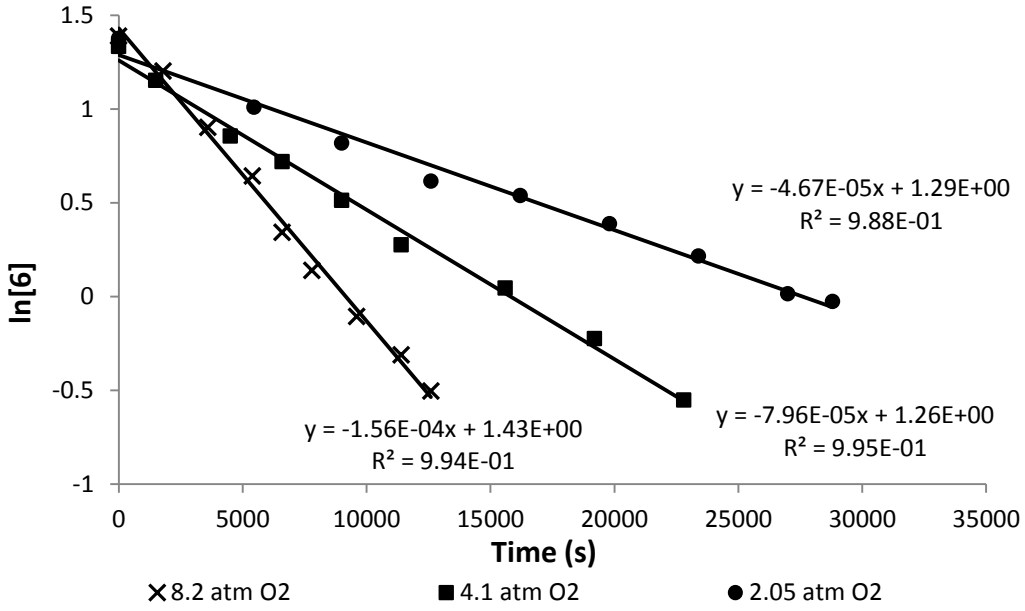

Figure 3.7. 1st order plot of the reaction of **6** with O_2 at various pressures of O_2.

At elevated pD (> 11) or temperature (> 80 °C) a new NNO product was observed in the ^{1}H NMR spectrum of the products with signals at 6.32 and 2.57 ppm consistent with the platinum(IV) complex, κ^3-NNOPt^{IV}(OD)$_3$ (**12**). Complex **12** was independently synthesized from the addition of H_2O_2 to **7** (Figure 3.8). Complex **7** is likely the source of **12** as the sum of the concentration of **7** and **12** was consistently equal to the concentration of **11** (Table 3.1: Entries 3, 4, 7 and 8). The relationship to production of **12** with pD and temperature may simply be that high pD and temperature enhance methyl transfer and therefore the [**7**].

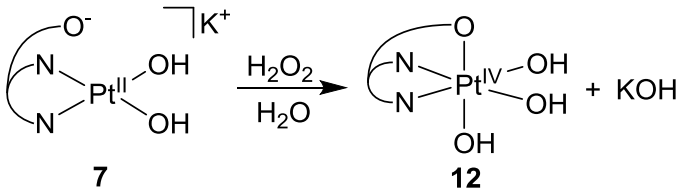

Figure 3.8. Independent synthesis of **12**.

Continued heating of the product mixture from the reaction of **6** with O_2 for 24 h after complete conversion of **6** had no effect on the ratio of **7**:**12**. Conversely, addition of H_2O_2 to the products resulted

in rapid conversion of **7** to **12**. The formation of **12** under the reaction conditions appears to indicate that a stronger oxidant than O_2 is produced during the reaction of **6** with O_2 and it is this oxidant that is capable of oxidizing **7**. A Pt^{IV} methyl hydroperoxide (**I_1**, Figure 3.9) similar to the intermediate described by Labinger and Bercaw seems most likely (Figure 3.6).[3b] A Pt^{IV} methyl hydroperoxide was not observed by ^1H NMR spectroscopy but this is not surprising as the concentration of the intermediate is likely very low. Also, when the hydroperoxide is deuterated, the intermediate would be nearly identical to the hydroxide product **10**.[3b,5] Finally, the monomethyl hydroxide Pt^{IV} (**10**) produced when **7** is oxidized by the mono methyl hydroperoxide Pt^{IV} is indistinguishable from the product of oxidation of **6** (Figure 3.9).

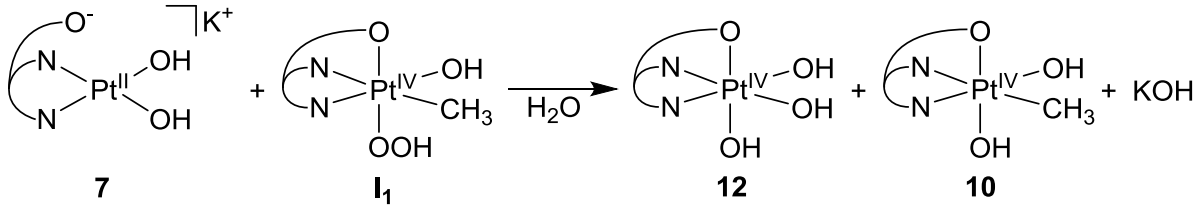

Figure 3.9. Proposed in situ synthesis of **12**.

Having identified the products and a likely intermediate of the reaction of **6** and O_2 the effect of pD on the product distribution was examined. Increasing the alkalinity of the solution through the addition of KOH (4 mM) resulted in increased methyl transfer to produce a 23% yield of the Pt^{IV} dimethyl product **11** (Table 3.1: Entry 4). Thus, under these conditions, almost 50% of **6** undergoes methyl transfer. The addition of KOH also slowed the reaction as seen by the first half-life more than doubling relative to the reaction without added KOH (Table 3.1: Entries 3 and 4). This inhibition of the reaction by hydroxide is also consistent with the slowing of the reaction that is observed as KOD is produced in the reaction of **6** with O_2 to form **10** (see above).

Table 3.1. Effects of temperature, alkalinity and pressure of O_2 on the rate and product distribution of the reaction of 6 with O_2 ([**6**] = 4 mM, *added 4 mM KOH, $^{\dagger}H_3PO_4/H_3BO_3$/KOH buffered, $^{\blacklozenge}H_3BO_3$/KOH buffered).

Entry	Temp. (°C)	pD	pO_2 (atm)	1st half-life (hr)	Conv. of **6** (%)	Yield (%)			
						10	**11**	**7**	**12**
1	~22	-	8.2	30	95	89	3	3	0
2	40	-	8.2	14	99	89	6	5	0
3	80	-	8.2	1	99	72	12	9	4
4	80	-*	8.2	2.4	98	51	23	16	7
5	80	6.5†	3.4	0.29	98	91	2	3	0
6	80	8.6†	3.4	0.067	99	95	2	2	0
7	80	11.2$^{\blacklozenge}$	8.2	1.2	99	62	17	9	8
8	80	11.2$^{\blacklozenge}$	4.1	2.4	98	63	16	10	6

The oxidative methyl transfer reaction has less precedent than the direct oxidation of Pt^{II}-CH_3 with oxygen.[4b,c] Notably, no reaction was observed between the monomethyl Pt^{II} starting material **6** and the monomethyl Pt^{IV} product **10** under anaerobic conditions that were otherwise optimized for methyl transfer (80 °C, 4 mM added KOH). This lack of reactivity eliminated **10** as the source of the additional methyl group in **11**. However, it has been shown that for efficient nucleophilic attack on a Pt^{IV} methyl group, an open site or good leaving group in the trans position is required.[6]

While it did not prove possible to isolate the isomer of **10** in which the methyl bound to platinum is trans to the carboxylate arm, the dimethyl **11** does contain such a methyl group. Thus, to observe the potential reactivity between **6** and a Pt^{IV}-CH_3 with the methyl group trans to the hemilabile carboxylate arm isotopically labelled **6**-d_5 (Deuterium in Pt-CD_3, Pt-OD and methine (R_3C-D in NNO) was heated with **11** under anaerobic conditions optimized for methyl transfer (80 °C, 4 mM added KOH, Figure 3.10). After 1.5 hours the Pt^{II}-CH_3 signal (δ = 0.69 ppm) associated with **6** appeared supporting the production of **6** (6.6 μmol) due to the conversion of 19% of **6**-d_5 to **6**. A closely matching decrease (8.5%) of the integration of the *two* Pt^{IV}-CH_3 signals (δ = 1.75 and 1.99 ppm) associated with **11** was observed. The ratio of [**6** + **6**-d_5]:[**11** + **11**-d_5] was unchanged based on a comparison of the aromatic

protons in the NNO ligand. The increase in the [**6**] slowed until after 15 h the [**6**] (7.7 mM) made up 50% of [**6** + **6**-d_5] (15.7 mM). Interestingly, the integration of the two Pt^{IV}-CH_3 groups in **11**/**11**-d_5 remained nearly 1:1 through the reaction supporting a faster rate of isomerization of **11** than the rate of methyl transfer. While the possibility of methyl transfer of the equatorial Pt^{IV}-CH_3 in **11** cannot be ruled out the lack of reactivity between **6** and **10** (see above) as well as Vedernikov's finding that methyl transfer from C_s-NNO$Pt^{IV}(CH_3)(OH)_2$ is much faster than transfer from C_1-NNO$Pt^{IV}(CH_3)(OH)_2$ support more facile methyl transfer when the Pt^{IV}-CH_3 is trans to a good leaving group.[4c]

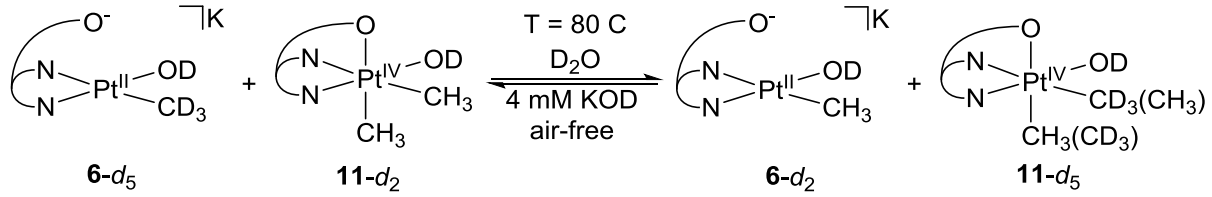

Figure 3.10. Methyl group transfer from **11** to **6**.

Based on the similarity of the observed oxidation reaction with that reported by Labinger and Bercaw along with the apparent need for a Pt^{IV}-CH_3 trans to a good leaving group to perform methyl transfer we propose a competitive oxidation/oxidative methyl transfer mechanism that incorporates both pathways (Figure 3.11). A first-order dependence on [**6**] and on [O_2] (second-order overall) is consistent with an initial rate determining reaction of **6** with dioxygen to produce $\mathbf{I_1}$ (k_1, Figure 3.11). The similarity in the product ratios of [**10**]/[**11**] (and thus the rates of formation) when the pressure of oxygen is doubled is suggestive of a shared initial reaction path for the two types of Pt^{IV} products, albeit two separate paths cannot be ruled out.[7b,c] Reaction of $\mathbf{I_1}$ with a second equivalent of **6** is proposed to lead to two equivalents of **10** (k_2, Figure 3.11). Again, this mechanism is analogous to that suggested by Labinger and Bercaw for their Pt^{II}-$(CH_3)_2$ oxidation.[3b] To enable efficient methyl group transfer, we propose that $\mathbf{I_1}$ isomerizes to $\mathbf{I_2}$ which then reacts with **6** to produce **11**. The position of the CH_3 group trans to the carboxylate moiety (a competent leaving group) in $\mathbf{I_2}$ should facilitate the nucleophilic

attack by **6** leading to methyl transfer.[4a,c] The difference in the propensity of $\mathbf{I_1}$ versus **10** to undergo isomerization may be attributed to the greater trans influence of OOH versus OH which may ease access to a 5 coordinate intermediate.[4b]

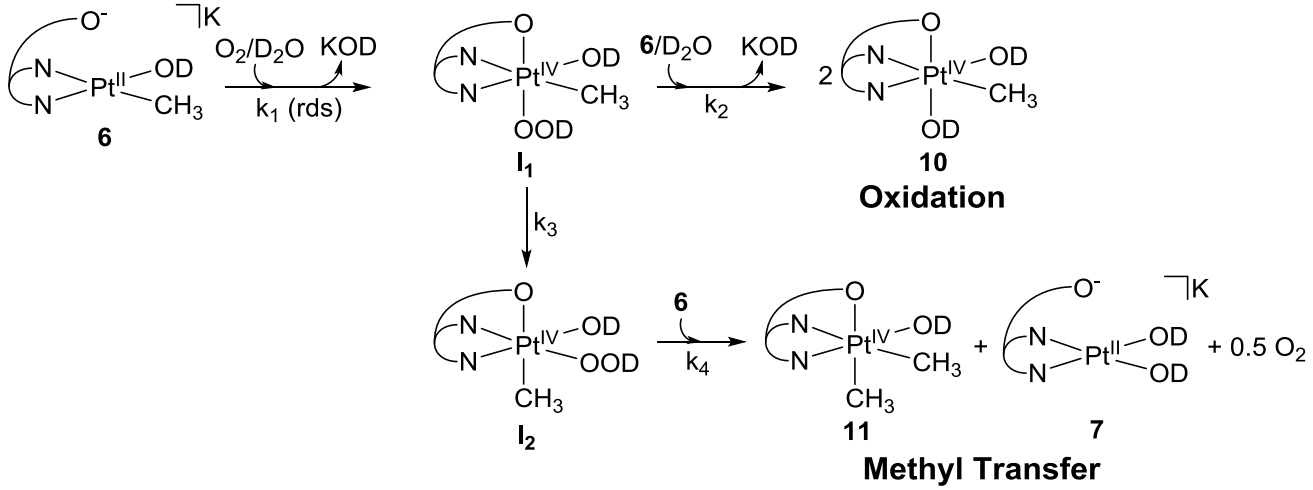

Figure 3.11. Proposed mechanism for the reaction of **6** with O_2 in alkaline solutions.

As stated above, methyl transfer becomes more competitive with oxidation with increasing pD. In our proposed mechanism partitioning between oxidation and methyl transfer occurs wherein $\mathbf{I_1}$ reacts with **6** or undergoes isomerization to $\mathbf{I_2}$. Notably, the rate of isomerization of $\mathbf{I_1}$ is expected to positively correlate with pD; in the related dpms system Vedernikov found that isomerization of monomethyl Pt^{IV} hydroxide was considerably faster at higher pH (more details on pH-dependent isomerization of $NNOPt^{IV}CH_3(OH)_2$ in Chapter 4).[4a] An increase in the rate of isomerization of $\mathbf{I_1}$ with increasing pD can explain the more significant contribution of the methyl transfer pathway at high pD.

The effect of pD on the reaction rate of $NNOPt^{II}(CH_3)L$ (L = H_2O/OH^-) with O_2 was also examined. At low pD (6.5) when nearly all of $NNOPt^{II}(CH_3)L$ is in the $\mathbf{6}D^+$ form (Table 3.2) the reaction is 1st order in $\mathbf{6}D^+$ (k_{obs} = 7.3 (0.4) x 10^{-5} s^{-1}, Figure 3.12). At high pD (11.2) when **6** is the major species the reaction is also 1st order in **6** (k_{obs} = 8.2 (0.1) x 10^{-5} s^{-1}, Figure 3.7). At pD = 8.6 (*ca.* the pK_a of $\mathbf{6}D^+$) excellent fit to 1st-order in [$\mathbf{6}/\mathbf{6}D^+$] was observed through the first two half-lives with a

significantly faster k_{obs} = 2.6 (0.4) x 10^{-4} s^{-1} (Figure 3.13a). However, slowing was observed during the 3rd half-life and may be due to the slower k_2 step becoming the rate-determining step for oxidation at very low [**6**] (Figure 3.13b).[3c]

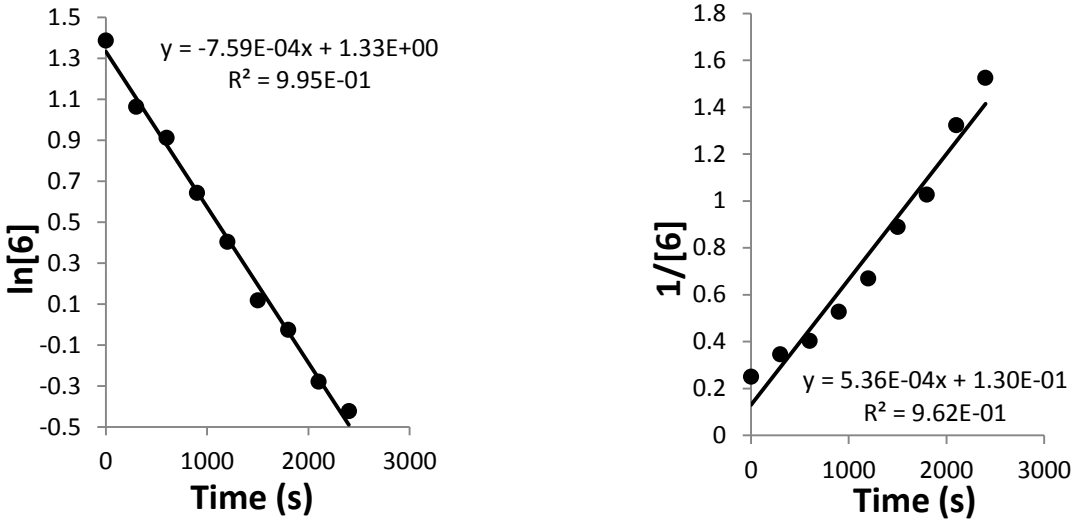

Figure 3.12. First and second-order plots of the reaction of **6** with O_2 at pD = 6.5 ($[\mathbf{6}]_{init}$ = 4 mM, pO_2 = 3.4 atm, T = 80 °C).

a)

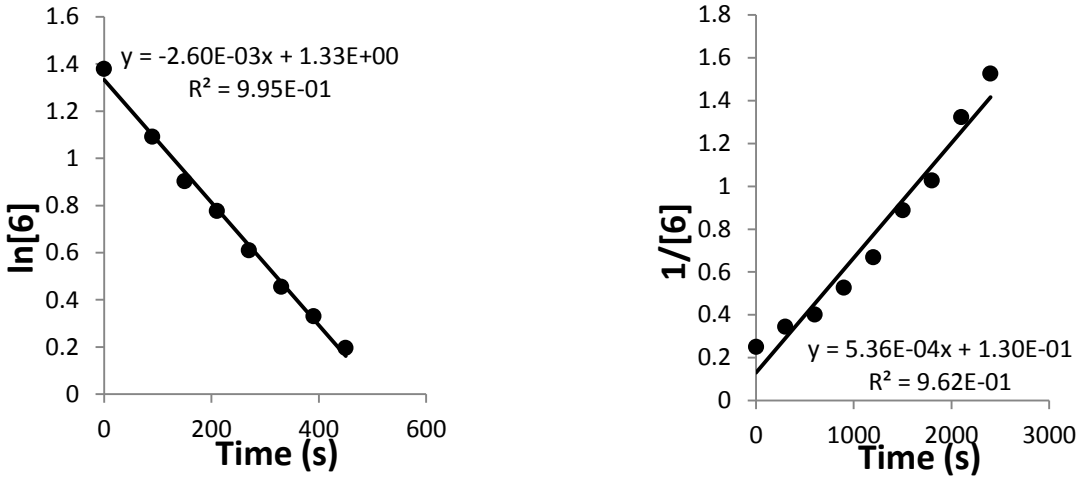

b)

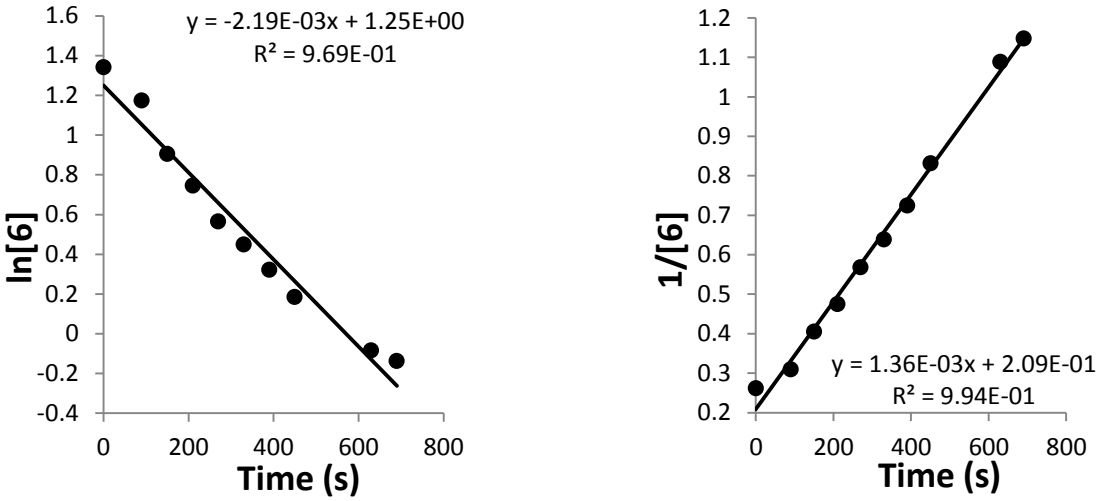

Figure 3.13. First and second-order plots of the reaction of **6** with O_2 at pD = 8.5 (data through the 2nd half-life, $[\mathbf{6}]_{init}$ = 4 mM, pO_2 = 3.4 atm, T = 80 °C): a) Data through the 2nd half-life. b) Data through the 3rd half-life.

Based on the 1st half-life (Table 3.2) the reaction rate increases as the pD of the solution approaches the pKa of $\mathbf{6}D^+$. A similar peak in the reaction rate with respect to pH was observed in the Vedernikov dpms system.[4b] The increase in the rate of the reaction with increasing pD at pD values lower than the pK_a is consistent with a faster reaction of **6** with O_2 relative to the reaction of $\mathbf{6}D^+$ with O_2. A similar explanation was offered by Vedernikov with respect to the relative reactivity of the dpms

hydroxide and aquo complexes.[4b,c] As shown in Figure 3.11, we propose that reaction of **6**/**6**D$^+$ and dioxygen forms a hydroperoxo intermediate $\mathbf{I_1}$ that decomposes by competing oxidation and methyl transfer pathways. Notably, to form the hydroperoxo intermediate $\mathbf{I_1}$ from **6** and O_2, a proton is also needed, presenting an explanation for the observed decrease in reaction rate at high pD.

Table 3.2. Effects of pD on the ratio of **6** to **6**D$^+$ based on pK_a = 8.6. ([**6**+ **6**D$^+$] = 4 mM, $^{\dagger}H_3PO_4/H_3BO_3$/KOH buffered, $^{\blacklozenge}H_3BO_3$/KOH buffered).

pD	Initial (%)		pO_2	1st half-life
	6	**6**D$^+$	(atm)	(hr)
6.5†	1	99	3.4	0.29
8.6†	52	48	3.4	0.067
11.2$^{\blacklozenge}$	99	< 1	8.2	1.2

In addition to the reaction of $\mathbf{I_1}$ with **6** and/or **6**D$^+$, $\mathbf{I_1}$ can also react with the bis-hydroxo Pt^{II} product **7** to generate the Pt^{IV} product **12** (Figure 3.9). This reaction between **7** and $\mathbf{I_1}$ should impose a limit on methyl transfer as **7** can compete with methyl transfer for reaction with $\mathbf{I_1}$ resulting in the oxidation product (Figure 3.14). In terms of the effect on the product distribution, increasing the [**7**] would be similar to increasing the [**6**] (see below) which results in an increase in oxidation relative to methyl transfer. This would explain why increasing [KOH] above 4 mM had little effect on the production of the methyl transfer product **11**. At 8 and 200 mM [KOH] the yield of **11** was 47 and 49% respectively similar to the 50% yield at [KOH] of 4 mM. In the Vedernikov system where oxidation of the demethylated product of methyl transfer is not oxidized the dimethyl Pt^{IV} methyl transfer product reached as high as 70% at pH = 14.[4b]

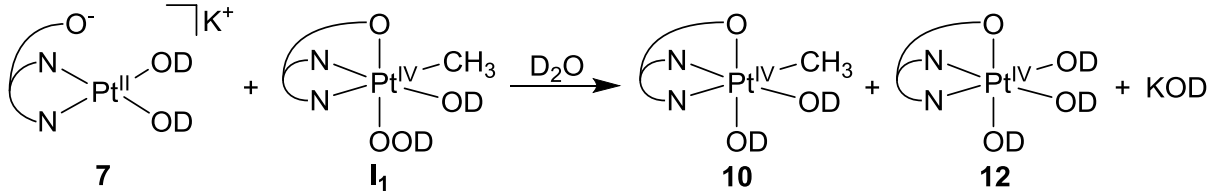

Figure 3.14. Proposed Oxidation of **7** by intermediate $\mathbf{I_1}$ generated from the reaction of **6** and O_2.

Modification of the temperature of the reaction between **6** and dioxygen was also investigated. As the temperature was raised, reaction times decreased as expected, but an increase in the proportion of the methyl transfer product **11** relative to the oxidation product **10** was also observed. At 80 °C, the reaction was complete within 24 hours, and **11** accounted for 12% of the Pt containing product (Table 3.1: Entry 3) compared with a lower yield of **11** at 22 °C (3%, Table 3.1: Entry 1). The use of higher temperatures (> 80 °C) resulted in decomposition of the Pt product **10** to methanol and **7** (more details in Chapter 4) and thus, further studies were limited to 80°C.

As outlined in our proposed mechanism the competition for $\mathbf{I_1}$ determines the products. The two different paths, either associative reaction between **7** and $\mathbf{I_1}$ or isomerization of $\mathbf{I_1}$ (likely through dissociation of the carboxylate hemilabile arm) should have considerable differences in $\Delta S^{\ddagger}$. The associative reaction would likely have $\Delta S^{\ddagger} < 0$ which would inhibit the reaction at higher temperature. Comparatively, "dissociative" isomerization which likely has a near zero contribution from $\Delta S^{\ddagger}$ thereby conserving any temperature related increase in rate. The differential response to increasing temperature would result in an increase in the methyl transfer relative to oxidation at higher temperature as observed. Unfortunately, activation parameters determined from the change in the [**6**] would only provide information on the initial reaction of **6** with O_2 to form $\mathbf{I_1}$.

Following the formation of the oxidation product **10** and the methyl transfer product **11** could provide useful activation parameters however the ratio of **10**:**11** changes over the course of the reaction (Figure 3.15). As described in Figure 3.11, competition for $\mathbf{I_1}$ determines the ratio of [**10**]:[**11**]. The oxidation product determining step (k_2) is expected to be 2^{nd} order in [**6**] while the methyl transfer product determining step (k_3) remains 1^{st} order in [**6**] (assuming a sufficiently high [**6**] preventing a change in the rds for methyl transfer to k_4). Due to the differential response to [**6**] between oxidation and methyl transfer we would expect to see the production of **10** decreasing, as the [**6**] decreases, relative to

the production of **11** which matches our observations. The increasing methyl transfer relative to oxidation with time was also observed in Vedernikov's dpms system.[4c]

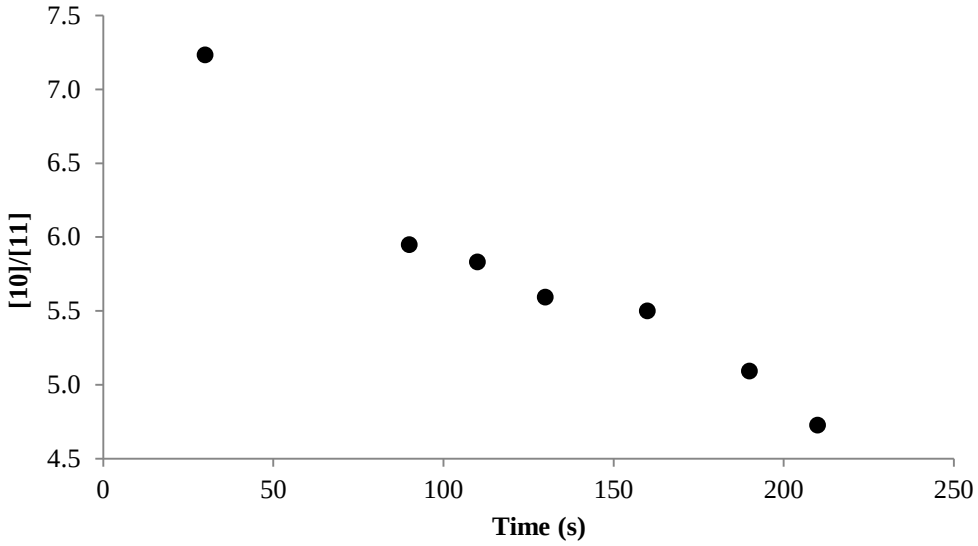

Figure 3.15. Increasing methyl transfer (**11**) relative to oxidation (**10**) during the reaction of **6** with O_2. See Table 3.1: entry 7 for conditions.

In contrast to our results, in the related dpms system, a change from 1st to 2nd order kinetics was observed with respect to aerobic oxidation of the Pt^{II}-Me species (**6v**, Figure 3.16) when the pH was increased above 10.[4b,c] A change in the rate determining step from the reaction with O_2 (k_1, Figure 3.16) to the reaction of the Pt^{IV}-OOH intermediate with the Pt^{II}-CH_3 species (k_2, Figure 3.16) was suggested. Meanwhile the methyl transfer reaction was noted to maintain 1st order kinetic behavior and dominated at high pH. The authors conclude that two distinct pathways are responsible for the oxidation and methyl transfer. While we cannot rule out two pathways in our system, our results are fully consistent with the mechanism shown in Figure 3.11.

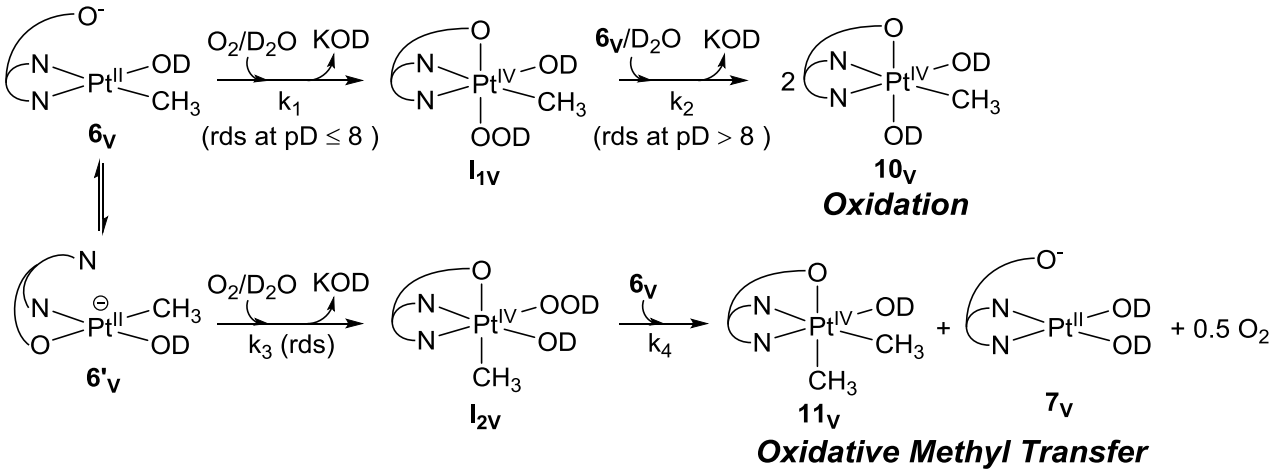

Figure 3.16. Vedernikov's proposed mechanism of competitive oxidation and methyl transfer.[4b,c]

Interestingly, we were able to get a good fit to 2nd order kinetics in [**6**] when the reaction of **6** with O_2 was performed in non-buffered solution at pD_i = 10.2 (Figure 3.17a). However, this fit to 2nd order kinetics is likely fortuitous due to slowing of the reaction with increasing pD (pD_f = 12.4) Thus we propose that this is a coincidental fit to 2nd order kinetics. Supporting this conclusion is that when the reaction was repeated under nearly identical conditions but using a 100 mM boric acid/D_2O buffered solution that was adjusted to pD = 10.2 by the addition of KOH, the data clearly fit best to 1st order kinetic expression with respect to [**6**] (Figure 3.17b). This result supports the need for sufficient buffer capacity. This is particularly important at pH farther from the pK_a of the buffers which may not have been considered in Vedernikov's studies.

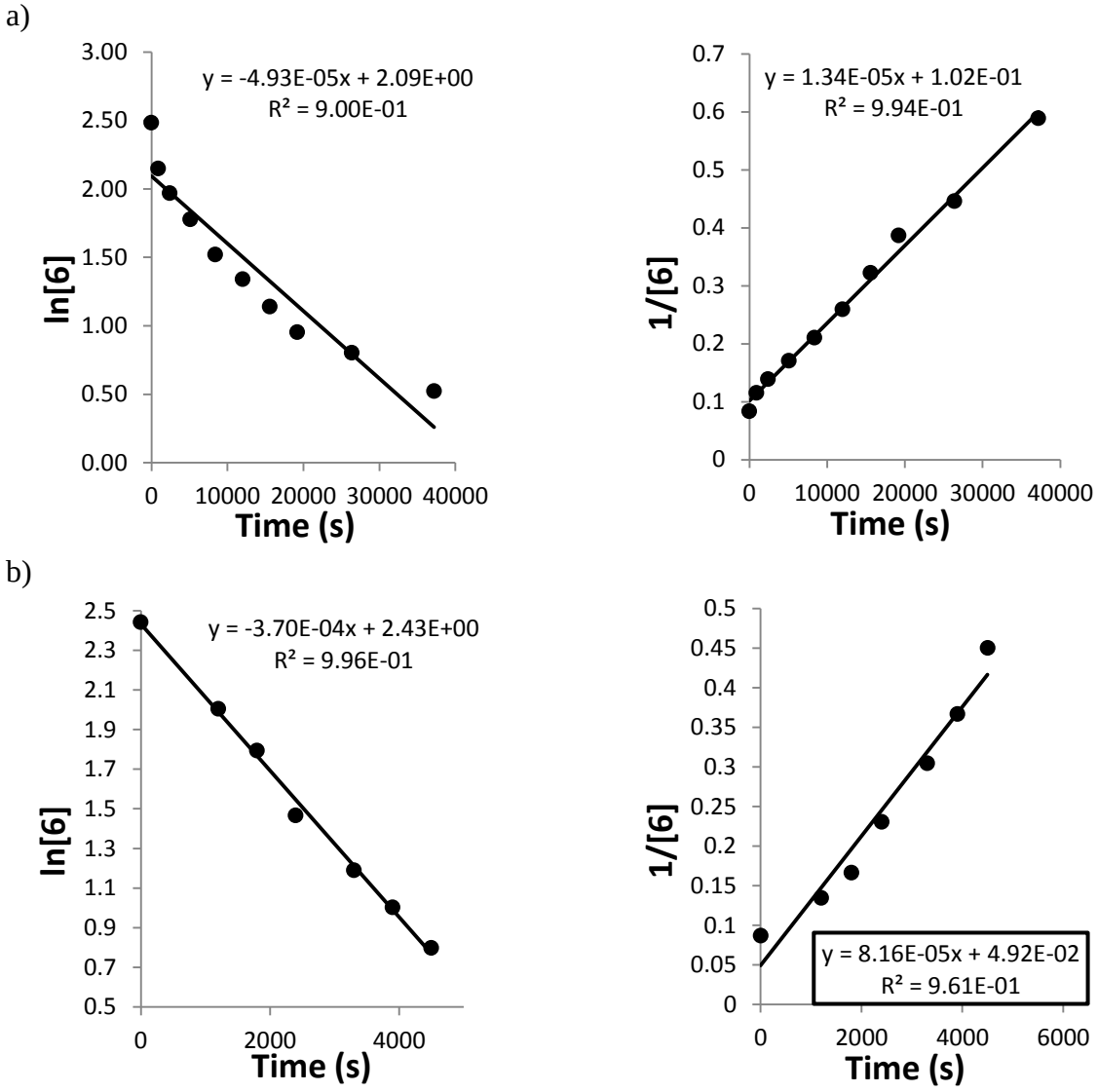

Figure 3.17. Coincidental pH dependent fit to a second-order kinetic expression: a) Apparent second-order fit of the reaction of **6** with O_2 in non-buffered D_2O (pD_{init} = 10.2, pD_{fin} = 12.4, $[\mathbf{6}]_{init}$ = 4 mM, pO_2 = 8.2 atm, T = 80 °C). b) First-order fit of the reaction of **6** with O_2 in buffered D_2O (100 mN boric acid/KOD buffered, pD = 10.2, $[\mathbf{6}]_{init}$ = 4 mM, pO_2 = 8.2 atm, T = 80 °C).

Due to the instability of dimethyl Pt^{II} complex **5** in water through protonolysis, aerobic oxidation of monomethyl **6** was prioritized. Not surprisingly, **5** can be oxidized under similar conditions as oxidation of **6**. Addition of H_2O_2 (0.17 mmol) to a CH_2Cl_2 solution of the dimethyl Pt^{II} complex **5** (0.01 mmol) resulted in clean oxidation to the C_s-symmetric isomer of the dimethyl Pt^{IV} complex, κ^3-$NNOPt^{IV}(CH_3)_2(OH)$ (**13**, Figure 3.18). Complex **13** was identified by single Pt-CH_3 resonance at 1.21

ppm with coupling to ^{195}Pt of 69.9 Hz that integrated to 6H against the NNO backbone supporting a higher symmetry than its isomer **11**. Crystals grown from DCM/Et_2O were suitable for analysis by X-ray crystallography (Figure 3.19). The carboxylate arm of NNO is coordinated to the Pt^{IV} center trans to a hydroxide while the two methyl groups are trans to the pyrazolyl resulting in an octahedral geometry. A mixture of **5** and **13** was detected by ^1H NMR spectroscopy after accidental exposure of a CH_2Cl_2 solution of **5** to air. Previous reports support rapid reaction of dimethyl Pt^{II} with O_2 but to eliminate competing protonolysis the oxidation is best performed in an aprotic solvent.[3]

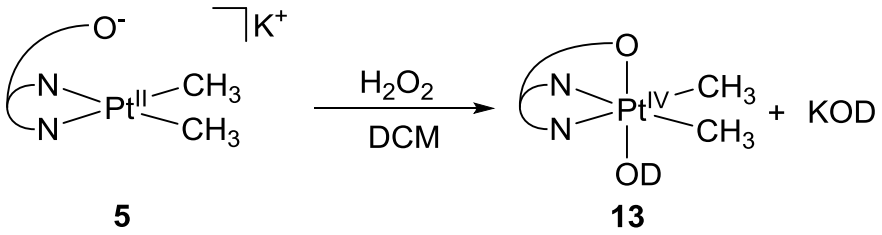

Figure 3.18. Oxidation of dimethyl $NNOPt^{II}$.

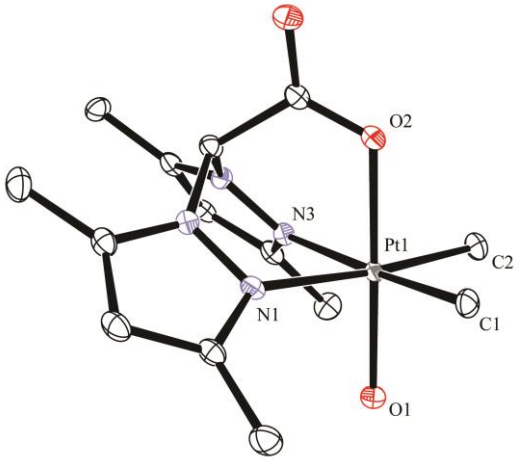

Figure 3.19. ORTEP of **13**. Displacement ellipsoids at the 50% probability level. Hydrogen atoms are excluded for clarity. Selected bond distances (Å) and angles (°):Pt1-C1 2.020(3), Pt1-C2 = 2.031(3), Pt1-N1 = 2.196(3), Pt1-N3 = 2.150(3), Pt1-O1 = 1.987(2), Pt1-O2 = 2.062(2), O2-C3 = 1.277(4), O3-C3 = 1.224(4), C_1-Pt-C_2 = 87.32(14), C_1-Pt-N_1 = 94.15(12), C_1-Pt-O_1 = 89.48(12), C_1-Pt-O_2 = 90.54(11).

Conclusions

Reaction of the monomethyl κ^2-NNO ligated Pt^{II} (**6**/**6**D^+) with dioxygen in D_2O resulted in direct oxidation yielding the monomethyl κ^3-NNO Pt^{IV} complex **10** in competition with a rare methyl transfer reaction to form the dimethyl κ^3-NNO Pt^{IV} complex **11**. The methyl transfer product is favored at high temperatures and high pD. A mechanism is proposed in which **6**/**6**D^+ reacts with O_2 in the rate-determining step to generate a hydroperoxo species $\mathbf{I_1}$. The reaction of **6** with oxygen is apparently faster than **6**D^+ as the reaction rate increases as pD approaches the pK_a of **6**D^+. Subsequent competition between the reaction of $\mathbf{I_1}$ with **6**/**6**D^+ and the isomerization to $\mathbf{I_2}$ controls the ratio of the observed Pt^{IV} products. Methyl transfer is proposed to occur between $\mathbf{I_2}$ and unreacted **6**/**6**D^+.

Oxidation by oxygen to produce Pt^{IV} methyl hydroxide complexes from Pt^{II} methyl species has potential application in methane to methanol catalysis,[1,2] and this κ^3-NNOPt work extends the generality and mechanistic understanding of such reactions.[3,4] The reactivity of the NNO system with O_2 was very slow relative to the Vedernikov system (dpms).[4] At pH 8 the half-life of oxidation of $NNOPt^{II}$ to $NNOPt^{IV}$ was 4 m in both our systems and the Vedernikov system. However, in the Vedernikov system the reaction was performed at 21 °C and 1 atm O_2 while our experiments was carried out at much higher temperature 80 °C and 3.4 atm of O_2. This result was unexpected as the more basic carboxylate arm, compared with a sulfonate group in dpms, would seem to make our NNO ligand better at coordinating to Pt^{II} and thereby oxidation to Pt^{IV}. The methyl groups on pyrazolyl rings and the resulting steric congestion around platinum are most likely the cause of the slow reaction with O_2 in the NNO system. Labinger and Bercaw demonstrated that steric bulk around platinum(II) tends to slow its reaction with O_2 and oxidation to platinum(IV).[3b]

The observed methyl group transfer to produce a Pt^{IV} dimethyl species upon oxidation of a Pt^{II} monomethyl with O_2 is highly unusual,[4b,c,7] and represents a reaction pathway that could have novel

applications, for example, in methane oligomerization.[8] C-H activation of methane at Pt^{II} to yield monomethyl Pt^{II} complexes is known[9] and C-C reductive elimination of ethane from Pt^{IV} is also a well-established reaction.[6] The knowledge gained from the studies described herein, particularly with respect to the dependence on pH and temperature, may be applicable to the development of methane functionalization catalysts using an environmentally benign oxidant and solvent (dioxygen and water).

Experimental

All air-free manipulations were performed in a N_2 glove box, or using a Schlenk or high vacuum line. Solvents were purified by passage through two columns of activated alumina in the case of THF and diethyl ether, and a column of activated alumina followed by a column of Q5 reactant in the case of benzene, pentane, and toluene. NMR solvents were obtained from Cambridge Isotope Laboratories. Benzene-d_6 and THF-d_8 were dried over Na/benzophenone then vacuum transferred prior to use. Chloroform-d_1 was dried over CaH_2 and vacuum transferred prior to use. NMR spectra were referenced from the residual protiated solvent signal and chemical shifts are reported in parts per million (ppm) from tetramethylsilane (TMS). KH was obtained as a suspension in oil and was purified by washing with pentane. All other chemicals were purchased from Sigma-Aldrich or Fisher Scientific and were used as received. pH/pD measurements were obtained using a Hach company ISFET pH Stainless Steel NMR Tube Probe calibrated using phosphate buffered H_2O solutions of pH 4, 7 and 10 from EMD Millipore. Readings from pH meter of D_2O solutions are reported as pD. Elemental analyses were performed by the CENTC Elemental Analysis Facility at the University of Rochester.

***C*$_1$-symmetric κ^3-NNOPt^{IV}(CH$_3$)(OH)$_2$ (10).** A Teflon valve-sealed medium-walled round-bottom flask was charged with **5** (550 mg, 1.08 mmol) and 5 mL of N_2-sparged H_2O. The container was sealed under an atmosphere of N_2 and heated at 40 °C for 24 h. The solution was filtered and 30% H_2O_2 (170 μL, 1.62 mmol) was added. After stirring under air for 1 h, the water was removed under low pressure.

The resulting light orange solid was dissolved in methanol and filtered through 1 inch of alumina in a pipette fitted with a small piece of glass wool. The methanol was removed under vacuum giving a faint yellow solid which was dissolved in a 5 mL of H_2O. Crystals were grown from the resulting solution by slow evaporation at room temperature. Yield: 340 mg (64%). ^{1}H NMR (300 MHz, D_2O, 298 K): δ 2.41 (s, 3H, CH_3), 2.42 (s, 3H, CH_3), 2.48 (s, $^2J_{Pt-H}$ = 72.4 Hz, 3H, CH_3), 2.50 (s, 3H, CH_3), 2.53 (s, 3H, CH_3), 6.25 (s, 1H, H_{pz}), 6.27 (s, 1H, H_{pz}), 6.86 (s, 1H, CH). ^{13}C NMR (500 MHz, D_2O, 298 K): δ 1.63 ($^1J_{Pt-C}$ = 547 Hz), 10.02, 10.67, 11.62, 11.97, 109.76, 143.35, 145.01, 152.89, 153.65, 167.35. Anal. Calcd for $C_{13}H_{20}N_4O_4Pt$: C, 31.8; H, 4.1; N, 11.4. Found: C, 31.0; H, 3.9; N, 10.9.

***C*$_1$-κ^3-NNOPt^{IV}(CH$_3$)$_2$OH (11).** A 25 mL round bottom flask was charged with complex **6** (500 mg, 0.974 mmol) and 10 mL THF. Methyl iodide (99.5%, 300 μL, 2.92 mmol) was added and the reaction mixture was stirred for 1 h. A precipitate from the reaction was collected, washed with 3 mL x 3 THF and then dissolved in CH_2Cl_2 and filtered. The volatiles were removed under low pressure leaving a light yellow solid. Colorless crystals were grown by diffusion of diethyl ether into a solution of methanol. Yield: 326 mg (65 %). ^{1}H NMR (300 MHz, D_2O, 298 K): δ 1.75 (s, $^2J_{Pt-H}$ = 69.8 Hz, 3H, CH_3), 2.01 (s, $^2J_{Pt-H}$ = 76.7Hz, 3H, CH_3), 2.50(s, 3H, CH_3), 2.48 (s, 3H, CH_3), 2.36 (s, 3H, CH_3), 2.30 (s, 3H, CH_3), 6.22 (s, 1H, H_{pz}), 6.21 (s, 1H, H_{pz}), 6.65 (s, 1H, CH). ^{13}C NMR (500 MHz, D_2O, 298 K): δ -11.20 ($^1J_{Pt-C}$ = 659 Hz), -6.65 ($^1J_{Pt-C}$ = 627 Hz), 8.03, 8.71, 9.95, 10.73, 64.6, 106.68, 107.68, 140.61, 142.09, 150.22, 151.59, 169.08. Anal. Calcd for $C_{14}H_{22}N_4O_3Pt$: C, 34.4; H, 4.5; N, 11.4. Found: C, 34.3; H, 4.4; N, 11.2.

κ^3-NNOPt^{IV}(OH)$_3$ (12). A sample of **6** (100 mg, 0.19 mmol) was dissolved in 6 mL of N_2-sparged H_2O. Five drops of 50% H_2O/HBF_4 were added and the reaction was heated in a Teflon cap sealed NMR tube at 60 °C for 24 h (complete conversion to **7** by ^{1}H NMR spectroscopy). 1M KOH was added until the solution was at near neutral pH by litmus paper then 30% H_2O_2 (1 mL) was added. Complete conversion to **12** was observed by ^{1}H NMR spectroscopy. ^{1}H NMR (300 MHz, D_2O, 298 K): δ 2.55 (s,

6H, CH_3), 2.59 (s, 6H, CH_3), 6.33 (s, 2H, H_{pz}), 7.05 (s, 1H, CH). ^{13}C NMR (500 MHz, D_2O, 298 K): δ 10.55, 11.71, 110.02, 145.65, 154.38, 154.41, 165.69, 166.99.

Determination of pKa for $6D^+$. Complex **6** (5.2 mg, 0.010 mmol) was dissolved in 2.0 mL of N_2-sparged D_2O under N_2. A 50 mM KOD solution was prepared by dissolving KOH (6.6 mg, 0.118 mmol) in 2.4 mL N_2-sparged D_2O. The KOD solution was added drop-wise to the solution of **6** to a pD of 11.3. A 50 mM H_2SO_4 solution was prepared by addition of 2.8 μL of conc. H_2SO_4 to 1.0 mL of N_2-sparged D_2O. The dilute H_2SO_4 solution was then added in measured aliquots while monitoring changes in pD (Figure 3.2a). Upon complete conversion of **6** to $\mathbf{6}D^+$ the change in pD was monitored while adding measured aliquots of the dilute KOH solution (Figure 3.2b).

Reaction of aqueous 6 with O_2. An 8 mM stock solution of **6** was prepared under an atmosphere of N_2 by dissolving in **6** (26.8 mg, 0.052 mmol) 6.5 mL of N_2-sparged D_2O with dioxane (0.1 μL, int. std.). Samples were made 4 mM in **6** by addition of 0.375 mL of the 8 mM stock solution to 0.375 mL D_2O. These diluted solutions were found to have a pD of 10 (measured in air). The solutions were transferred to Teflon cap sealed NMR tubes and then frozen. The solutions were degased by 3 successive freeze/pump/thaw cycles then pressurized with O_2 (30 - 120 p.s.i.) while frozen in a dry ice bath. The frozen solution was rapidly thawed in a 25 °C water bath then placed in a preheated oil bath (40 - 80 °C) or left to react at room temperature. At timed intervals the NMR tube was removed from the oil bath, rapidly cooled in a 25 °C water bath (10s) and then examined by ^1H NMR spectroscopy. This procedure was repeated until **6** was no longer detectable by ^1H NMR spectroscopy.

Reaction of 6 and O_2 with added KOH. A reaction sample that is 4 mM in KOH was prepared by combining a 0.375 mM aliquot of the 8 mM stock solution of **6**, 0.1875 mL D_2O and 0.1875 mL of a 16 mM stock solution of KOH. The reaction was then followed at T = 80 °C by H NMR spectroscopy similar to the method described above.

Kinetic studies for the reaction of 6 with O_2.

pD = 11.2. A 20 mM stock solution of **6** was prepared by dissolving **6** (16.5 mg, 0.032 mmol) in 1.6 mL D_2O and dioxane (0.1 μL, int. std.). A 50 mM boric acid buffer was prepared by dissolving boric acid (31.1 mg, 0.503 mmol) in 8.87 mL D_2O with dioxane (0.1 μL, int. std.). The solution was made basic by the addition of 1.13 mL of a 490 mM KOH solution. 4 mM solutions of **6** were prepared by combining 0.08 mL of the 20 mM stock solution of **6** and 0.32 mL of the 50 mM boric acid stock solution giving a pD of 11. The solutions were transferred to Teflon cap sealed NMR tubes, degassed, pressurized with O_2, heated at 80 °C and followed by ^{1}H NMR spectroscopy as described above. Upon complete conversion of **6** as determined by ^{1}H NMR spectroscopy, the sample was heated at 80 °C for an additional 20 h with no change in the product distribution (**7**: 7%, **12**: 7%). An NMR spectrum taken 5 h after the addition of 1.2 μL of ~10 M H_2O_2 at room temperature showed conversion of **7** (0%) to **12** (14%). See Figure 3.17 for fits of the data to the 1st order kinetics with respect to [**6**].

pD = 6.5. A buffer system that was 100 mM in phosphoric acid and boric acid was prepared by combining 85% H_3PO_4 (67.6 μL, 1.00 mmol) and $B(OH)_3$ (62 mg, 1.05 mmol). D_2O was added to 10 mL total. A 50 mM in phosphoric acid and boric acid buffer at the appropriate pD was made by adding 81 μL of 1.5 M KOH/D_2O (0.842 g/15 mmol KOH diluted to 10 mL with D_2O) to 1 mL of the 100 mM stock solution then D_2O was added to a total volume of 2 mL (pD = 6.14). Complex **6** (1.8 mg, 0.0035 mmol) was dissolved in 876 μL of buffer resulting in a pD of 6.5. The reaction of **6** with O_2 was carried out as described above. See Figure 3.12 for fits of the data to the 1st and 2nd order kinetics with respect to [**6**].

pD = 8.5. 155 μL of 1.5 M KOH/D_2O was added to 1 mL of the 100 mM stock solution (see above) then D_2O was added to a total volume of 2 mL (pD = 8.24). Complex **6** (1.92 mg, 0.0037 mmol) was dissolved in 935 μL of 50 mM phosphoric acid and boric acid buffer resulting in a pD of 8.5. The

reaction of **6** with O_2 carried out as described above. See Figure 3.13 for fits of the data to the 1st and 2nd order kinetics with respect to [**6**].

Attempted kinetics under non-buffered conditions. A 12 mM solution of **6** (25 mg, 0.049 mmol) in D_2O (4.0 mL) was heated at 80 °C under 8.2 atm O_2. The reaction was followed by ^1H NMR spectroscopy until nearly complete conversion of **6** (99%). Over the course of the reaction the pD changed from 10.2 to 12.4. The data from this reaction shows a best-fit to 2nd order kinetics (Figure 3.17). However, this fit to 2nd order kinetics is likely fortuitous due to slowing of the reaction with increasing pD (i.e. coincidental fit to 2nd order kinetics). Supporting this conclusion is that when the reaction was repeated under nearly identical conditions but using a 100 mM boric acid/D_2O buffered solution that was adjusted to pD = 10.2 by the addition of KOH, the data clearly fit best to 1st order kinetics with respect to [**6**] (Figure 3.17).

Methyl Transfer Studies

Demonstration that methyl transfer does not occur between complexes 6 and 10. Complexes **6** (1.2 mg, 0.002 mmol) and **10** (1.0 mg, 0.002 mmol) were dissolved in 0.27 mL N_2-sparged D_2O with 0.03 mL of 40 mM KOH/D_2O (Figure 3.20). The sample was heated in a Teflon cap sealed NMR tube at 80 °C for 14 h and monitored by ^1H NMR spectroscopy. After heating, 95% of **6** (0.00189 mmol) and 99% of **10** (0.00198 mmol) remained unchanged.

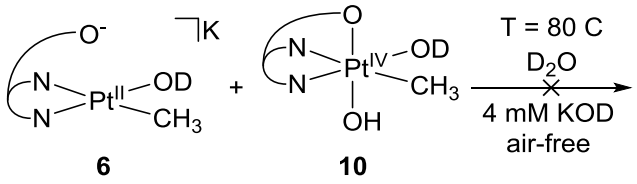

Figure 3.20. No methyl transfer observed between **6** and 10.

Methyl transfer between 6-d_5 and 11. Complex **5** (5.4 mg, 0.0102 mmol) was dissolved in 0.75 mL N_2-sparged D_2O and heated in a Teflon cap sealed NMR tube at 80 °C for 24 h to yield a **6**-d_5. Under an N_2 atmosphere, 5.2 mg of **11** (0.0106 mmol) and 0.075 mL of N_2-sparged 40 mM KOH/D_2O were

added to the solution of **6**-d_5. The sample was then heated at 80 °C and monitored by ^{1}H NMR spectroscopy (Figure 3.21). After 1.5 h the Pt^{II}-CH_3 signal (δ = 0.69 ppm) associated with **6** appeared supporting the production of **6** (6.6 μmol) due to the conversion of 19% of **6**-d_5 to **6**. A closely matching decrease (8.5%) of the integration of the two Pt^{IV}-CH_3 signals (δ = 1.75 and 1.99 ppm) associated with **11** was observed. The ratio of [**6** + **6**-d_5] : [**11**+ **11**-d_5] was unchanged based on a comparison of the aromatic protons in the NNO ligand.

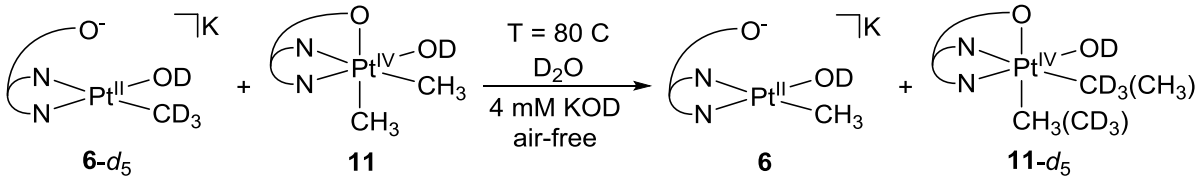

Figure 3.21. Methyl transfer observed between deuterium labelled **6** and **11**.

Crystallographic characterization of compound 10

A colorless prism, measuring 0.17 x 0.06 x 0.05 mm^3 was mounted on a glass capillary with oil. Data was collected at -163°C on a Bruker APEX II single crystal X-ray diffractometer, Mo-radiation. Crystal-to-detector distance was 40 mm and exposure time was 10 seconds per degree for all sets. The scan width was 0.5°. Data collection was 99.5% complete to 33.32° and 100% complete to 25° in ϑ. A total of 33805 (merged) reflections were collected covering the indices, h = -12 to 12, k = -15 to 15, l = -15 to 15. 5683 reflections were symmetry independent and the R_{int} = 0.0256 indicated that the data was brilliant (average quality 0.07). Indexing and unit cell refinement indicated a triclinic P lattice. The space group was found to be P $\bar{1}$ (No.2). The data was integrated and scaled using SAINT, SADABS within the APEX2 software package by Bruker.[10] Solution by direct methods (SHELXS, SIR97[11]) produced a complete heavy atom phasing model consistent with the proposed structure. The structure was completed by difference Fourier synthesis with SHELXL97.[12,13] Scattering factors are from Waasmair and Kirfel[14]. Hydrogen atoms were placed in geometrically idealized positions and constrained to ride on their parent atoms with C---H distances in the range 0.95-1.00 Angstrom.

Isotropic thermal parameters U_{eq} were fixed such that they were $1.2U_{eq}$ of their parent atom U_{eq} for CH's and $1.5U_{eq}$ of their parent atom U_{eq} in case of methyl groups. All non-hydrogen atoms were refined anisotropically by full-matrix least-squares. The hydrogen of O1 has no immediate acceptor, however the hydrogen is found in the plane through O1, O2 and Pt1, as close to O2 as possible within the restriction of being a hydroxyl hydrogen atom.

Table 3.3. Crystallographic data for **10**.

Parameter	**10**
Empirical formula	C13 H20 N4 O4 Pt
Formula weight	491.42
Temperature	110(2) K
Wavelength	0.71073 Å
Crystal system	Triclinic
Space group	P -1
Unit cell dimensions	a = 8.0081(2) Å, α= 78.2810(10)° b = 9.9680(2) Å, β= 69.1000(10)° c = 10.1253(2) Å, γ = 88.7940(10)°
Volume	738.16(3) $Å^3$
Z	2
Density (calculated)	2.211 Mg/m^3
Absorption coefficient	9.529 mm^{-1}
F(000)	472
Crystal size	0.17 x 0.06 x 0.05 mm^3
Theta range for data collection	2.09 to 33.32°.
Index ranges	-12<=h<=12, -15<=k<=15, -15<=l<=15
Reflections collected	33805
Independent reflections	5683 [R(int) = 0.0256]
Completeness to theta = 25.00°	100.0 %
Max. and min. transmission	0.6473 and 0.2942
Refinement method	Full-matrix least-squares on F^2
Data / restraints / parameters	5683 / 0 / 206
Goodness-of-fit on F^2	1.105

Final R indices [I>2sigma(I)]	R1 = 0.0132, wR2 = 0.0310
R indices (all data)	R1 = 0.0145, wR2 = 0.0313
Largest diff. peak and hole	1.062 and -1.464 e.Å^{-3}

Crystallographic characterization of compound 11

A colorless prism, measuring 0.15 x 0.14 x 0.13 mm^3 was mounted on a glass capillary with oil. Data was collected at -163^{o}C on a Bruker APEX II single crystal X-ray diffractometer, Mo-radiation. Crystal-to-detector distance was 40 mm and exposure time was 10 seconds per degree for all sets. The scan width was 0.5^o. Data collection was 100% complete to 25^o in ϑ. A total of 68113 (merged) reflections were collected covering the indices, h = -15 to 15, k = -16 to 16, l = -19 to 19. 5111 reflections were symmetry independent and the R_{int} = 0.0300 indicated that the data was brilliant (average quality 0.07). Indexing and unit cell refinement indicated primitive monoclinic lattice. The space group was found to be P 2_1/n (No.14). The data was integrated and scaled using SAINT, SADABS within the APEX2 software package by Bruker.[10] Solution by direct methods (SHELXS, SIR97[11]) produced a complete heavy atom phasing model consistent with the proposed structure. The structure was completed by difference Fourier synthesis with SHELXL97.[12,13] Scattering factors are from Waasmair and Kirfel[14]. Hydrogen atoms were placed in geometrically idealized positions and constrained to ride on their parent atoms with C---H distances in the range 0.95-1.00 Angstrom. Isotropic thermal parameters U_{eq} were fixed such that they were 1.2U_{eq} of their parent atom U_{eq} for CH's and 1.5U_{eq} of their parent atom U_{eq} in case of methyl groups. All non-hydrogen atoms were refined anisotropically by full-matrix least-squares. The water is hydrogen bonding to the acetates of two molecules, the hydroxyl hydrogen bonds to the water.

Table 3.4. Crystallographic data for **11**.

Parameter	**11**
Empirical formula	C14 H24 N4 O4 Pt

Formula weight	507.46
Temperature	110(2) K
Wavelength	0.71073 Å
Crystal system	Monoclinic
Space group	P 1 21/n 1
Unit cell dimensions	a = 10.6758(4) Å, α= 90° b = 11.4708(5) Å, β= 103.510(2)° c = 13.9846(5) Å, γ = 90°
Volume	1665.17(11) $Å^3$
Z	4
Density (calculated)	2.024 Mg/m^3
Absorption coefficient	8.452 mm^{-1}
F(000)	984
Crystal size	0.15 x 0.14 x 0.13 mm^3
Theta range for data collection	2.17 to 30.60°.
Index ranges	-15<=h<=15, -16<=k<=16, -19<=l<=19
Reflections collected	68113
Independent reflections	5111 [R(int) = 0.0300]
Completeness to theta = 25.00°	100.0 %
Max. and min. transmission	0.4062 and 0.3637
Refinement method	Full-matrix least-squares on F^2
Data / restraints / parameters	5111 / 0 / 214
Goodness-of-fit on F^2	1.036
Final R indices [I>2sigma(I)]	R1 = 0.0170, wR2 = 0.0400
R indices (all data)	R1 = 0.0213, wR2 = 0.0417
Largest diff. peak and hole	1.271 and -0.885 $e.Å^{-3}$

Crystallographic characterization of compound 13

A colorless prism, measuring 0.15 x 0.14 x 0.13 mm^3 was mounted on a glass capillary with oil. Data was collected at -163°C on a Bruker APEX II single crystal X-ray diffractometer, Mo-radiation. Crystal-to-detector distance was 40 mm and exposure time was 10 seconds per degree for all sets. The scan width was 0.5°. Data collection was 100% complete to 25° in ϑ. A total of 68113 (merged)

reflections were collected covering the indices, h = -15 to 15, k = -16 to 16, l = -19 to 19. 5111 reflections were symmetry independent and the R_{int} = 0.0300 indicated that the data was brilliant (average quality 0.07). Indexing and unit cell refinement indicated primitive monoclinic lattice. The space group was found to be P 2_1/n (No.14). The data was integrated and scaled using SAINT, SADABS within the APEX2 software package by Bruker.[10] Solution by direct methods (SHELXS, SIR97[11]) produced a complete heavy atom phasing model consistent with the proposed structure. The structure was completed by difference Fourier synthesis with SHELXL97.[12,13] Scattering factors are from Waasmair and Kirfel[14]. Hydrogen atoms were placed in geometrically idealized positions and constrained to ride on their parent atoms with C---H distances in the range 0.95-1.00 Angstrom. Isotropic thermal parameters U_{eq} were fixed such that they were 1.2U_{eq} of their parent atom U_{eq} for CH's and 1.5U_{eq} of their parent atom U_{eq} in case of methyl groups. All non-hydrogen atoms were refined anisotropically by full-matrix least-squares. The water is hydrogen bonding to the acetates of two molecules, the hydroxyl hydrogen bonds to the water.

Table 3.5. Crystallographic data for **13**.

Parameter	**13**
Empirical formula	C14 H24 N4 O4 Pt
Formula weight	507.46
Temperature	110(2) K
Wavelength	0.71073 Å
Crystal system	Monoclinic
Space group	P 1 21/n 1
Unit cell dimensions	a = 10.6758(4) Å, α= 90° b = 11.4708(5) Å, β= 103.510(2)° c = 13.9846(5) Å, γ = 90°
Volume	1665.17(11) $Å^3$
Z	4
Density (calculated)	2.024 Mg/m^3
Absorption coefficient	8.452 mm^{-1}

F(000)	984
Crystal size	0.15 x 0.14 x 0.13 mm^3
Theta range for data collection	2.17 to 30.60°.
Index ranges	-15<=h<=15, -16<=k<=16, -19<=l<=19
Reflections collected	68113
Independent reflections	5111 [R(int) = 0.0300]
Completeness to theta = 25.00°	100.0 %
Max. and min. transmission	0.4062 and 0.3637
Refinement method	Full-matrix least-squares on F^2
Data / restraints / parameters	5111 / 0 / 214
Goodness-of-fit on F^2	1.036
Final R indices [I>2sigma(I)]	R1 = 0.0170, wR2 = 0.0400
R indices (all data)	R1 = 0.0213, wR2 = 0.0417
Largest diff. peak and hole	1.271 and -0.885 e.$Å^{-3}$

[1] (a) Shilov, A. E.; Shulpin, G. B. *Russ. Chem. Rev.* **1987**, *56*, 442. (b) Shilov, A. E.; Shul'pin, G. B. *Activation and Catalytic Reactions of Saturated Hydrocarbons in the Presence of Metal Complexes*; Kluwer Academic Publishers: Boston, 2000.

[2] (a) Periana, R. A.; Douglas, R. J.; Taube, D. J.; Gamble, S.; Taube, H.; Satoh, T.; Fujii, H. *Science* **1998**, *280*, 560. (b) Mironov, O. A.; Bischof, S. M.; Konnick, M. M.; Hashiguchi, B. G.; Ziatdinov, V. R.; Goddard, W. A.; Ahlquist, M.; Periana, R. A. *J. Am. Chem. Soc*. **2013**, *135*, 14644.

[3] (a) E. M. Prokopchuk, H. A. Jenkins and R. J. Puddephatt, Organometallics, **1999**, *18*, 2861. (b) Rostovtsev, V. V.; Lasseter, T. L.; Goldberg, K. I.; Labinger, J. A.; Bercaw, J. E. *Organometallics* **1998**, *17*, 4530. (c) Rostovtsev, V. V; Henling, L. M.; Labinger, J. A.; Bercaw, J. E. *Inorg. Chem.* **2002**, *41*, 3608.

[4] (a) Binfield, S. A.; Zavalij, P. Y.; Khusnutdinova, J. R.; Vedernikov, A. N. *J. Am. Chem. Soc.* **2006**, 1*28*, 82. (b) Liu, W. G.; Sberegaeva, A. V.; Nielsen, R. J.; Goddard, W. A.; Vedernikov, A. N. *J. Am. Chem. Soc*. **2014**, *136*, 2335 (c) Sberegaeva, A. V.; Liu, W. G.; Nielsen, R. J.; Goddard, W. A.; Vedernikov, A. N. *J. Am. Chem. Soc*. **2014**, *136*, 4761

[5] Wick, D. D.; Goldberg, K. I. *J. Am. Chem. Soc.* **1999,** *121*, 11900

[6] Grice, K. A.; Scheuermann, M. L.; Goldberg, K. I. *Top. Organomet. Chem.* **2011**, *35*, 1 and references therein

[7] (a) Khusnutdinova, J. R.; Rath, N. P.; Mirica, L. M. *J. Am. Chem. Soc.* **2010**, *132*, 7303. (b) Khusnutdinova, J. R.; Rath, N. P.; Mirica, L. M. *J. Am. Chem. Soc.* **2012**, *134*, 2414.

[8] Lanci, M. P.; Remy, M.S.; Lao, D. B.; Sanford, M. S.; Mayer, J. M. *Organometallics* **2011**, *30*, 3704 and references therein.

[9] (a) Stahl, S. S.; Labinger, J. A.; Bercaw, J. E. *Angew. Chem. Int. Ed*. **1998**, *37*, 2180 (b) Labinger, J. A.; Bercaw, J. E. *Nature* **2002**, *417*, 507. (c) Fekl, U.; Goldberg, K. I. *Adv. Inorg. Chem*. **2003**, *54*, 259. (d) Lersch, M.; Tilset, M. *Chem. Rev.* **2005**, *105*, 2471. (e) Vedernikov, A. N. *Chem. Commun.* **2009**, *32*, 4781.

[10] Bruker (**2007**) APEX2 (Version 2.1-4), SAINT (version 7.34A), SADABS (version 2007/4), BrukerAXS Inc, Madison, Wisconsin, USA.

[11] (a) Altomare, A.; Burla, C.; Camalli M.; Cascarano L.; Giacovazzo C.; Guagliardi A.; Moliterni A.G.G.; Polidori G.; Spagna R. J. Appl. Cryst. 1999, **32**, 115-119; (b) Altomare, A., Cascarano, G., Giacovazzo, C., Guagliardi, A., J. Appl. Cryst. 1993, **26**, 343.
[12] Sheldrick, G. M. SHELXL-97: Program for the Refinement of Crystal Structures 1997 University of Gottingen, Germany.
[13] Mackay, S.; Edwards, C.; Henderson, A.; Gilmore, C.; Stewart, N.; Shankland, K.; Donald, A.; *MaXus: a computer program for the solution and refinement of crystal structures from diffraction data*. University of Glasgow, Scotland, 1997.
[14] Waasmaier, D.; Kirfel, A. Acta Crystallogr. A. 1995, **51**, 416.

Chapter 4 : Reductive elimination of methanol from monomethylhydroxo platinum(IV)

Introduction

Reductive elimination is often the key product release step in homogeneous catalysis driven by late transition metals. Of particular interest are reductive eliminations that generate new carbon-heteroatom bonds. The formation of a C-O bond through reductive elimination of a methyl group from a metal center is a particularly important as it is the proposed final step in catalytic oxidations of methane to methanol (Figure 1.2).[1] In general, the results of studies of carbon-heteroatom reductive elimination reactions from Pt^{IV} complexes are consistent with a common mechanism, dissociation of the anionic heteroatom group (e.g. OH^-) followed by nucleophilic attack at a methyl group on the Pt^{IV} five-coordinate cationic intermediate (Figure 4.1).[2] Notable in these proposed mechanisms is that nucleophilic attack of the heteroatom group occurs on the Pt^{IV}-CH_3 group trans to an open site on the metal center, such that the leaving group is a square planar Pt^{II} species.[3] Thus, the mechanism is similar to the microscopic reverse C-I oxidative addition of methyl iodide to the square-planar Ir^I Vaska's complex ($IrCl(CO)[P(C_6H_5)_3]_2$).[3]

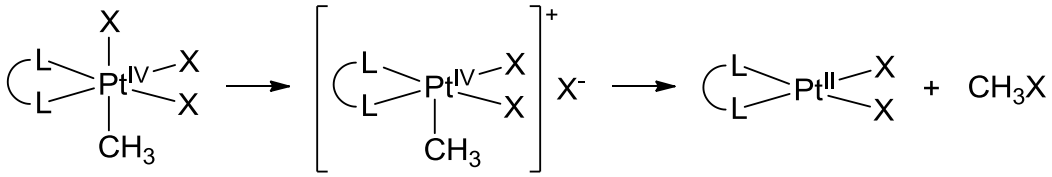

Figure 4.1. C-X coupling from Pt^{IV}.[2]

This mechanism of nucleophilic attack on a Pt^{IV} methyl group was proposed by Vedernikov for the reductive elimination of methanol from $(dpms)Pt^{IV}(CH_3)(OH)_2$ (dpms = di(2-pyridyl)methanesulfonate) in aqueous solution.[4] Notable in this system is the hemilabile character of the tridentate ligand dpms. Isomerization of the monomethyl Pt^{IV} complex (**10_V**, Figure 4.2), orienting the Pt^{IV}-CH_3 group trans to the sulfonate oxygen, was shown to occur prior to S_N2 attack on the methyl by H_2O (Figure 4.2). The isomerization was proposed to occur via dissociation of the sulfonate group and rearrangement of the five-coordinate intermediate. Kinetic studies revealed that the isomerization was inhibited by the addition of acid to the solution (Figure 4.3).[4b] It was proposed that decreased pH led to protonation of the hydroxide ligands generating cationic species which, in turn, disfavored dissociation of the negatively charged sulfonate group. In contrast, the rate of S_N2 step was found to increase with increasing $[H^+]$ as nucleophilic attack at a protonated cationic complex is favored. Ultimately, sulfonate group dissociation and nucleophilic attack by water on the Pt^{IV} methyl group produces methanol and a square-planar Pt^{II} product.

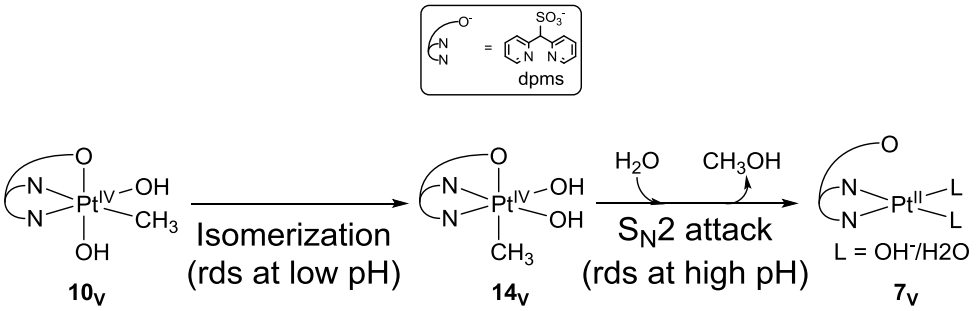

Figure 4.2. Two-step reductive elimination in dpms system.[4b]

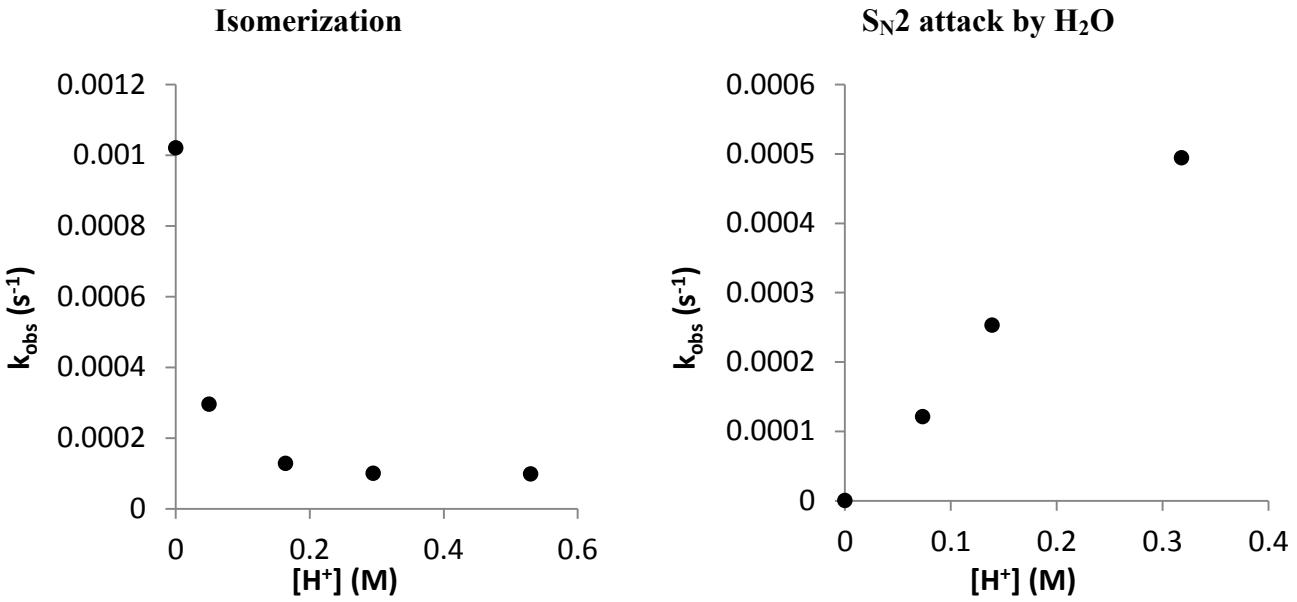

Figure 4.3. Isomerization of $\mathbf{10_V}$ to $\mathbf{14_V}$ at T = 94 °C with added HBF_4 (0 – 0.53 M). C-O coupling from $\mathbf{14_V}$ producing $\mathbf{7_V}$ and methanol at T = 65.5 °C with added HBF_4 (0 – 0.32 M).[4b] Reprinted with permission from: Khusnutdinova, J. R.; Zavalij, P, Y.; Vedernikov, A. N. *Organometallics* **2007**, *26*, 3466. Copyright 2007 American Chemical Society.

The hemilability of the sulfonate group in the dpms system plays a significant role in the C-O reductive elimination reaction. Dissociation of this group is involved in both the isomerization and in the C-O bond forming step. Aside from potential environmental benefits, using water as the solvent allows for the use of pH to control reactivity. In the case of reductive elimination of methanol from **10v**, controlling reactivity by altering the pH is challenging as the isomerization and S_N2 attack steps respond differently to [H+]. Perhaps the isomerization step could be accelerated if protonation occurred at the sulfonyl group bound to Pt^{IV} thereby weakening the SO_3-Pt^{IV} bond. Protonation of the sulfonyl would likely require extremely acidic conditions (e.g. fuming sulfuric acid) because the sulfonate moiety is a

relatively weak base (pKa of methanesulfonic acid (H_2O) = -1.9 at 25 ^oC)[5] and thus the ability to control its lability with pH is limited.

Herein is described an aqueous platinum system with a facially coordinating NNO ligand containing a carboxylate hemilabile arm (NNO = bis(3,5-dimethylpyrazol-1-yl)-acetate (**1**)).[6] The stronger base functionality (pK_a of acetic acid (H_2O) = 4.76 at 25 ^oC)[7] might allow for better control of the hemilability of the facially coordinating ligand with pH. In particular, if protonation were to occur at the carboxylate oxygen bound to Pt^{IV} this would likely weaken the Pt^{IV}-O bond. Also, the dissociated arm should be a neutral acid removing the charge separation problem proposed by Vedernikov (Figure 4.4). In this contribution, we report C-O reductive elimination from a κ^3-NNO *carboxylate* ligated monomethyl platinum(IV) complex. Significant differences in reactivity were observed under acidic and basic conditions. To facilitate presentation, the results of thermolysis under these different conditions will be addressed separately.

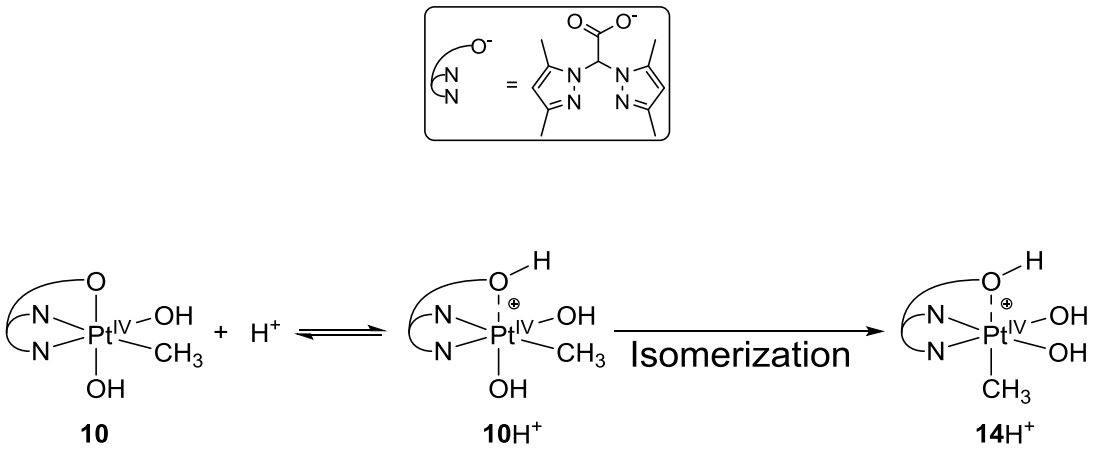

Figure 4.4. Proposed acceleration of isomerization at low pH due to protonation of Pt^{IV} bound hemilabile arm.

Part I. Reductive elimination of methanol from (NNO)$Pt^{IV}(CH_3)(OH)_2$ (10) in alkaline solution

Results and Discussion

When a sample of the Pt^{IV} complex **10** was dissolved in D_2O (9 mM), the pD of the solution was measured to be significantly alkaline (pD = 9.8). The high pD of the solution is likely the result of protonation of **10** to **10**D^+ (pK_a: 7.3 ± 0.1) by the solvent (Figure 4.5). The exact location of the added deuteron cannot be determined so addition to the Pt-OD in **10** rather than the carboxylate bound to Pt in **10** is arbitrary, After heating the solution of **10** at 140 ^oC for 1 h, examination by ^1H NMR spectroscopy indicated that, along with unreacted **10** (*ca*. 80% remained)**,** the solution contained 7% of the dimethyl Pt^{IV} complex **11** (Figure 4.6). Complex **11** was identified in the ^1H NMR spectrum by signals due to the Pt^{IV}-CH_3 groups at 2.01ppm ($^2J_{Pt\text{-}H}$ = 78.7 Hz) and 1.76 ppm ($^2J_{Pt\text{-}H}$ = 70.4 Hz). The reaction mixture also contained an equivalent amount (6%) of the demethylated Pt^{II} species **7**, characterized by a ^1H NMR signal at 6.08 ppm attributed to a pyrazolyl bound hydrogen atom (Figure 4.6). Additionally, the C_s-symmetric isomer of **10**, complex **14** (9%, Figure 4.6), was identified by a Pt^{IV}-CH_3 signal at 2.73 ppm ($^2J_{Pt\text{-}H}$ = 76 Hz). Although methanol was eventually produced after heating at higher temperature (165 °C, see below) no methanol was produced after one hour at 140 °C.

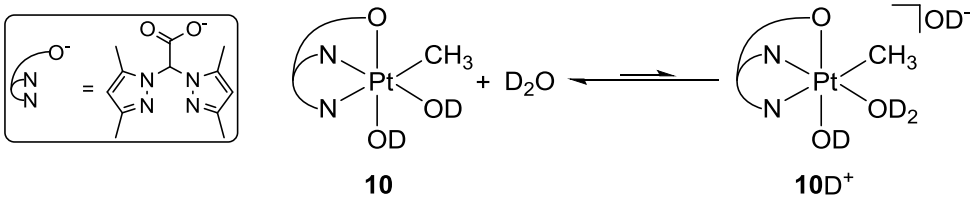

10 **10**D^+

Figure 4.5. Production of OD^- upon dissolution of **10** in D_2O.

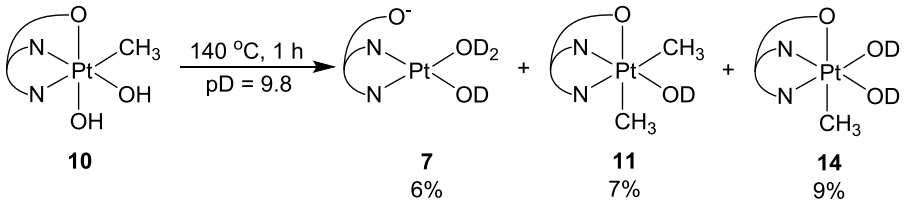

10 **7** 6% **11** 7% **14** 9%

Figure 4.6. Thermolysis of *ca*. 20% of **10** in D_2O.

To increase the rate of the reaction, the temperature was increased to 165 °C. The change in the concentration of the products **7, 11**, **14** and methanol over the course of the reaction is shown in Figure 4.7. Heating at 165 °C for 1 h resulted in an increase in the [**14**], to 32% of the initial [**10**]. Subsequent heating (165 °C) saw a decrease in [**14**] until it was no longer detectable after 7 h during which the concentration of methanol had increased to a maximum yield of 24% (Figure 4.7, See Experimental for discussion of low methanol yields). The concentration of **11** reached a maximum yield of 16% at 5.5 h then decreased to 1% after an additional 14 days of heating with no observed production of ethane. Dimerization of **7** to both **8** and **9** was observed over time (see Chapter 2: Figure 2.7 and Figure 2.10) with some black solid observed near the end of the reaction.

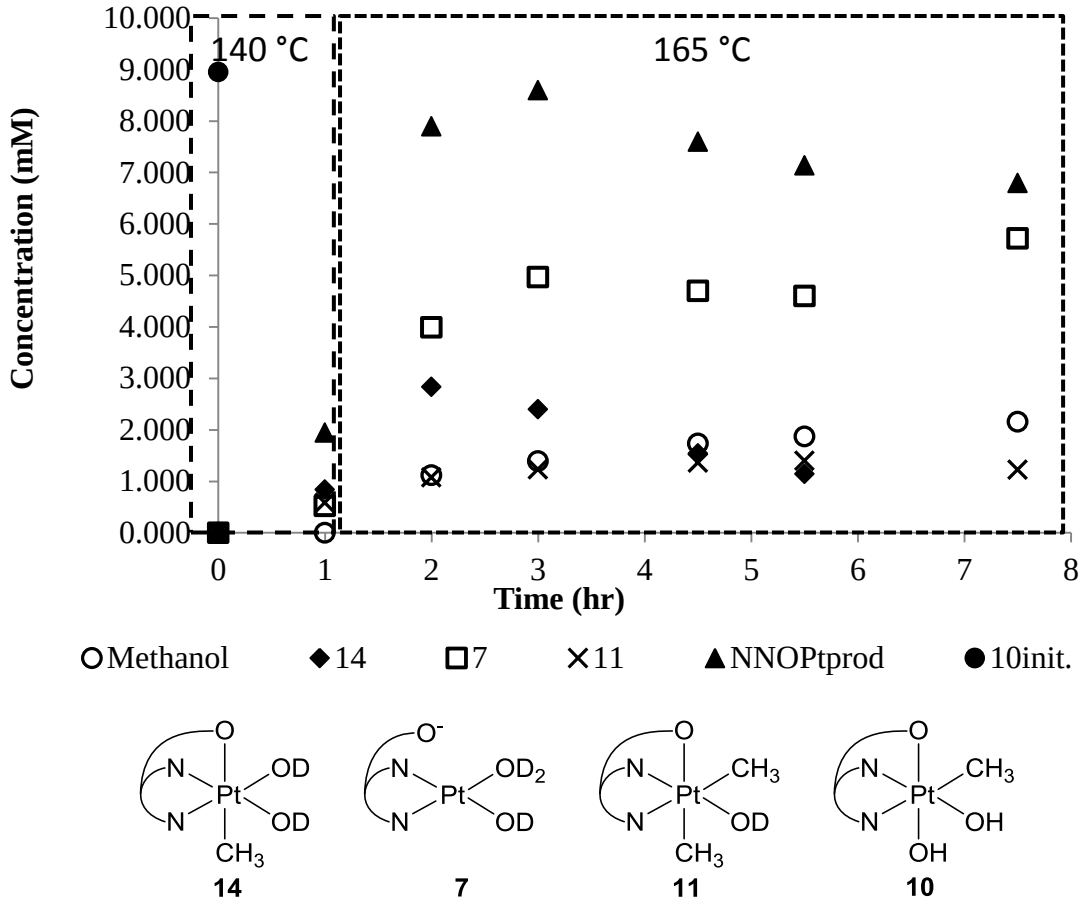

Figure 4.7. Products and intermediates from the thermolysis of **10** in D_2O at 140 -165 °C ([$NNOPt_{prod}$] = [**7**] + [**11**] + [**14**]).

After heating the aqueous solution of **10** for 3 h (1 h at 140 °C followed by 2 h at 165 °C) the total concentration of observed platinum products ([**7**] + [**11**] + [**14**]) was 8.5 mM. The combination of these products accounts for 95% of the starting concentration of **10** (9 mM, Figure 4.7) which was no longer observed in the ^{1}H NMR spectrum. Further heating (14 days) leads to a decrease in the total integration of the signals due to the Pt products. This is likely due to the dimerization of **7** to poorly soluble **9** which in the solid state appears to degrade to Pt^0 at 165 °C. This may be avoided by running the reaction a low initial concentration of **10** (< 2mM).

The concurrent increase in the concentration of methanol and decrease in the [**14**] is consistent with the isomerization of **10** to **14**, followed by reductive elimination of methanol from **14** (Figure 4.8). An analogous isomerization was previously reported in the reductive elimination of methanol from dpmsPt^{IV}(CH_3)$(OH)_2$ (Figure 4.2) with the C_1-symmetric NNOPt^{IV}-CH_3 observed as an intermediate at near neutral pH.[4]

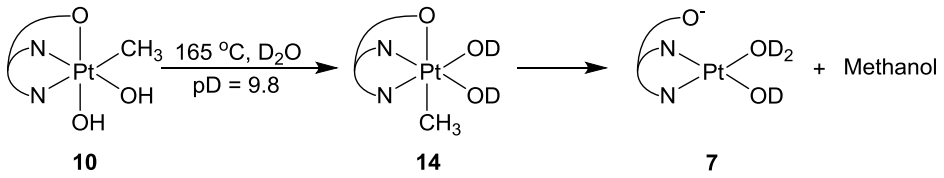

10 **14** **7**

Figure 4.8. Thermolysis of **10** in D_2O.

While the transformation of the Pt^{IV}-CH_3 in **10** to methanol is exciting, the observed decomposition of **11** is also intriguing as the formation of the expected products methanol or ethane can be considered key steps in methane functionalization or oligomerization. However, ethane was not observed in the ^{1}H NMR spectrum of the products (Figure 4.9a). The elimination of methanol from **11** would presumably produce **6,** which could then undergo aerobic oxidization (reaction performed in air) to **10** subsequently producing an additional equivalent of methanol and the demethylated product **7** (Figure 4.9b). If protonolysis of **6** is competitive with aerobic oxidation of **6**, methane should be produced (Figure 4.9b). However, methane was not observed in the reaction mixture. Although protonolysis might be expected in a protic media at high temperature, Labinger and Bercaw found that the ratio of oxidation to protonolysis of monomethyl Pt^{II} increased at higher temperatures.[8] It is possible that the route depicted in Figure 4.9b accurately describes the decomposition of **11** but methane is not observed due to a combination of competitive oxidation at high temperature (165 °C) and low [D_3O^+] (pD = 9.8) resulting in oxidation of **6** over protonolysis. In summary, reductive elimination of two

equivalents of methanol from **11** is likely the mechanism of decomposition of **11.** Unfortunately, the predicted products from C-O reductive elimination from **11** (**7**, **10** and methanol) are all also observed from the reductive elimination of **10** so their presence alone cannot be used as evidence to explain the fate of **11**.

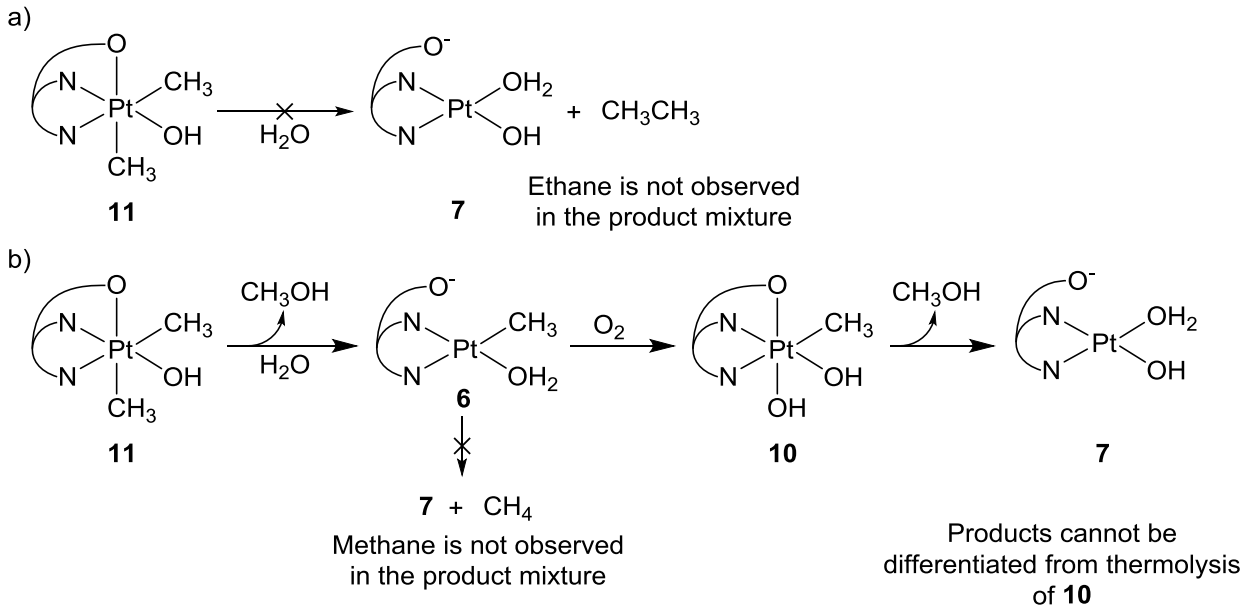

Figure 4.9. Proposed routes for the decomposition of **11**: a) Reductive elimination of ethane from dimethyl **11**. b) Reductive elimination of two equivalents of methanol from dimethyl **11**.

In addition to reductive elimination of methanol a methyl transfer reaction producing **11** was observed. A better understanding of the mechanism of methyl transfer that produced **11** could have tremendous value towards the design a system for methane oligomerization. In Chapter 3 I proposed that the observed methyl transfer generating **11** occurred through attack of **6** on a Pt^{IV}-CH_3 group positioned *trans* to the hemilabile carboxylate arm (Figure 4.10). This general methyl transfer mechanism was proposed to operate in Vedernikov's dpms system as well.[4c]

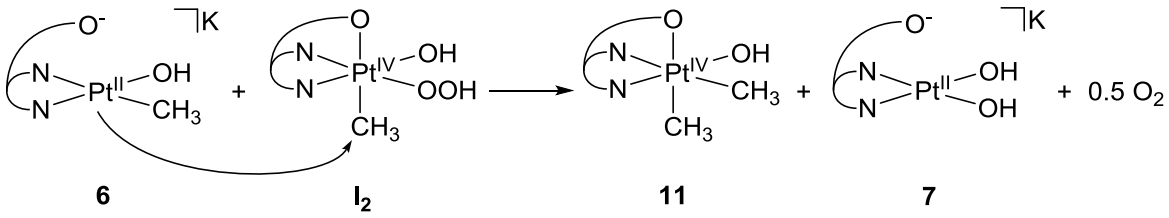

Figure 4.10. Proposed mechanism for methyl transfer from Pt^{IV}-CH_3 to Pt^{II}.

During the thermolysis of **10**, isomerization produced **14** which possesses a Pt^{IV}-CH_3 group *trans* to the carboxylate arm (Figure 4.8). This positioning of the Pt^{IV}-CH_3 group should make **14** an excellent methyl group donor. The identity of the methyl group acceptor is more difficult to determine as a complex containing a Pt^{II}-CH_3 group such as **6** is not observed or expected based on our understanding of reductive elimination of methanol from NNOPt^{IV}-CH_3. The possibility of reduction of **10** producing **6** is inconsistent with Labinger and Bercaw's finding that oxidation to (tmeda)$Pt^{IV}(CH_3)_2(OH)$ is irreversible.[9] Specifically, they did not observe the production of $^{18}O_2$ during the decomposition (tmeda)$Pt^{IV}(^{18}O_2H)(OCH_3)(CH_3)_2$ which is an intermediate generated during aerobic oxidation of (tmeda)$Pt^{II}(CH_3)_2$.

An alternative to nucleophilic methyl transfer mechanism involving Pt^{II} and Pt^{IV} may be methyl transfer occurring through a Pt^{III}-CH_3 intermediate. Methyl transfer mechanisms that propose a Pt^{III}/Pd^{III}-CH_3 intermediate have been reported but the M^{III}-CH_3 was produced through 1-electron oxidation of a Pt^{II}-CH_3.[10] Both mononuclear and dinuclear Pt^{III} compounds possessing an octahedral geometry around the Pt have been reported suggesting that Pt^{III} may be stabilized by a facially coordinating ligand like NNO.[11] A pathway in which a Pt^{III}-CH_3 species is generated by 1 electron reduction of Pt^{IV} through the loss of •OH from **10**, was considered (Figure 4.11).[12] A similar reduction from a d^6 to d^7 metal from homolysis of a M-OH bond generating •OH was reported from rhodium(III)

porphrin hydroxide (Figure 4.12).[13] However, efforts to induce methyl transfer by the addition of known 1 electron reductant Cp_2Co^{II} to a solution of **10** did not result in methyl transfer but rather a 2 electron reduction to **6**.

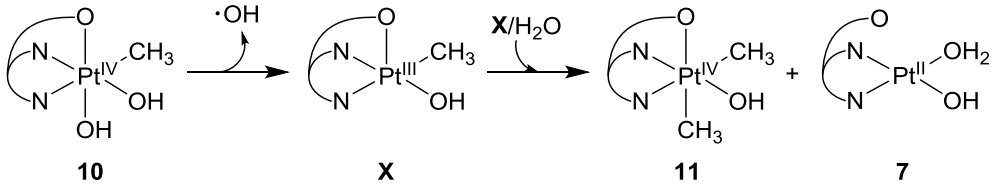

Figure 4.11. Possible production of **11** through a Pt^{III}-CH_3 intermediate.

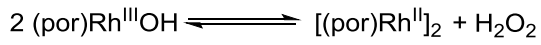

Figure 4.12. 1-electron reduction of Rh^{III} by OH^-.[13]

In summary, the thermolysis of the monomethyl Pt^{IV} **10** under basic conditions produces the expected products methanol and **7**. Isomerization of **10** to place the CH_3 group trans to the carboxyl producing **14** is proposed as an intermediate on the pathway to produce methanol (Figure 4.8), consistent with a reductive elimination mechanism described by Vedernikov that involves isomerization followed by S_N2 attack (Figure 4.2).[4a] Additionally, a rare methyl transfer reaction occurred producing the dimethyl platinum **11**. While the production of **14** during the thermolysis of **10** provides an excellent methyl group donor, we were unable to determine an appropriate Pt^{II}-CH_3 methyl group acceptor to generate **11**. A disproportionation of Pt^{III}-CH_3, proposed from homolysis of a Pt^{IV}-OH in **10** was also considered but further investigation is required (Figure 4.11). Thermolysis of **11** was observed and it seems likely that decomposition occurred through reductive elimination of methanol followed by oxidation to **10** and a second elimination of methanol to produce **7** (Figure 4.9). Unfortunately the products of this mechanism cannot be discerned from the products of the concurrent thermolysis of **10**.

A methyl transfer that occurs from monomethyl Pt^{IV} could find a use in catalytic oligomerization of methane. Previous proposed catalytic cycles which incorporate reported methyl transfer through 1-electron oxidation of dimethyl Pd^{II}[10b] would likely be hindered by the need to develop a high concentration of dimethyl Pd^{II} for the bimolecular step (Figure 4.13a). High concentrations of methylated transition metals are unlikely due to the reversible nature of C-H activation of methane. Trapping the product of C-H activation (M^n-CH_3) through irreversible oxidation to M^{n+2}-CH_3 could produce a high enough concentration of M-CH_3 to allow for methyl transfer and potential elimination of oligomerized product ethane (Figure 4.13b).

a) b)

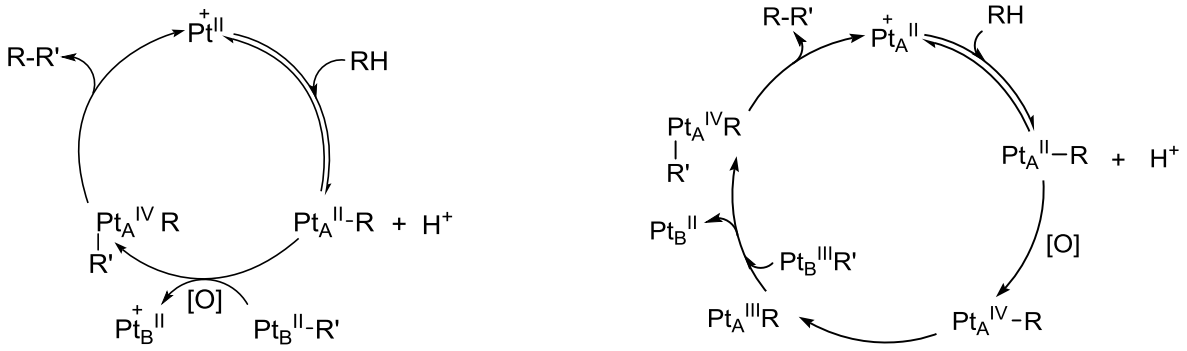

Figure 4.13. Proposed catalytic cycles for alkane oligomerization. a) Methyl transfer occurs from Pt^{II}-R. b) Methyl transfer occurs from Pt^{IV}-R.

Part II. Reductive elimination from $(NNO)Pt^{IV}(CH_3)(OH)_2$ (10) in acidic solution

Results and Discussion

Protonation of 10

As discussed in the introduction, in Vedernikov's dpms system reductive elimination of methanol from monomethyl Pt^{IV} was slowed considerably by the addition of acid.[4a] To improve reductive elimination under acidic conditions we propose that a sufficiently basic hemilabile arm

(carboxylate in NNO) could be protonated resulting in faster reductive elimination (Figure 4.4). Protonation of **10** (pK_a for **10**H^+ = 7.3 ± 0.1, Figure 4.30) is expected to occur at either the carboxylate or the hydroxides bound to Pt^{IV}. Some insight into the site of protonation may be gained by a comparison of the X-ray crystal structures of **10** (Figure 4.14a) and **10**H^+ (Figure 4.14b). The structure of **10** was determined from crystals grown in an aqueous solution while the structure of **10**H^+ was determined from crystals grown in an aqueous solution with HBF_4 added to a pH of 1.1.

a)

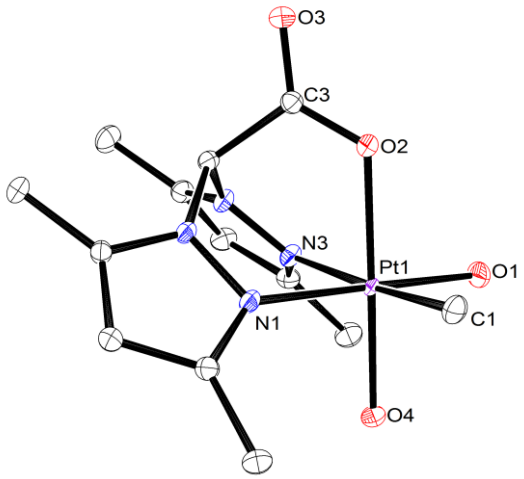

b)

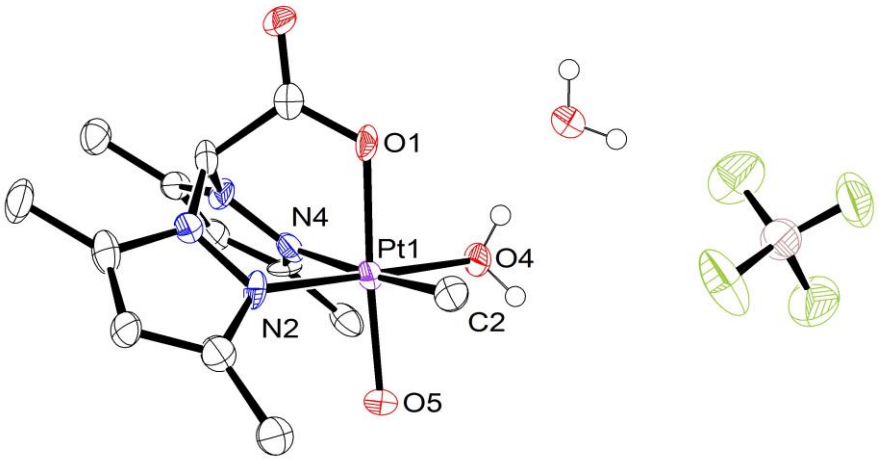

Figure 4.14. 10 ellipsoids at the 50% probability level. Hydrogen atoms are excluded for clarity. a) **10** (see Figure 3.4 for selected bond lengths and angles). b) Selected bond distances (Å) and angles (°): Pt1-C2 = 2.019(15), Pt1-O4 = 2.029(9), Pt1-O1 = 2.010(10), Pt1-O5 = 1.982(10), Pt1-N2 = 2.006(11), Pt1-N4 = 2.169(13), N4-Pt1-O4 = 90.5(4), C2-Pt1-N2 = 92.4(6), C2-Pt1-O4 = 89.0(5), C2-Pt1-O1 = 88.9(5), O5-Pt1-C2 = 89.6(5), N2-Pt1-N4 = 88.0(5).

The presence of a BF_4^- counter anion in the x-ray crystal structure of **10**H^+ supports protonation of neutral **10** to the cationic **10**H^+. The longer equatorial Pt-O bond in **10**H^+ (Pt1-O4 = 2.029(9) Å) when compared to the similar bond in **10** (Pt1-O1 = 1.9806(12) Å) may be due to protonation of **10** resulting in a Pt-OH_2 in **10**H^+. Additionally, the bond Pt-N bond located trans to equatorial Pt-O is shorter in the protonated product (**10**: Pt1-N1 = 2.0353(13) Å, **10**H^+: Pt1-N2 = 2.006(11) Å) consistent with a lower trans influence of H_2O versus OH^-.

Of particular consequence to reductive elimination is the bond length between Pt and the O in the carboxylate arm. The Pt-O bond shortens on protonation from **10** (Pt1 – O2 = 2.0706(12) Å) to **10**H^+ (Pt1 – O1 = 2.010(10) Å). Dissociation of the carboxylate arm requiring breaking of the Pt-O bond is a required during isomerization. Therefore a stronger Pt-carboxylate arm in **10**H^+ is expected to result in slower reductive elimination. Vedernikov's finding that the rate determining isomerization step is slower at lower pH (Figure 4.2and Figure 4.3) is consistent with our observed decrease in the length of the bond between Pt and the hemilabile arm due to protonation. Protonation could be steered towards the hemilabile carboxylate arm in NNO by removing the more basic Pt-OH groups. This may be done by substituting the Pt^{IV} bound OH^-/H_2O with anionic species that are not susceptible to protonation like Cl^-. While addition of the Bronsted-Lowry acid H^+ did not result in rate acceleration, described below is an observed acceleration of reductive elimination of methanol from **10** in the presence of the Lewis acid **7**.

Thermolysis of 10 under acidic conditions

Heating an aqueous acidic (100 mM HBF_4/H_2O) solution of **10** (6 mM) at 120 °C for 48 hours resulted in complete consumption of **10** as determined by ^{1}H NMR spectroscopy (2.84 ppm, $^2J_{Pt\text{-}H}$ = 66 Hz). The product mixture contained methanol (3.4 ppm, yield = 49%) and two NNO ligand containing

species identified as **7** and the dimer species **8** (Figure 4.15). The combination of **7** (43%) and **8** (43%) accounted for 86% of the original **10.** No other species were observed.

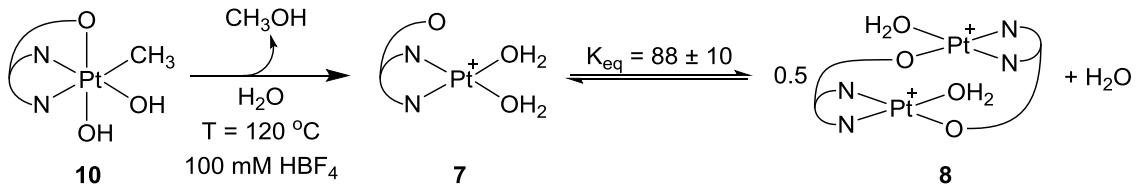

Figure 4.15. Reductive elimination of methanol from **10** in H_2O under acidic conditions.

Under similar conditions ([HBF_4] = 100 mM) but at higher temperature to make kinetic studies more practical (T = 140 °C) the thermolysis of **10** (6 mM) in D_2O was monitored by ^1H NMR spectroscopy. A first-order plot of the decomposition of **10** is not linear but curves downward as the reaction progresses (Figure 4.16). The data also did not fit half or second order kinetic expressions. There was no change in pD (1.4) over the course of the reaction. To examine the possibility that the products were causing the reaction rate to increase at later reaction times, reductive elimination was studied in the presence of the products **7**, **8** and methanol.

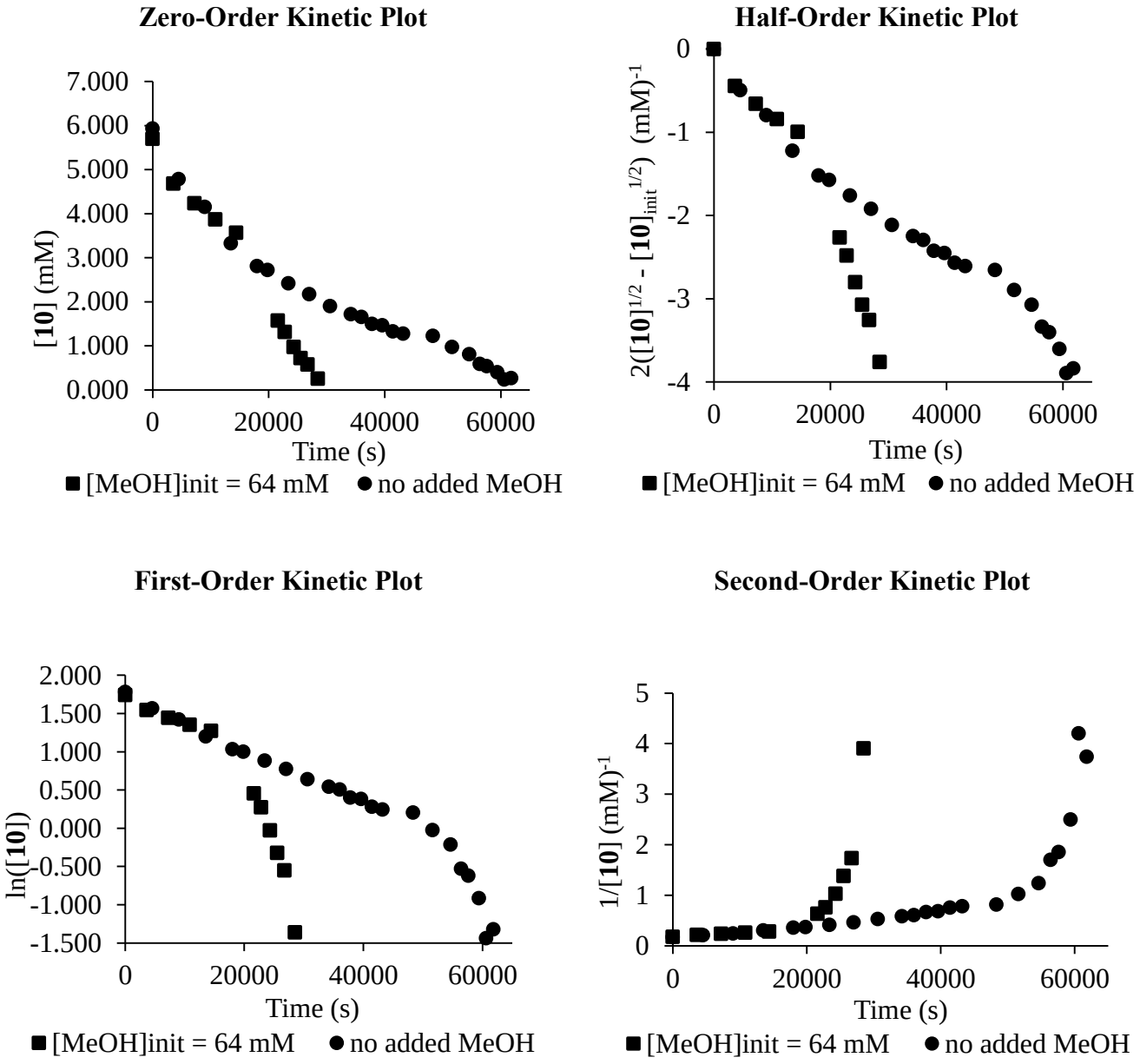

Figure 4.16. Kinetic plots of thermolysis (T = 140 °C) of **10** (6 mM) under acidic conditions (100 mM HBF_4) with (■) and without (●) added methanol (64 mM).

To examine the effect of methanol, the thermolysis of **10** (5.7 mM) was carried out with added methanol (64 mM). Similar to the reaction in which no methanol was added, a large increase in rate occurs during the reaction (Figure 4.16). However the increase in rate began earlier in the reaction i.e. at

a higher concentration of **10**. Again, no change in pD (1.4) was observed over the course of the reaction. Based on these results, methanol is not solely responsible for the observed rate increase.

To investigate the effects on the reaction rate due to the [$\mathbf{Pt_{prod}}$] ($\mathbf{Pt_{prod}}$ = [**7**] + [**8**]) a thermolysis of **10** (2 mM) was monitored in the presence of 4 equivalents of $\mathbf{Pt_{prod}}$ (from a previous thermolysis of **10** (8 mM)) and 50 equivalents of CD_3OD (100 mM, Figure 4.17) in 100 mM HBF_4/D_2O (Figure 4.17). It was clear that the addition of **Ptprod** increased the rate of decomposition of **10**. The reaction temperature was reduced to 100 °C due to the significant increase in the rate of conversion of **10**.

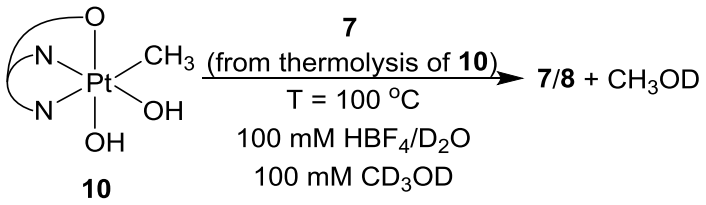

Figure 4.17. Thermolysis (100 °C) of **10** (2 mM) in the presence of **7** and **8** from previous thermolysis of **10** (8 mM) with CD_3OD (100 mM) added in excess of **10**.

Under these conditions, the reaction followed first-order kinetics (k_{obs} = 1.75 x 10^{-4} s^{-1}) through 3 half-lives (Figure 4.18). A four-fold increase in the concentration of $\mathbf{Pt_{prod}}$ (32 mM) resulted in an increase in k_{obs} to 5.53 x 10^{-4} s^{-1} (Figure 4.18). To determine the species (**7** or **8**) involved in the increased rate of decomposition of **10** the expected change in the [**7**] and [**8**] upon quadrupling of [$\mathbf{Pt_{prod}}$] (using the K_{eq} (85 ± 5) for **7**/**8** at 100 °C, see Chapter 2 and Figure 4.15) was calculated.[14] The relative increase in k_{obs} (3.2) upon quadrupling [$\mathbf{Pt_{prod}}$] is a closer match to the expected increase based on a first-order contribution from **7** (2.5) than from **8** (6.0). The increase in rate supports a direct interaction of **10** and **7** during, or prior to, the rate determining step.

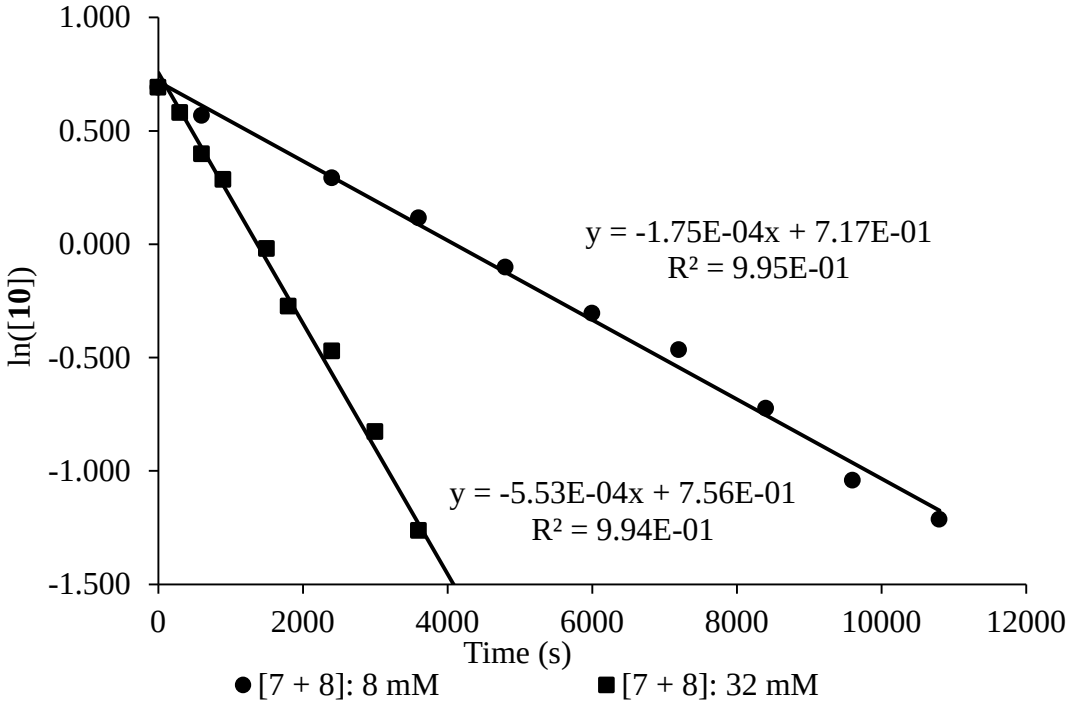

Figure 4.18. First order decomposition of **10** (2 mM) in 100 mM HBF_4/D_2O and 100 mM CD_3OD at 100 °C in the presence of **7** and **8** from previous decomposition of **10**.

Having found conditions (excess **7**) under which pseudo first-order behavior of the decomposition of **10** was maintained, the effect of methanol on reactivity was reconsidered. The results (Figure 4.19) showed that the concentration of methanol does not alter the rate of decomposition of **10**. Doubling the $[CH_3OH]$ from 75 to 150 mM while following the decomposition of **10** (3 mM) at 140 °C in the presence of **7** (from thermolysis of **10** (12 mM)) in 100 mM HBF_4/D_2O made very little difference in the rate of the reaction (k_{obs}: 8.0 and 8.2 x 10^{-4} s^{-1} respectively, Figure 4.19) consistent with a zero order dependence on methanol under these conditions.

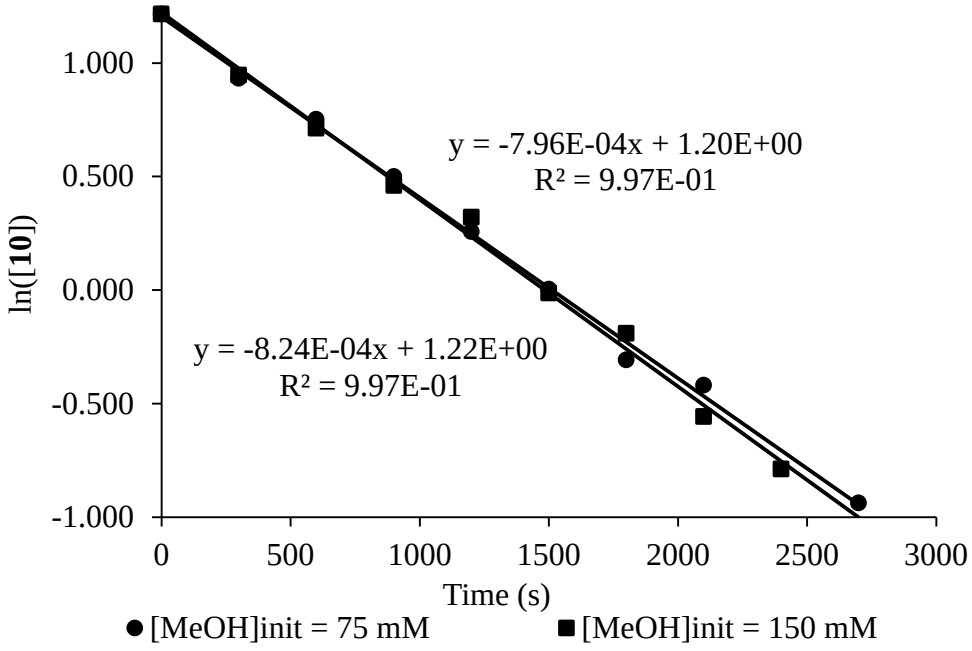

Figure 4.19. First order decomposition of 10 (3 mM) at 140 °C in 100 mM HBF_4/D_2O of **7** and **8** from previous decomposition of **10** (12 mM) with varying amount of added CH_3OH.

Summarizing the kinetic data, the thermolysis of **10** is first-order in **10** and **7** (when in excess) and zero-order in methanol. While **7** clearly plays a role, the thermolysis of **10** is also observed before **7** is produced. A two pathway reaction scheme is proposed in which the reaction occurs in the absence of **7** (Figure 4.20a) then at sufficiently high concentration, **7** acts as a catalyst in the decomposition of **10** (Figure 4.20b). This mechanism is consistent with the rate acceleration observed during the thermolysis of **10** due to increasing [**7**] over the course of the reaction. As there is no **7** present at the start of the reaction the initial slow rate (Figure 4.21a) may be associated with the thermolysis of **10** that occurs without interaction with another Pt center (Section a, Figure 4.20). Later in the reaction when [**7**] becomes sufficiently high (> 2^{nd} $t_{1/2}$), a significant increase in the rate of thermolysis of **10** is observed (Section b, Figure 4.21) likely due to a contribution from **7**.

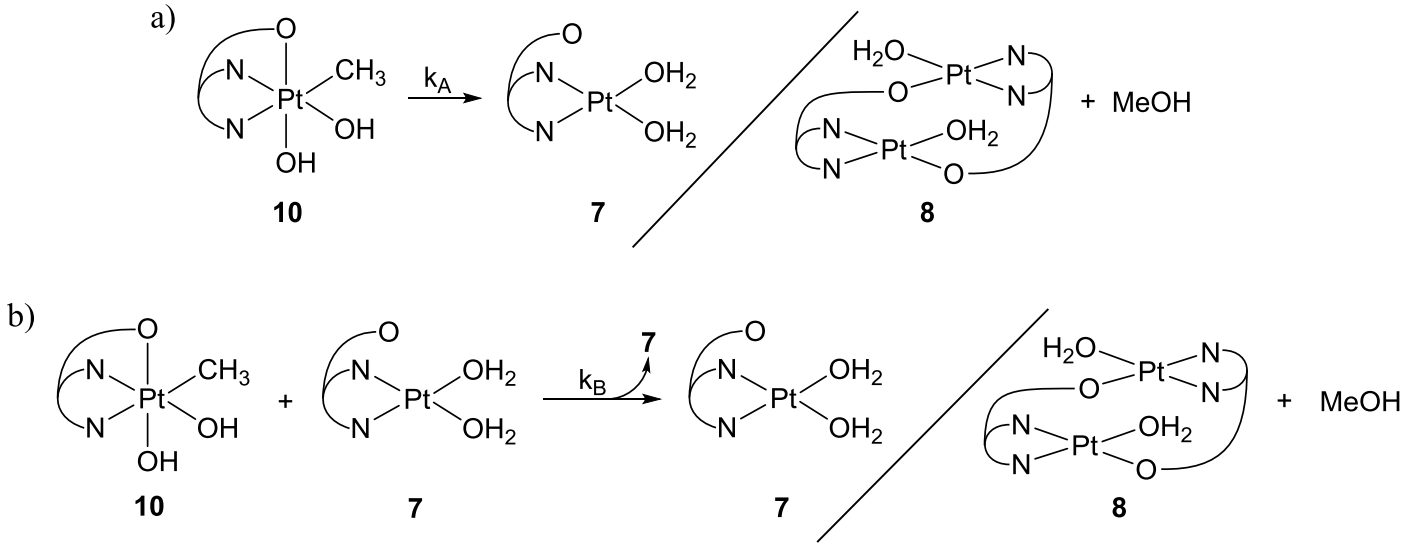

Figure 4.20. Two competing mechanisms for the decomposition of **10** where $k_B[\mathbf{7}] > k_A$. a) low [**7**] b) high [**7**].

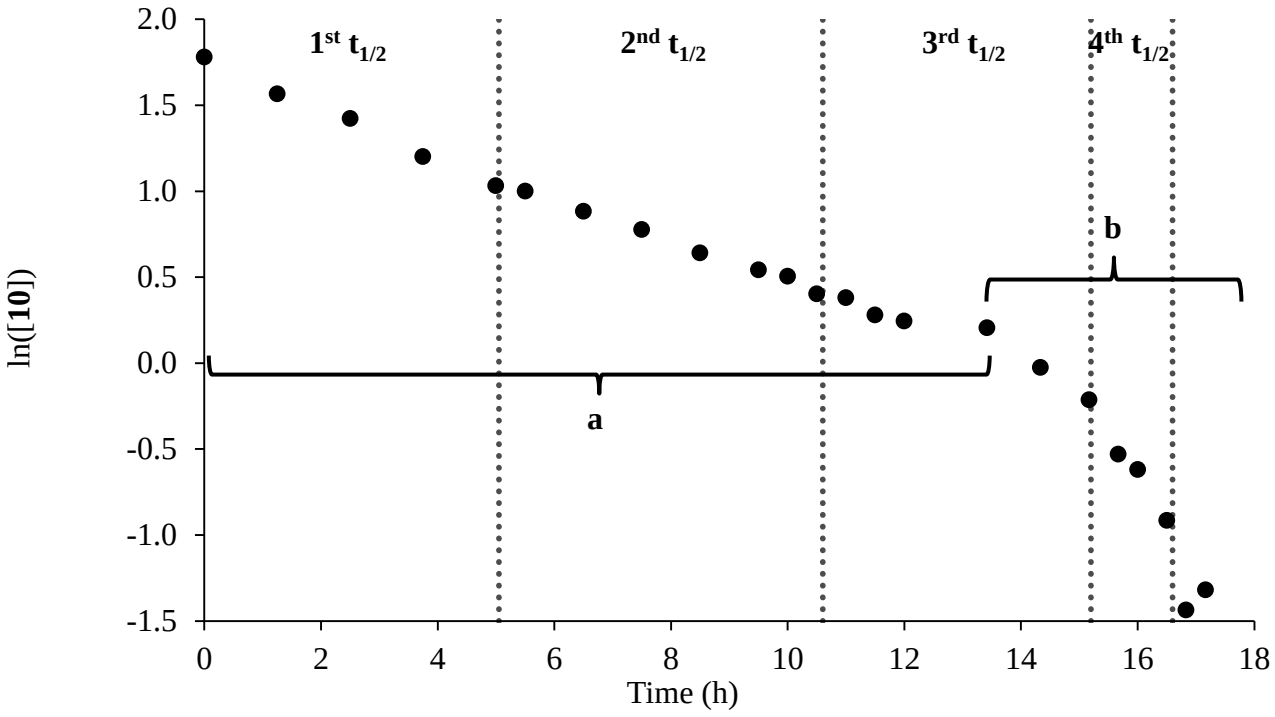

Figure 4.21. First-order plot of the thermolysis of **10** (6 mM) at 120 °C in 100 mM HBF_4 including estimation of when pathway a or pathway b is the dominant reaction pathway.

As described above, previous studies of C-O bond formation from platinum(IV) revealed S_N2 attack of the oxygen containing species on the platinum bound alkyl that is *trans* to an open site or a good leaving group (Figure 4.2).[4] Given the significant precedent for this mechanism, it seems prudent to propose a two-step mechanism for reductive elimination (Figure 4.22). The first step is isomerization moving the Pt^{IV}-CH_3 group trans to the hemilabile carboxylate arm followed by nucleophilic attack by water forming the C-O bond of methanol.

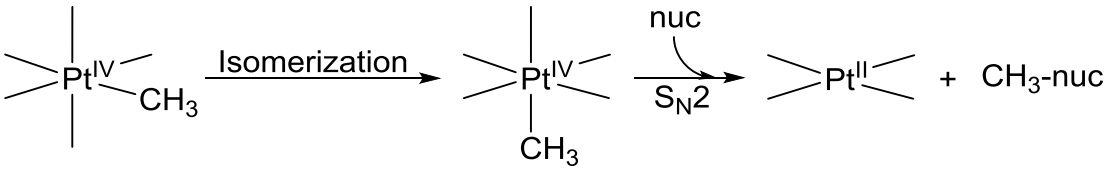

Figure 4.22. Two-step C-O bond formation from monoalkyl platinum(IV).

The role that added **7** would play in promoting this reductive elimination reaction is not clear. One possibility is that **7** might interact with **10** and assist in the isomerization step resulting in the observed rate increase. This assumes that isomerization is the rate determining step under acidic conditions which is consistent with Vedernikov's findings using the similar dpms system (Figure 4.3). During the thermolysis of **10** in basic solution (see above) the observation of **14** indicated that the S_N2 attack is the rate determining step (Figure 4.8). Under acidic conditions **14** was not observed during the thermolysis of **10** and the production of methanol.

Acceleration of the isomerization could be due to the formation of a dinuclear combination of **10** and **7** through the carboxylate arm (**I_3** or **I_4**, Figure 4.23). The structure of **I_3** is analogous to the formation of the dimer **8** (Figure 2.7 and Figure 2.8). In both **I_3** and **I_4** the bridging of two platinum centers through the oxygen of the carboxylate arm bound to Pt^{IV} may weaken the Pt^{IV}-carboxylate bond. The result would likely be facile conversion to a 5-coordinate Pt^{IV} species, which has been shown to be a key intermediate in other reductive elimination reactions.[15]

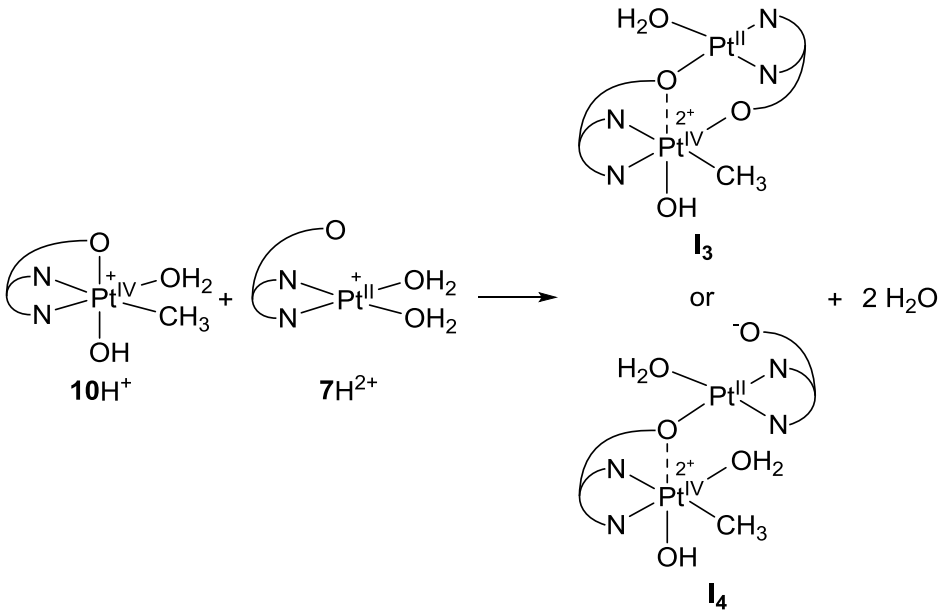

Figure 4.23. Proposed dinuclear complexes from **10** and **7** in acidic solution.

Coordination of the oxygen atom in an NNO ligand to two separate iron centers in a manner similar to that proposed in $\mathbf{I_3}$ was observed by X-ray crystallography (Figure 4.24).[16] The dimer structure supports the ability for the NNO ligand type to bridge two metal centers with the potential for weakening the M-O bond when compared with the tridentate coordinated monomer.

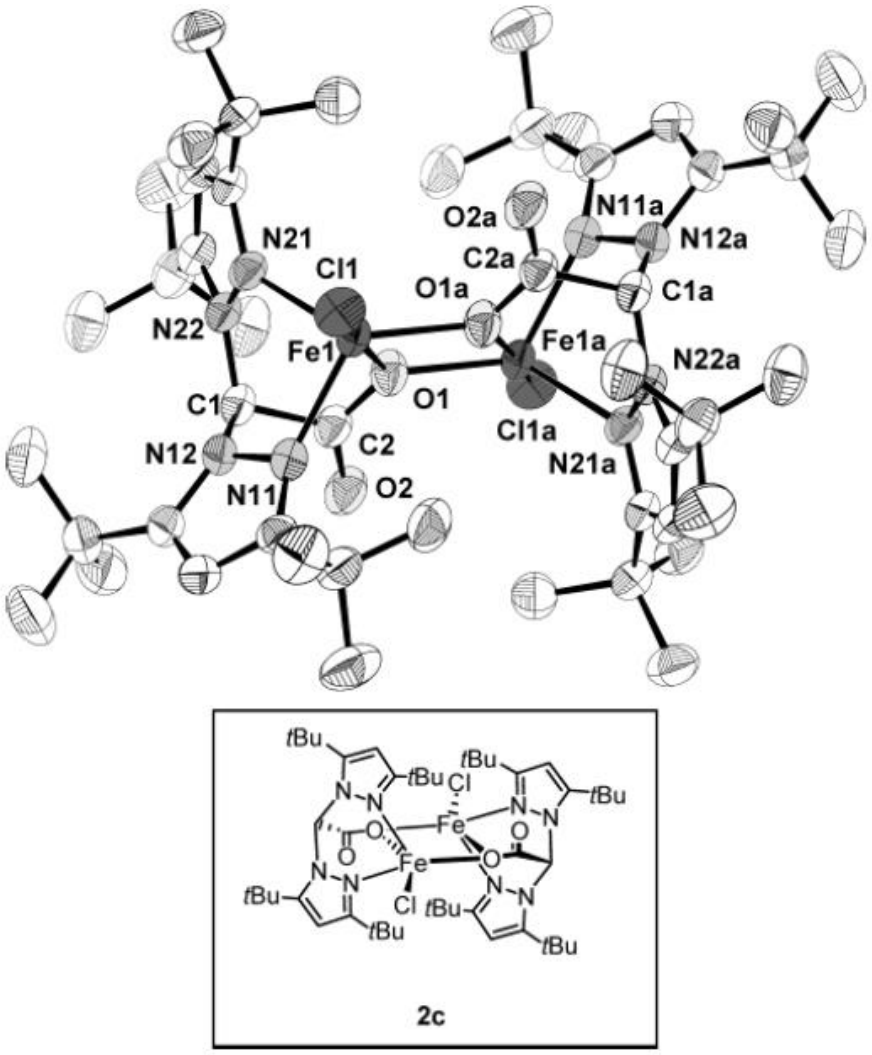

Figure 4.24. Structure of NNOFe dimer with bridging oxygen atoms in the carboxylate arm of the NNO ligand.[16] Reprinted with permission from: Beck, A.; Barth, A.; Hubner, H.; Burzlaff, N. *Inorg. Chem.* **2003**, *42*, 7182. Copyright 2003 American Chemical Society.

No mixed valent species such as $\mathbf{I_3}$ from Figure 4.23 were observed by ^{1}H NMR spectroscopy during the reaction. However, if the formation of a dinuclear species is entropically favored, as in formation of **8** (Figure 2.9), the high temperatures required to generate $\mathbf{I_3}$ may provide sufficient energy for rapid isomerization and S_N2 attack keeping the concentration of the intermediates very low. Also,

based on the kinetic data, the formation of **I_3** cannot be ruled out as the rate determining step in which case the intermediate would not be observed.

Simple coordination of the Pt^{II} center of **7** to the oxygen of the carboxylate arm from **10** (without reciprocal binding of the carboxylate arm of **7** to the Pt^{IV} center of **10**) as in **I_4** may also occur (Figure 4.23). The resulting weakening of the Pt^{IV}-O bond may make coordination of the carboxylate arm of **7** to the Pt^{IV} center through both carboxylate arms unnecessary for acceleration of C-O coupling. In this model of rate acceleration a Lewis acid of sufficient strength should serve as a substitute for **7**. To test this proposal, boric acid (100 mM) and $ZnBF_4$ (42 mM) were each added separately to the thermolysis of **10** instead of methanol. When boric acid was added the kinetic profile was nearly identical to the reaction in which excess methanol was present (Figure 4.25). If the mechanism proposed above is appropriate, then boric acid lacks sufficient strength to accelerate reductive elimination. It also seems that boric acid can perform the same role as methanol in terms of its effect on the decomposition of **10**. Although the reaction was not followed to completion, adding $Zn(BF_4)_2$ also did not give a significant increase in the rate of decomposition of **10** (Figure 4.25).

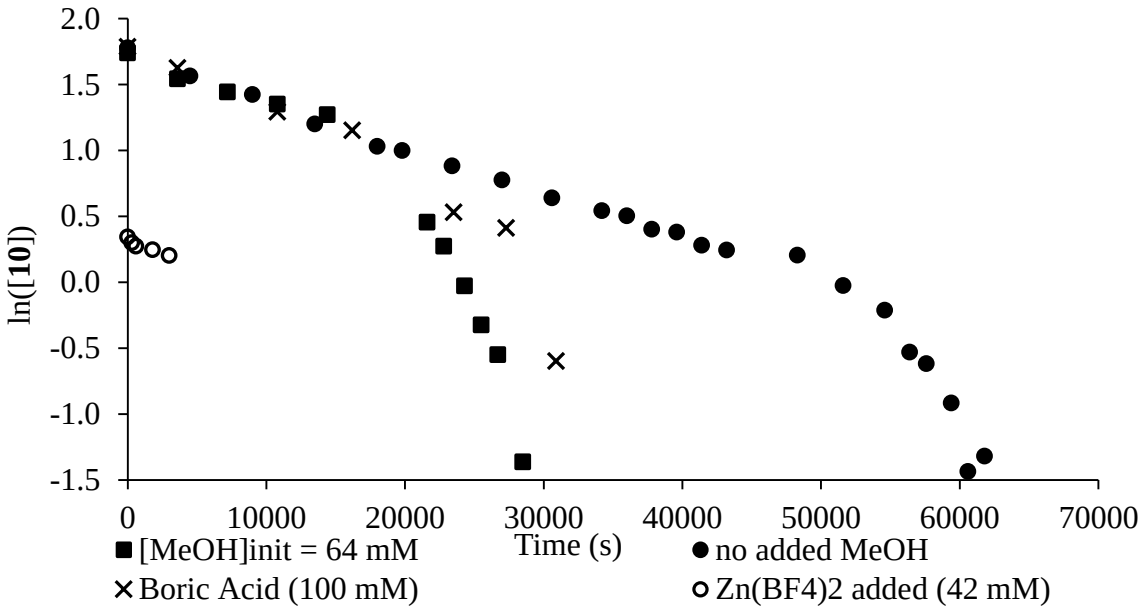

Figure 4.25. 1st order plot of thermolysis (T = 140 °C) of **10** (6 mM, 2 mM in added $Zn(BF_4)_2$ version) under acidic conditions (100 mM HBF_4) (■) with added methanol (64 mM) (●) no added methanol (64 mM) (x) with H_3BO_3 (100 mM, no added methanol) (○) added $Zn(BF_4)_2$ (42 mM).

Along with potential weakening of the Pt^{IV}-carboxylate arm in the dinuclear species **I_3** and **I_4** an increase in charge may occur upon formation of the dinuclear species. The stability of the Pt^{IV}-CH_3 bond in **10** requires isomerization to move the methyl group trans to the hemilabile arm before S_N2 attack by H_2O can form the C-O bond in CH_3OH. Alternatively, increasing the charge may sufficiently enhance the electrophilicity of the Pt^{IV}-CH_3 containing group thereby allowing removal of the methyl group by S_N2 attack from H_2O without isomerization (Figure 4.26). Assuming the formation of the dinuclear species is rate determining this mechanism would be first-order in both **10** and **7** matching the kinetic data from reductive elimination from **10**.

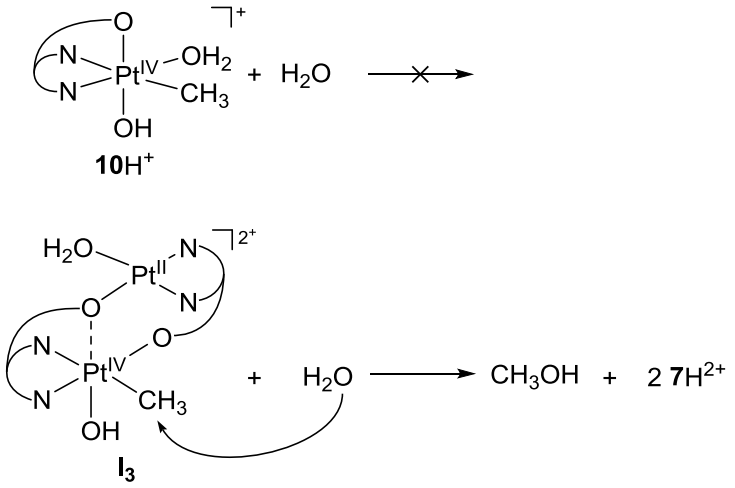

Figure 4.26. Proposed enhancement of nucleophilic attack on equatorial Pt^{IV}-CH_3 group due to increased cationic character in $\mathbf{I_3}$.

Other mechanisms that would require cooperation between **7** and **10** were also considered. Vedernikov found that reductive elimination of methanol from the C_s-symmetric (dpms)$Pt^{IV}(CH_3)(OH)_2$ ($\mathbf{14_V}$) isomer is accelerated in the presence of (dpms)$Pt^{II}(OH_2)_2$ ($\mathbf{7_V}$, Figure 4.27).[4b] They proposed that the increased rate was due to an observed mixed valent Pt^{IV}/Pt^{II} hydroxide bridged dinuclear intermediate ($\mathbf{I_V}$, Figure 4.27). The coordination of the cationic $\mathbf{7_V}$ with $\mathbf{14_V}$ resulting in a cationic $\mathbf{I_V}$ was suggested to enhance the electrophilicity of the Pt^{IV}-CH_3 containing complex, compared to neutral $\mathbf{14_V}$, resulting in faster S_N2 attack by H_2O. Formation of the dinuclear $\mathbf{I_V}$ was not observed during reductive elimination from the C_1-symmetric (dpms)$Pt^{IV}(CH_3)(OH)_2$ ($\mathbf{10_V}$) isomer in the presence of $\mathbf{7_V}$. Returning to our NNO system, **14** is not observed during the thermolysis of **10** under acidic conditions thus isomerization from **10** to **14** is likely the rate determining step. Based on this understanding, dimerization between **14** and **7** similar to $\mathbf{I_V}$ would not be expected to enhance that rate of decomposition of **10**.

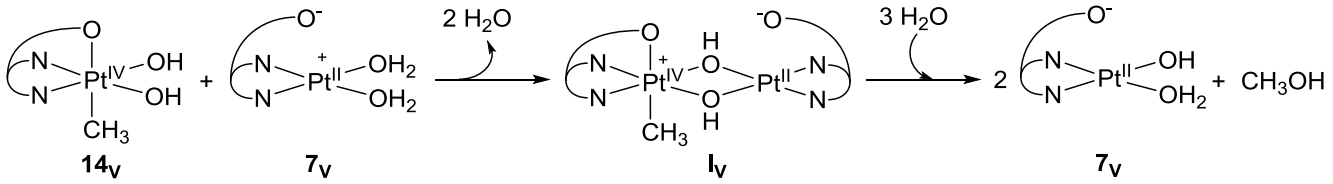

Figure 4.27. Proposed mechanism for the acceleration of reductive elimination from *Cs*-$NNOPt^{II}(CH_3)(OH)_2$ by the addition of $NNOPt^{II}(OH)_2$ in the Vedernikov system.[4b]

Nucleophilic attack through the oxygen atom of a hydroxo in **7** on the Pt^{IV}-CH_3 of **10** was also considered (Figure 4.28). This reaction would result in a Pt^{II}-($OHCH_3$) containing product (**7**CH_3OH) which could undergo ligand exchange with the solvent producing methanol. The relative stability of the Pt^{IV}-CH_3 in **10** towards nucleophilic attack by **6**, a likely stronger nucleophile than **7**, as described in Figure 3.20 is inconsistent with this type of mechanism. And while the low pH likely results in protonation of **10** which should improve its performance as an electrophile similar protonation of **7** would reduce its nucleophilicity. In the similar dpms system, nucleophilic attack by $\mathbf{7_V}$ was found to be insufficiently nucleophilic to remove the Pt^{IV}-CH_3 group in $\mathbf{14_V}$.[4] $\mathbf{14_V}$ possesses a Pt^{IV}-CH_3 group trans to the hemilabile arm, enhancing C-O bond formation. Removal of the Pt^{IV}-CH_3 group in **10** by S_N2 attack from **7** is highly unlikely as the Pt^{IV}-CH_3 group is trans to a pyrazolyl.

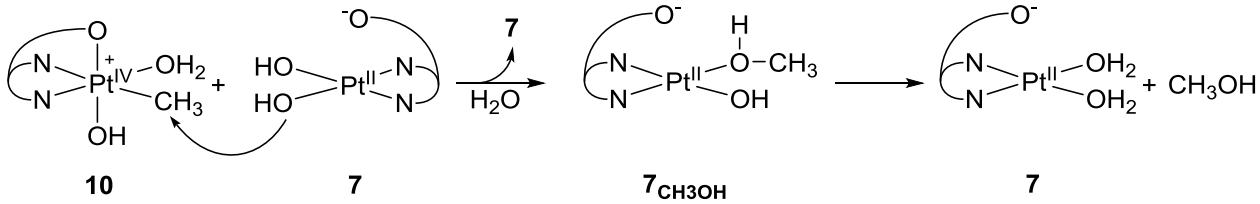

Figure 4.28. Potential mechanism for the acceleration of reductive elimination from *C1*-$NNOPt^{II}(CH_3)(OH)_2$ (**10**) through nucleophilic attack by $NNOPt^{II}(OH)_2$ (**7**) followed by solvent substitution.

In summary, with isomerization controlling the rate of reductive elimination from **10** enhancement of the overall rate must come through increasing the rate of isomerization. The proposed

weakening of the Pt^{IV}-carboxylate due to the formation of **I_3**/**I_4** would likely ease the transition to a 5-coordinate intermediate thereby increasing the rate of isomerization. Increased charge on the Pt^{IV}-CH_3 upon generation of **I_3**/**I_4** containing species may sufficiently activate the Pt^{IV}-CH_3 group to allow for direct C-O coupling through nucleophilic attack by H_2O without preceding isomerization. Both proposed mechanisms are expected to be first-order in **10** and **7** matching our empirical findings. Of the alternative mechanisms considered none were expected to enhance the rate of isomerization. Precedent from the Vedernikov group support that the Pt^{IV}-CH_3 containing species can be activated towards S_N2 attack through protonation or the addition of a cationic Pt species however increasing the rate of S_N2 attack would have no effect on the observed rate of reductive elimination of **10** under acidic conditions when isomerization is the rate determining step.

Conclusions

A facially coordinating NNO ligand containing a hemilabile carboxylate moiety allows for reductive elimination of methanol from a monomethyl platinum(IV) (**10**). Our results are consistent with a two-step mechanism similar to that determined by Vedernikov for the related dpms system.[4a] In the first step, isomerization of **10** to **14** moves the methyl group bound to platinum(IV) *trans* to a good leaving group (Figure 4.29). The second step then involves nucleophilic attack on the platinum bound methyl. Under alkaline conditions the S_N2 attack appears to be rate limiting supported by the appearance of the C_s-symmetric intermediate **14** during reductive elimination from **10** (Figure 4.8). The mechanism under acidic conditions is more complex, but **14** is not observed over the course of the reaction suggesting isomerization is the rate determining step. This pH-dependent change in the rate determining step is also consistent with the mechanism thought to occur in the dpms system.[4a]

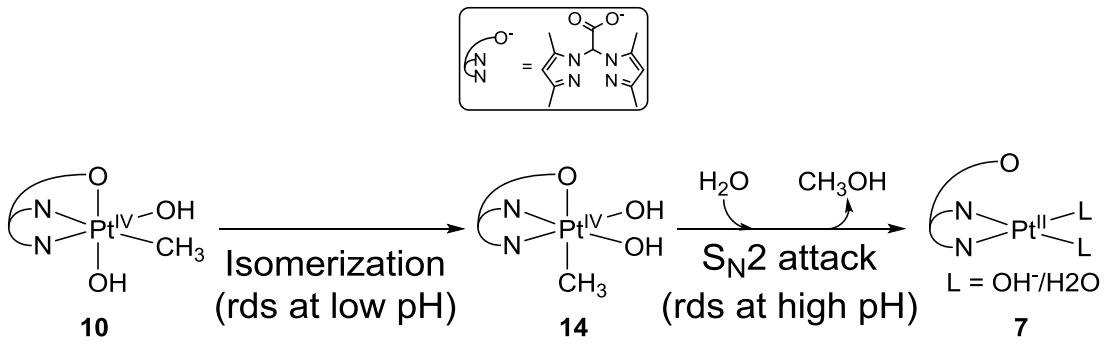

Figure 4.29. Proposed two-step pH-dependent reductive elimination of methanol from monomethyl $NNOPt^{IV}$

Under acidic conditions the rate of reductive elimination from **10** is enhanced by the product of reductive elimination (**7**/**8**). Although **7** and **8** are in equilibrium, the change in the rate of thermolysis of **10** was more consistent with a first-order dependence on **7** rather than **8**. Rate determining formation of a dinuclear Pt^{II}/Pt^{IV} species, perhaps similar to $\mathbf{I_3}/\mathbf{I_4}$ (Figure 4.23) is consistent with kinetic studies. Further, we propose that the rate of reductive elimination from $\mathbf{I_3}/\mathbf{I_4}$ is faster than from **10** due to a weaker bond between Pt^{IV} and the carboxylate arm in $\mathbf{I_3}/\mathbf{I_4}$. The bond may be weakened by coordination of a Pt^{II} center to the carboxylate oxygen also bound to **10**. This should result in more facile access to a 5-coordinate intermediate, thereby accelerating isomerization which is thought to be the rate determining step under acidic conditions.

Facially coordinating ligands have shown great promise as components in potential methane to methanol catalysts. Two key steps in these types of systems are oxidation and reductive elimination. Aerobic oxidation of the monomethyl Pt^{II} occurs at room temperature but higher temperatures are required for reductive elimination of methanol in both the NNO (100 °C) and dpms systems (75 °C).[4] Reductive elimination clearly has a higher barrier than oxidation. Under acidic conditions, the rate of reductive elimination has been shown to be under control of the isomerization step. As both the Shilov

and Periana systems operate at very low pH enhancement of the isomerization step when using a facially coordinating ligand may be a crucial for an effective catalytic system.

The determination of conditions that enhances the rate of reductive elimination from methyl Pt^{IV} stabilized by a facially coordinating ligand as observed in the NNO system may be an useful component in a catalytic system. Assuming that dimerization similar to **I_3/I_4** (Figure 4.23) is required to accelerate reductive elimination, the accelerant need not be a product of the reaction. In all likelihood using a separate ligand-metal combination specifically designed to coordinate to the hemilabile arm of a methyl Pt^{IV} would further enhance reductive elimination.

Experimental

All air-free manipulations were performed in a N_2 glove box, on a Schlenk line, or on a high vacuum line. Solvents were purified by passage through two columns of activated alumina in the case of THF and diethyl ether, and a column of activated alumina followed by a column of Q5 reactant in the case of benzene, pentane, and toluene. NMR solvents were obtained from Cambridge Isotope Laboratories. Benzene-d_6 and THF-d_8 were dried over Na/benzophenone then vacuum transferred prior to use. Chloroform-d_1 was dried over CaH_2 and vacuum transferred prior to use. ^{1}H NMR spectra were referenced from the residual protiated solvent signal and chemical shifts are reported in parts per million (ppm) from tetramethylsilane (TMS). KH was obtained as a suspension in oil and was purified by washing with pentane. All other chemicals were purchased and were used as received. pH/pD measurements were obtained using a Hach company ISFET pH Stainless Steel NMR Tube Probe calibrated using phosphate buffered H_2O solutions of pH 4, 7 and 10. Readings from pH meter of D_2O solutions are reported as pD. Elemental analyses were performed by the CENTC Elemental Analysis Facility at the University of Rochester.

Determination of pKa for 10H$^+$. Complex **10** (80 mg, 0.163 mmol) was dissolved in 2.0 mL of H_2O with a pH probe was submerged in the solution (pD: 10.2). A 0.16 M HBF_4 solution was prepared by dissolving 50% HBF_4/H_2O (200 μL, 1.59 mmol) in 10 mL H_2O. The HBF_4 solution was added drop-wise to the solution of **10** to a pH of 4.6 (Figure 4.30a). The procedure was repeated with a different solution of **10** (41 mM) and HBF_4 (0.3 M, Figure 4.30b).

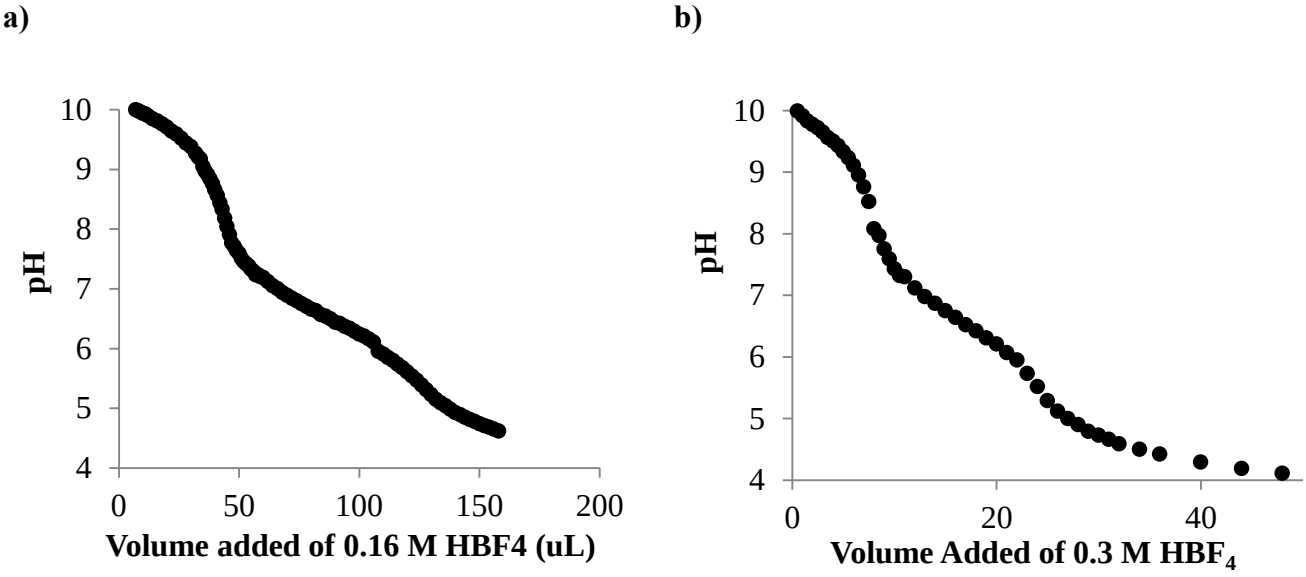

Figure 4.30. Determination of pK_a of **10**H$^+$ by titration of **10** with HBF_4: a) [**10**] = 81 mM, [HBF_4] = 0.16 M. b) [**10**] = 41 mM, [HBF_4] = 0.3 M.

Thermolysis of 10 in D_2O. Complex **10** (3.3 mg, 0.007 mmol) was dissolved in 0.75 mL D_2O with dioxane (0.2 μL, int. std.). The addition of **10** elevated the pD from 7.2 to 9.8. The solution was transferred to a Teflon valve sealed NMR tube and heated in a 140 °C oil bath for 1 h. The temperature was then increase to 165 °C and the sample was heated for an additional 4 d with periodic examination by ^{1}H NMR spectroscopy.

Attempted 1 electron reduction of 10. A Teflon cap sealed NMR tube was charged with **10** (8.0 mg, 0.016 mmol) and dioxane (0.1 μL, int. std.) in 0.4 mL of N_2-sparged D_2O. The ^{1}H NMR spectrum of the sample was then recorded. $(Cp)_2Co^{II}$ (3.0 mg, 0.016 mmol) was then added. Upon addition of $(Cp)_2Co^{II}$

to the D_2O solution of **10,** the previously colorless solution changed to a brown supernatant over a black solid. The ^1H NMR spectrum of the mixture consisted of very broad peaks with chemical shifts consistent with both **10** and $(Cp)_2Co^{II}$. Heating the solution at 100 °C for 1 h resulted in the production of **6** (0.0072 mmol, 45%) however all of the signals in the ^1H NMR spectrum remained broad. Heating at 100 °C for an additional 3 h resulted in a small increase in the concentration of **6** (0.0075 mmol, 47%) but the signals were significantly sharper.

Thermolysis of methanol in acidic solution. A Teflon valve sealed NMR tube was charged with methanol (0.1 μL, 0.002 mmol), 50% HBF_4/H_2O (4.4 μL, 0.035 mmol) and dioxane (0.1 μL, int. std.) dissolved in 0.35 mL D_2O. The sample was then placed in a 130 °C oil bath and the signal due to methanol (3.34 ppm) was examined periodically by ^1H NMR spectroscopy. Over the course of the observation (8 d) the concentration of methanol slowly decreased from 7 to 5 mM. For a more detailed discussion of the results see Appendix A: Low methanol yield and accompanied text below.

Decomposition of methanol after production from thermolysis of 10. A Teflon cap sealed NMR tube was charged with **10** (1.2 mg, 0.002 mmol), 50% HBF_4/H_2O (4.4 μL, 0.035 mmol) and dioxane (0.1 μL, int. std.) dissolved in 0.35 mL D_2O. The sample was placed in a 130 °C oil bath and examined periodically by ^1H NMR spectroscopy. Signals for methanol (3.34 ppm) and the Pt^{IV}-CH_3 of **10** (2.83 ppm, $^2J_{Pt\text{-}H}$ = 66 Hz) were followed until both methanol and **10** were no longer observed (3 d). For a more detailed discussion of the results see **10** and accompanied text below.

Mercury drop test for the production of methanol from thermolysis of 10 in acidic solution. A Teflon cap sealed NMR tube was charged with 1.7 mg (0.0035 mmol) of **10**, 50% HBF_4/H_2O (4.4 μL, 0.035 mmol) and dioxane (0.1 μL, int. std.) dissolved in D_2O (0.35 mL) with a drop of mercury. The sample was then placed in a 130 °C oil bath and examined periodically by ^1H NMR spectroscopy.

Signals for methanol (3.34 ppm) and the Pt^{IV}-CH_3 of **10** (2.82 ppm, $^2J_{Pt-H}$ = 63 Hz) were followed until the concentration of methanol stabilized (3.5 mM) and **10** was no longer observed (73 h). For a more detailed discussion of the results see Figure 4.31 and accompanied text below.

Thermolysis of 10 in acidic H_2O solution. A Teflon valve sealed NMR tube was charged with **10** (1.2 mg, 0.002 mmol), 50% HBF_4/H_2O (5.0 μL, 0.04 mmol) and dioxane (0.1 μL, int. std.) dissolved in 0.4 mL of H_2O (0.4 mL). The sample was placed in a 120 °C oil bath and examined periodically by ^1H NMR spectroscopy until **10** was no longer observed (48 h). Upon completion signals consistent with 7 (2.38, 2.49, 6.17 and 6.88 ppm) **8** (2.03, 2.39, 2.4, 2.50, 6.04, 6.20 and 7.17 ppm) and methanol (3.35 ppm) were observed. Yield: methanol (49% from signal at 3.35 ppm), 7 (43% from methine signal at 6.88 ppm), **8** (43% from methine signal at 7.17 ppm).

Thermolysis of 10 in acidic D_2O solution. A stock solution was prepared from **10** (10.2 mg, 0.021 mmol), 50% HBF_4/H_2O (44 μL, 0.35 mmol) and dioxane (0.1 μL, int. std.) dissolved in 3.5 mL D_2O. A Teflon valve sealed NMR tube was charged with 0.75 mL of the stock solution. The sample was then placed in a 140 °C oil bath and examined periodically by ^1H NMR spectroscopy until **10** was no longer observed (17 h). Upon completion, signals consistent with **7** (2.38, 2.49 and 6.17 ppm) **8** (2.03, 2.38, 2.47, 2.49, 6.03 and 6.19 ppm) and methanol (3.34 ppm) were observed. Yield: methanol (49% from signal at 3.34 ppm), **7** (43% from methine signal at 6.17 ppm) and **8** (43% from methine signal at 6.03 ppm).

Thermolysis of 10 in acidic D_2O solution with excess methanol. A Teflon valve sealed NMR tube was charged with **10** (9.8 mg, 0.019 mmol), 50% HBF_4/H_2O (44 μL, 0.350 mmol), methanol (9 μL, 0.222 mmol) and dioxane (0.1 μL, int. std.) dissolved in 0.35 mL D_2O. The sample was then placed in a 140 °C oil bath and examined periodically by ^1H NMR spectroscopy. Signals for the Pt^{IV}-CH_3 of **10**

(2.83 ppm, $^{2}J_{Pt\text{-}H}$ = 69 Hz) were followed until **10** was no longer observed (8 h). Upon completion signals consistent with 7 (2.38, 2.49 and 6.17 ppm) **8** (2.03, 2.39, 2.47, 2.49, 6.03 and 6.19 ppm) and methanol (3.34 ppm) were observed. The yield of **7** and **8** were not determined due to loss of signal for the pyrazolyl protons. The methanol yield was negative likely due to the heterogeneous decomposition of methanol described below.

Kinetic studies of the thermolysis of 10 in the presence of 7 & 8. A stock solution was made 100 mM in HBF_4 and CD_3OD by adding 50% HBF_4/H_2O (0.125 mL, 0.996 mmol of HBF_4) and CD_3OD (0.041 mL, 1.01 mmol) to D_2O (9.83 mL). A stock solution that was 32 mM in **10** and 100 mM in HBF_4 and CD_3OD was prepared by dissolving **10** in (13.6 mg, 0.028 mmol) the HBF_4/CD_3OD stock solution (0.865 mL). A 0.4 mL aliquot was transferred to a Teflon cap sealed NMR tube. The sample was heated at 120 °C and examined periodically by ^{1}H NMR spectroscopy until **10** was no longer observed (20 h). Conversion of **10** to **7** and **8** (**Pt_{prod}**) was assumed to be 100% making the sample 32 mM in **Pt_{prod}**. A 0.1 mL aliquot of the **10**/HBF_4/CD_3OD stock solution was diluted by the addition of 0.3 mL of the HBF_4/CD_3OD stock solution. Similar to above, the sample was converted to **Pt_{prod}** (8 mM) but required between 21 and 36 h of heating at 120°C. Both samples (8 and 32 mM in **Pt_{prod}**) were made 2 mM in **10** by evaporating 0.1 mL aliquots of a stock solution of **10** (2.2 mg, 0.004 mmol) in D_2O (0.56 mL) then dissolving the residue in both the 8 mM and 32 mM **Pt_{prod}**/HBF_4/CD_3OD solutions. The **10**/ **Pt_{prod}** /HBF_4/ CD_3OD solutions were then heated at 100 °C and followed by ^{1}H NMR spectroscopy. Signals for the Pt^{IV}-CH_3 of **10** (2.82 ppm, $^{2}J_{Pt\text{-}H}$ = 66 Hz) were followed through at least three half-lives (3 h).

Calculated k_{obs} based on concentration of 7 and 8 determined from K_{eq}.

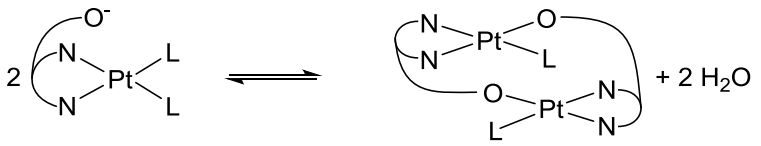

7 **8**

1) $K_{eq} = \frac{[\mathbf{8}][H_2O]^2}{[7]^2}$; $K_{eq}{}' = \frac{K_{eq}}{[H_2O]^2}$; Solve for [**8**]

2) $[NNOPt]_{tot} = [7] + 2[\mathbf{8}]$; Replace [**8**] with solution from equation 1

3) $2K_{eq}{}'[7]^2 + [7] - [NNOPt]_{tot} = 0$; Use quadradic equation to find [7]

$K_{eq}{}'$ = 85 ± 5; From Van't Hoff studies of equilibrium between **7** and **8** (see Chapter 2)

$[NNOPt]_{tot}$ = [**10**$_{init.}$] thermalized to **7** and **8** (assumes 100% conversion) = 8 or 32 mM

The change in [**7**], found when the [**Pt$_{prod}$**] changes from 8 to 32 mM, was used to calculate an expected k_{obs} (assuming a 1st order contribution from **7**). The procedure was repeated for **8** and **NNOPt$_{tot}$**.

Exp. k_{obs} (s^{-1}) when [NNOPt$_{tot}$] = 8 mM	1.75×10^{-4}
Exp. k_{obs} (s^{-1}) when [NNOPt$_{tot}$] = 32 mM	5.53×10^{-4}
Factor of increase in k_{obs}	3.2

	Calc. [7] (mM)	**Calc. [8] (mM)**
When [NNOPt$_{tot}$] = 8 mM	4.52	1.74
When [NNOPt$_{tot}$] = 32 mM	11.1	10.5

	If 1st order in 7	**If 1st order in 8**	**NNOPt$_{tot}$**
Exp. k_{obs} (s^{-1}) when [NNOPt$_{tot}$] = 8 mM	1.75×10^{-4}	1.75×10^{-4}	1.75×10^{-4}
Calc. k_{obs} (s^{-1}) when [NNOPt$_{tot}$] = 32 mM	4.29×10^{-4}	10.5×10^{-4}	7.00×10^{-4}
Factor of increase in k_{obs}	2.5	6.0	4

Thermolysis of 10 in the presence of Pt_{prod} with varying concentration of methanol (75 and 100 mM). A stock solution that was 100 mM in HBF_4 and 75 mM in methanol was prepared by combining 50% HBF_4/H_2O (0.215 mL, 15.9 mmol), methanol (0.061 mL, 1.51 mmol) and dioxane (2.0 μL, int. std.) diluted to 20 mL with D_2O. A Teflon valve sealed NMR tube was charged with **10** (1.98 mg, 0.004 mmol) dissolved in the HBF_4/methanol stock solution (0.35 mL). A 150 mM methanol stock solution was prepared by adding methanol (11 μL, 0.272 mmol) to a 3.5 mL aliquot of the HBF_4/methanol stock solution. A Teflon valve sealed NMR tube was charged with **10** (2.00 mg, 0.004 mmol) dissolved in 0.35 mL of the HBF_4/methanol stock solution. The samples were heated (140 °C for 4.5 h) until all of **10** had been converted to **7**, **8** and methanol by ^{1}H NMR spectroscopy. **10** was then added to each tube (580 mg : 75 mM methanol, 520 mg : 150 mM methanol). The samples were placed in a 140 °C oil bath and examined periodically by ^{1}H NMR spectroscopy. The signal for the Pt^{IV}-CH_3 of **10** (2.81 ppm, $^2J_{Pt\text{-}H}$ = 65 Hz) was followed through three half-lives of the decomposition of **10**. The resulting first-order rate constants for the decomposition of **10** were similar (k_{obs}(75 mM) = 8.0 x 10^{-4} s^{-1} and k_{obs}(150 mM) = 8.2 x 10^{-4} s^{-1}).

Thermolysis of 10 in acidic D_2O solution in the presence of 100 mM boric acid. A Teflon cap sealed NMR tube was charged with **10** (2.2 mg, 0.004 mmol), 50% HBF_4/H_2O (9.4 μL, 0.075 mmol), $B(OH)_3$ (4.8 mg, 0.078 mmol) and dioxane (0.1 μL, int. std.) dissolved in D_2O (0.75 mL). The sample was placed in a 140 °C oil bath and examined periodically by ^{1}H NMR spectroscopy. The signal for the Pt^{IV}-CH_3 of **10** (2.82 ppm, $^2J_{Pt\text{-}H}$ = 65 Hz) was followed through three half-lives of the decomposition of **10**. The resulting changes in the rate of decomposition of **10** were very similar to the decomposition of **10** without added $B(OH)_3$ (Figure 4.25).

Crystallographic characterization of compound $10H^+$.

Table 4.1. Crystallographic data for **10**H^+.

Parameter	**10**H^+
Empirical formula	C13 H21 B F4 N4 O5 Pt
Formula weight	595.24
Temperature	110(2) K
Wavelength	0.71073 Å
Crystal system	Triclinic
Space group	P -1
Unit cell dimensions	a = 9.021(3) Å b = 10.567(4) Å c = 11.231(5) Å
Volume	947.2(6) $Å^3$
Z	2
Density (calculated)	2.087 Mg/m^3
Absorption coefficient	7.478 mm^{-1}
F(000)	572
Crystal size	0.02 x 0.02 x 0.01 mm^3
Theta range for data collection	2.01 to 28.45°.
Index ranges	-11<=h<=12, -14<=k<=14, -14<=l<=14
Reflections collected	15340
Independent reflections	4650 [R(int) = 0.1606]
Completeness to theta = 25.00°	99.9 %
Max. and min. transmission	0.9290 and 0.8648
Refinement method	Full-matrix least-squares on F^2
Data / restraints / parameters	4650 / 0 / 258
Goodness-of-fit on F^2	0.993
Final R indices [I>2sigma(I)]	R1 = 0.0803, wR2 = 0.1779

Appendix A: Low methanol yield

As described above, complete thermolysis of **10** under both alkaline (pD = 9.8) and acidic (pD = 1.4) conditions resulted in significantly lower than expected production of methanol (24% and 40% yield respectively). Increasing the delay time from 2 s during collection of the methanol signal by ^{1}H NMR spectroscopy, which was used for calculating the yields above, to 120 s resulted in an increase of methanol yield from the alkaline solution to 40% and the acidic solution to 72 %. In both cases the yield increased by a factor of 1.7. However, insufficient delay time does not entirely correct the methanol yields to what seems reasonable (> 90%).

The reaction conditions under which the thermolysis of **10** was observed also caused the decomposition of methanol. In the absence of **10** no change in the [CH_3OH] (7 mM) was observed after heating a D_2O solution (100 mM HBF_4) at 100 °C for 1 d. Increasing the temperature to 130 °C (similar to the conditions under which the thermolysis of **10** was studied) resulted in slow decomposition of methanol (Figure 4.31). After 1.5 days, a similar amount of time required to completely thermalize a 7 mM solution of **10**, 15% of the methanol transformed to a combination of formaldehyde (4.81 ppm), formic acid (8.22 ppm) and methyl formate (8.21 and 3.65 ppm) by ^{1}H NMR spectroscopy. From these results it appears that methanol is unstable under the reaction conditions resulting in a low yield.

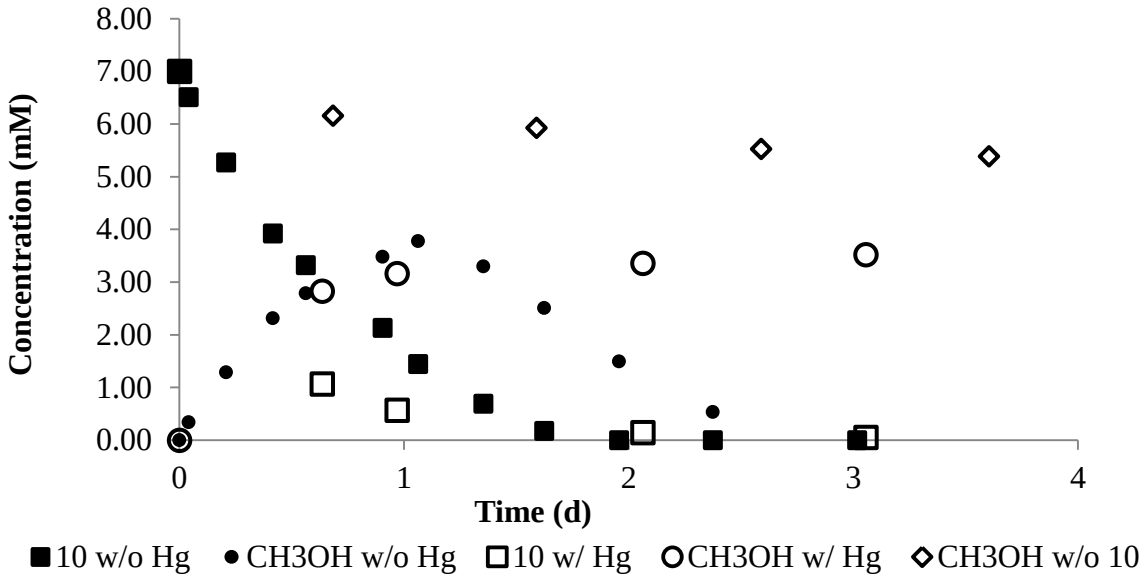

Figure 4.31. Thermolysis of **10** in 100 mM HBF_4/D_2O at 130 °C w/ and w/o a drop of Mercury as well as decomposition of methanol in the absence of NNOPt.

In addition to the acid assisted oxidation of methanol, a heterogeneously catalyzed decomposition of methanol was also observed. Following the thermolysis of **10** (7 mM) by ^{1}H NMR spectroscopy, a peak methanol yield of 54% was observed after 1 day at 130 °C in 100 mM HBF_4/D_2O (Figure 4.31). The yield of methanol then fell to zero after 3 days of heating. Thus this decomposition occurred at a faster rate ($t_{1/2}$: 1 d) than expected for the acid catalyzed oxidation of methanol ($t_{1/2}$: 8 d). Only **7**, **8** and methanol were observed as significant products by ^{1}H NMR spectroscopy. Due to this reaction profile, the possibility of a reaction between the products of thermolysis of **10** (**7**, **8** or Pt^0) with methanol was considered. The thermolysis of **10** and was followed by ^{1}H NMR spectroscopy but with the addition of a drop of Hg^0 (Figure 4.31). The conversion of **10** was similar to the reaction in which no Hg^0 was added. The maximum yield of methanol reached a similar peak (50%) to the reaction without Hg^0 (54%) but in the presence of Hg^0 the concentration of methanol stabilized (coincident with nearly

complete conversion of **10** (98%)) rather than decreasing to zero consistent with decomposition of methanol being catalyzed by a heterogeneous platinum material.

The product(s) of the acid catalyzed oxidation of methanol (formaldehyde, formic acid and methyl formate) were not detected during the thermolysis of **10** in the presence of Hg^0. In D_2O the only significant products from the thermolysis of **10** were **7**, **8** and methanol. The thermolysis of **10** in H_2O gave the same result eliminating deuteration as a cause of low methanol detection. Analyzing the products of thermolysis (T = 130°C) of **10** (33.44 mM) under acidic conditions ([HBF_4] = 132 mM) by ^{13}C NMR spectroscopy only **7**, **8** and methanol were observed. Complete oxidation of methanol to CO or CO_2 would leave the products undetectable by ^1H NMR spectroscopy and potentially at such low concentrations, due to dispersion in the head space of the sealed NMR tube, that they would be very difficult to detect by ^{13}C NMR spectroscopy.

In summary, the low methanol yield seems to be due to a combination of insufficient delay time when collecting ^1H NMR spectroscopy data, decomposition of methanol produced by thermolysis of **10** due to high temperature (> 120°C) and acidic conditions (pH < 2) and a heterogeneous decomposition route due to production of Pt^0. No products that could be associated with the decomposition of methanol were observed by ^1H NMR or ^{13}C NMR spectroscopy during the thermolysis of **10** in either alkaline or acidic solution. This may be due to oxidation of methanol to CO or CO_2.

---

[1] (a) Stahl, S. S.; Labinger, J. A,; Bercaw, J. E. *Angew. Chem. Int. Ed.* **1998**, *37*, 2180 and references therein. (b) Parshall, G. W.; Ittel, S. D. *Homogeneous Catalysis: The Applications and Chemistry of Catalysis by Soluble Transition Metal Complexes,* 2nd ed.; Wiley-Interscience: New York, 1992. (c) Gol'dshleger, N. F.; Es'kova, V. V.; Shilov, A. E.; Shteinman, A. A. *Zh. Fiz. Khim.* **1972**, *46*, 1353. (d) Shilov, A. E.; Shul'pin, G. B. *Activation and Catalytic Reactions of Saturated Hydrocarbons in the Presence of Metal Complexes*; Kluwer Academic Publishers: Boston, 2000. (e) Periana, R. A.; Taube, D. J.; Gamble, S.; Taube, H.; Satoh, T.; Fujii, H. *Science* **1998**, *280*, 560.

[2] (a) Luinstra, G. A.; Labinger, J. A.; Bercaw, J. E. *J. Am. Chem. Soc*. **1993**, *115*, 3004. (b) Williams, B. S.; Goldberg, K. I. *J. Am. Chem. Soc*. **2001**, *123*, 2576. (c) Pawlikowski, A. V.; Getty, A.; Goldberg, K. I. *J. Am. Chem. Soc*. **2007**, *129*, 10382.
[3] Spessard, G. O.; Miessler, G. L. *Organometallic Chemistry*, 2nd ed.; Oxford University Press: New York, 2010.
[4] (a) Binfield, S. A.; Zavalij, P. Y.; Khusnutdinova, J. R.; Vedernikov, A. N. *J. Am. Chem. Soc.* **2006**, 1*28*, 82. (b) Khusnutdinova, J. R.; Zavalij, P, Y.; Vedernikov, A. N. *Organometallics* **2007**, *26*, 3466.
[5] Patai, S.; Rappoport, Z.; Stirling, C. J. M. *The Chemistry of Sulphones and Sulphoxides* John Wiley & Sons: New York, 1988.
[6] Otero, A.; Fernández-Baeza, J.; Tejeda, J.; Antiñolo, A.; Carrillo-Hermosilla, F.; Díez-Barra, E.; Lara-Sánchez, A.; Fernández-López, M. *J. Chem. Soc., Dalton Trans*., **1999**, 3537.
[7] March, J.; Smith, M. B. *March's Advanced Organic Chemistry*, 6th ed.; John Wiley & Sons: Hoboken, 2007.
[8] Weinberg, D. R.; Labinger, J. A,; Bercaw, J. E. *Organometallics* **2007**, *26*, 167.
[9] Rostovtsev, V. V; Henling, L. M.; Labinger, J. A.; Bercaw, J. E. *Inorg. Chem.* **2002**, *41*, 3608.
[10] (a) Johansson, L.; Ryan, O. B.; Romming, C.; Tilset, M. *Organometallics* **1998**, *17*, 3957. (b) Lanci, M. P.; Remy, M.S.; Lao, D. B.; Sanford, M. S.; Mayer, J. M. *Organometallics* **2011**, *30*, 3704 (c) Khusnutdinova, J. R.; Rath, N. P.; Mirica, L. M. *J. Am. Chem. Soc.* **2010**, *132*, 7303. (d) Khusnutdinova, J. R.; Rath, N. P.; Mirica, L. M. *J. Am. Chem. Soc.* **2012**, *134*, 2414.
[11] (a) Stephen, E.; Blake, A. J.; Davies, E. S.; McMaster, J.; Schroder, M. *Chem. Commun.* **2008**, 5707. (b) Justin J. Wilson and Stephen J. Lippard *Inorg. Chem.* **2012**, *51*, 9852.
[12] Roberts, J. R.; Sawyer, D. T. *Acc. Chem. Res.* **1988**, *21*, 469.
[13] Choi, K. S.; Lai, T. H.; Lee, S. Y.; Chan, K. S. *Organometallics* **2011**, *30*, 2633.
[14] See experimental section of Chapter 4 for details
[15] Grice, K. A.; Scheuermann, M. L.; Goldberg, K. I. *Top. Organomet. Chem.* **2011**, *35*, 1.
[16] Beck, A.; Barth, A.; Hubner, H.; Burzlaff, N. *Inorg. Chem.* **2003**, *42*, 7182.

Chapter 5 : A novel facially coordinating NNN ligand containing a sulfonyl amidate hemilabile arm.

Introduction

In the catalytic cycle proposed by Shilov the platinum catalyst is required to transition between the Pt^{II} and Pt^{IV} oxidation states (Figure 5.1).[1] As a consequence, the geometric arrangement of ligands around the platinum center alternate between square planar (Pt^{II}) and octahedral geometry (Pt^{IV}). Tridentate ligands containing a hemilabile arm like the NNO ligand **1** (Figure 1.10) and Vedernikov's dpms system (Figure 1.7) are capable of accommodating square planar and octahedral arrangement.[2] The flexible coordination of these ligand systems enhances the aerobic oxidation of Pt^{II} to Pt^{IV} while still allowing for facile transformation back to the Pt^{II} state. In practice, these systems are competent for performing two key steps in the catalytic transformation of methane to methanol (oxidation and C-O coupling).[3]

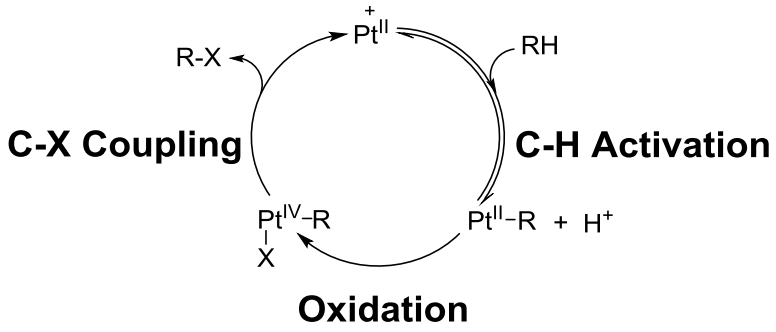

Figure 5.1. Proposed catalytic cycle for alkane functionalization.

The promise of this ligand architecture motivated the synthesis of a novel NNN ligand (bis(3,5-dimethylpyrazol-1-yl)-N-phenylsulfonylacetamide (**15**, Figure 5.2)). The electron-withdrawing sulfonyl and carbonyl groups attached to the nitrogen in the hemilabile arm are expected significantly reduce the basicity of the anionic nitrogen.[4,5] The result may be a stabile anionic nitrogen in an aqueous solution at near neutral pH rather than strongly basic conditions typically required. Of particular interest is the potential to tune the lability of the hemilabile arm by altering electronic and steric properties through a phenyl ring substituent (-R, Figure 5.2). With a focus on electronic properties, versions of **15** with a methyl, hydrogen and chloro substituent were synthesized.

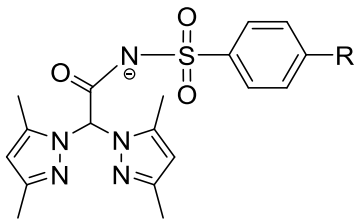

NNN

Figure 5.2. bis(3,5-dimethylpyrazol-1-yl)-N-phenylsulfonylacetamide R = H, CH_3 and Cl.

The substituents were chosen based on their Hammett para parameter (CH_3: -0.17, H: 0.00, Cl: 0.23) which when incorporated into **15** should provide a range of electron density at the amidate nitrogen. Assuming the amidate N is bound to Pt when NNN is facially coordinated to Pt^{IV}, the electron donating methyl group should produce a stronger Pt^{IV}-N bond whereas a weaker Pt^{IV}-N bond should result when the electron withdrawing chloro group is bound to the amidate arm. The variant in which R = H should have an intermediate Pt^{IV}-N bond strength. Ultimately, this should allow us to probe the effect of lability of the hemilabile arm on Shilov chemistry. In particular, is the need for ligand association to promote oxidation of the Pt center at odds with ligand dissociation required for facile C-O

coupling? With this system we should be able to compare the rates of oxidation and C-O coupling between NNNPt(CH_3) variants to improve the design of these types of ligands.

We were able to synthesize three different NNN variants (R = H, CH_3 and Cl), then bind the ligands to a Pt^{II} center. The reactivity of the NNNPt system, when R = H and CH_3, is very similar to the NNO system in regards to protonolysis of a $NNNPt^{II}$-CH_3 generating methane, oxidation of $NNNPt^{II}CH_3(OH)$ by H_2O_2 and reductive elimination of methanol from $NNNPt^{IV}CH_3(OH)_2$. This work was performed with assistance from undergraduate researcher Sarah Jablonski while Dr. Luc Boisvert made significant contributions to both the ligand design and synthesis.

Results and Discussion

Synthesis of NNN variants

The NNN ligands were synthesized by a pathway analogous to the synthesis of the NNO (**2**) ligand (Figure 5.3). Bis(3,5-dimethyl-1-pyrazolyl)methane was transformed into a strong nucleophile through removal of a methylene proton on the central carbon. Nucleophilic attack of the deprotonated bis(3,5-dimethyl-1-pyrazolyl)methane on the isocyanate C connected the two molecules through a C-C bond. Similar to the NNO ligand, platination of the lithium salt of NNN proved to be difficult. The ligand was far more reactive as a potassium salt which was produced by protonation of the NNN lithium salt followed by deprotonation by KH. Using this method three NNN variants where R = CH_3, H and Cl were synthesized.

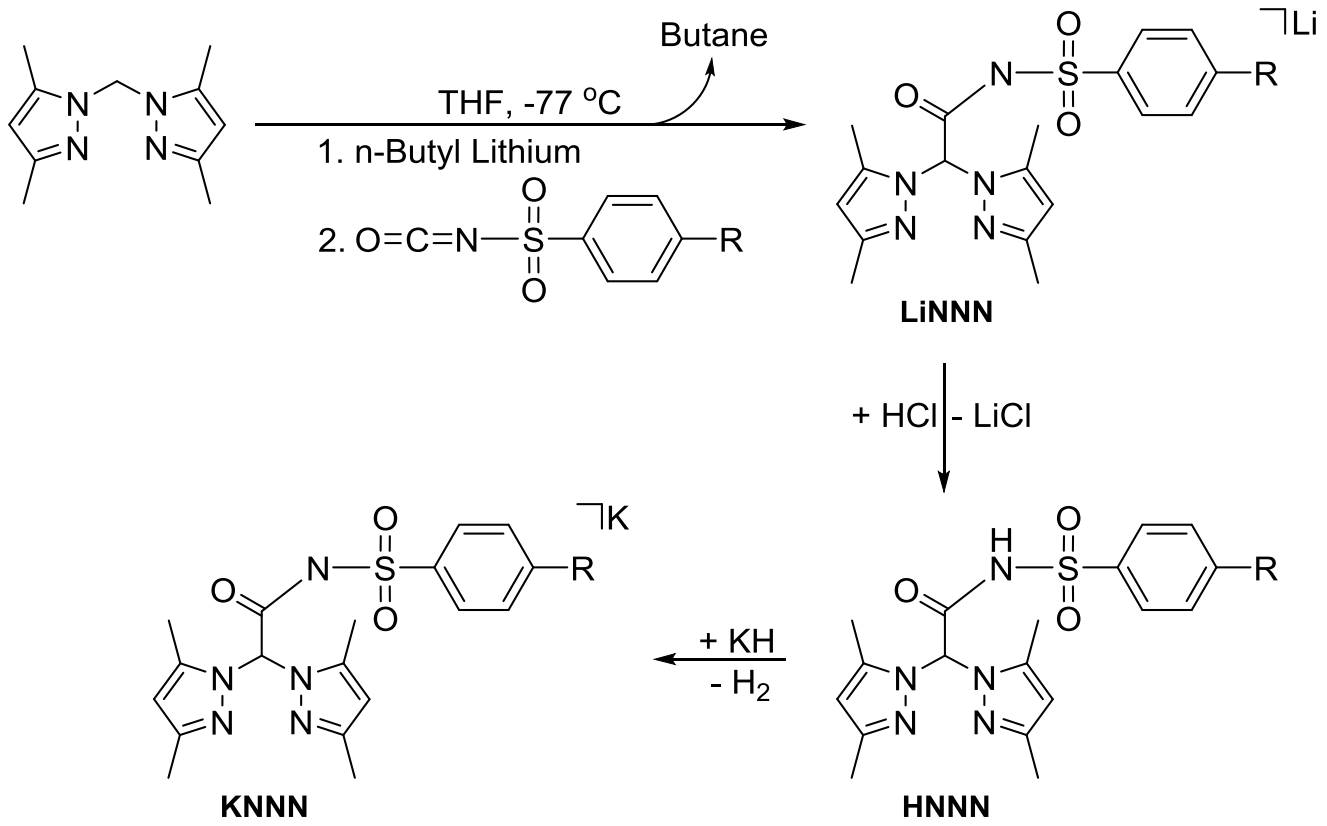

Figure 5.3. General scheme for synthesis of NNN ligand.

The structure of the ligands was determined using ^{1}H NMR spectroscopy. In the conjugate acid of the R = CH_3 version of NNN (**16**, Figure 5.4), the methyl group in the hemilabile arm was observed as a singlet (2.39 ppm). The two singlets associated with the methyl groups bound to the pyrazolyl rings (2.12 and 2.14 ppm) support a C_s symmetry. The aromatic hydrogens in sulfonyl amide arm were observed as two doublets (in all cases coupling beyond three bonds were not sufficiently resolved) centered at 7.28 ppm ($^{3}J_{H\text{-}H}$: 8 Hz) and 7.98 ppm ($^{3}J_{H\text{-}H}$: 8 Hz). The ^{1}H NMR spectrum of the potassium salt (**17**, Figure 5.4) was similar but shifted from **16**. A broad peak at 3.14 ppm may be due to the N bound proton in the sulfonyl amidate arm.

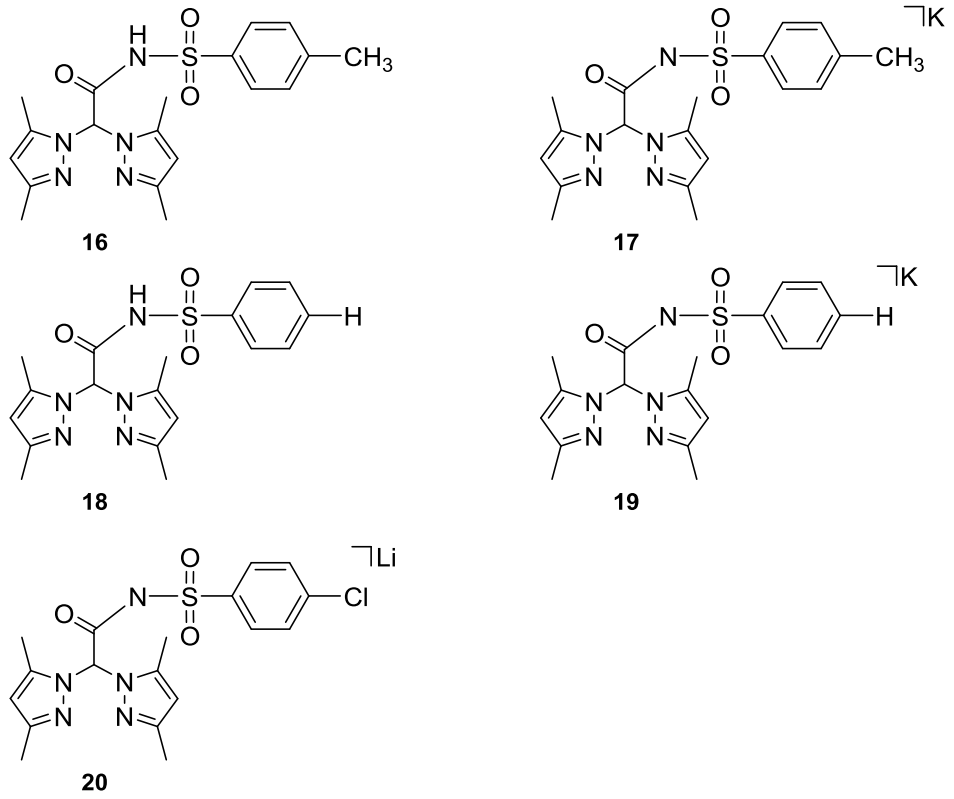

Figure 5.4. Conjugate acid and potassium salt of the R = CH and H and lithium salt of the R = Cl variants of the NNN ligand.

In the conjugate acid form of the R = H variant (**18**, Figure 5.4) the two ortho aromatic hydrogens in the sulfonyl amide arm appeared as a doublet at 8.16 ppm ($^3J_{H\text{-}H}$: 7 Hz), the two meta aromatic hydrogens appeared as a triplet at 7.55 ppm ($^3J_{H\text{-}H}$: 7 Hz) and the single para aromatic hydrogen appeared as a triplet at 7.65 ppm ($^3J_{H\text{-}H}$: 7 Hz). These signals were matched by signals associated with the other expected groups in the NNN ligand. In particular, the singlet (5.81 ppm) for the two aromatic hydrogens on the pyrazolyl rings supports a C_s symmetry. A signal consistent with a proton bound to the sulfonyl amidate was not observed which may be due to rapid exchange with H_2O present due to insufficient drying of sample after acidification. The formation of the $NNNPt^{IV}$ hydrido species (Figure 5.5) is consistent with reaction of the conjugate acid form of NNN (**18**) with Pt^{II}. The

potassium salt (**19**, Figure 5.4) was prepared *in situ* for platination but was not isolated or examined by ^{1}H NMR spectroscopy.

In the lithium salt of the NNN ligand R = Cl variant (**20**, Figure 5.4) the two ortho aromatic hydrogens in the sulfonyl amidate arm appeared as a doublet at 7.93 ppm ($^3J_{H\text{-}H}$: 9 Hz) while the two meta aromatic hydrogens appeared as a doublet at 7.45 ppm ($^3J_{H\text{-}H}$: 9 Hz). Indicative of a C_s symmetry, the two aromatic hydrogens on the pyrazolyl rings appeared as a singlet (5.81 ppm). Acidification of an H_2O solution (pH < 1) of **20** did not result in protonation based on identical ^{1}H NMR spectrum before and after acidification. Additionally, no reaction occurred upon the addition of **20** with $[Pt(CH_3)_2S(CH_3)_2]_2$ which is consistent with the low reactivity of the Li salt of the similar NNO ligand.

Platination of NNN ligands

Combining **18** with $[Pt(CH_3)_2S(CH_3)_2]_2$ in CD_2Cl_2 gave a mixture of C_s and C_1-symmetric κ^3-NNNPt^{IV}$(CH_3)_2$H isomers (**21$_{ax}$** and **21$_{eq}$** respectively, Figure 5.5). Early in the reaction the isomers were in a 9:1 ratio of **21$_{ax}$** : **21$_{eq}$** but after 24 h **21$_{eq}$** became the major species (1:4). This reactivity is the opposite from the NNO system (Chapter 2) which may be due to increased steric congestion from the bulky amidate arm.

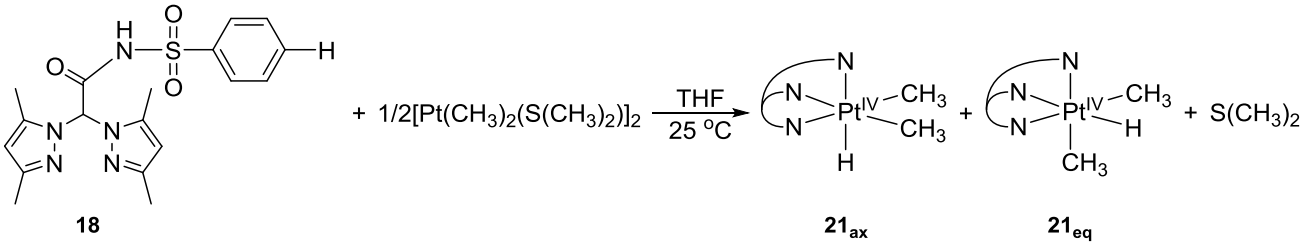

18 **21$_{ax}$** **21$_{eq}$**

Figure 5.5. Reaction of NNN acid (**18**) with dimethyl platinum(II) source.

The hydride in the C_s-symmetric isomer **21$_{ax}$** was observed in the ^{1}H NMR spectrum (CD_2Cl_2) as a singlet at -21.82 ppm with ^{195}Pt satellites ($^1J_{Pt\text{-}H}$: 1532 Hz). The upfield shift and large coupling

constant are characteristic of Pt hydrides and similar chemical shifts and coupling constants have been reported for a variety of Pt^{IV} hydrides.[6] The two chemically equivalent methyl groups bound to Pt were observed in the ^{1}H NMR spectrum as a singlet with a chemical shift of 1.59 ppm and ^{195}Pt satellites ($^{2}J_{Pt\text{-}H}$: 70 Hz). Similar chemical shifts and coupling constants have been reported for a variety of Pt^{IV} methyls.[7]

The hydride in the C_1-symmetric isomer **21$_{eq}$** was observed in the ^{1}H NMR spectrum as a singlet at -21.22 ppm with Pt satellites ($^{1}J_{Pt\text{-}H}$: 1451 Hz). The two Pt^{IV}-CH_3 groups in **21$_{eq}$** are not chemically equivalent with chemical shifts of 1.25 and 1.53 ppm and corresponding two-bond coupling with platinum of 70 and 71 Hz respectively. Again, for both the Pt^{IV}-H and Pt^{IV}-CH_3 complexes, similar chemical shifts and coupling constants have been reported for a variety of Pt^{IV} complexes.[7,8]

Dimethyl NNN Pt^{II} complexes K[κ^2-NNNPt$(CH_3)_2$] (**22** and **23**) were produced from the reaction of **17** or **19**, respectively, with $[PtMe_2(SMe_2)]_2$ in THF (Figure 5.6). Complex **22** was characterized by the six Pt^{II}-CH_3 hydrogens observed as a singlet at 0.41 with characteristic ^{195}Pt satellites (87 Hz) supporting C_2 symmetry. Complex **23** showed a similar ^{1}H NMR spectrum with the six Pt^{II}-CH_3 hydrogens observed as a singlet at 0.39 with characteristic ^{195}Pt satellites (83 Hz) supporting a C_2 symmetric structure.

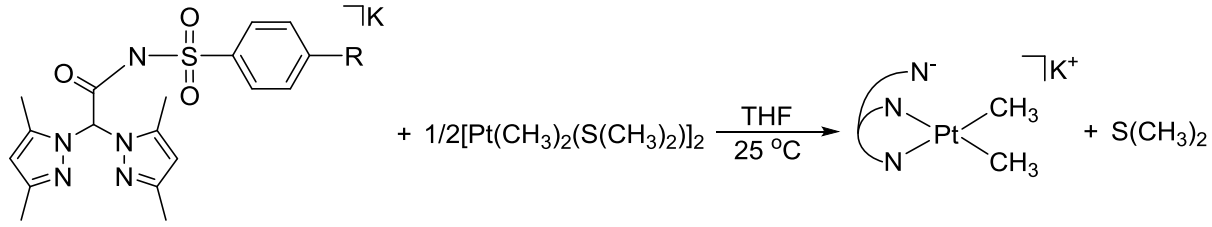

R: CH_3 (**17**) **22**

R: H (**19**) **23**

Figure 5.6. Reaction of NNN potassium salt with dimethyl platinum(II) source.

Reactivity of NNN Platinum(II) dimethyl compounds with H_2O

Dissolution of **22** or **23** in H_2O at 22 °C results in slow protonlysis of a Pt^{II}-CH_3 producing methane and a monomethyl Pt^{II} complex K[κ^2-NNNPt^{II}(CH_3)(OH)] (**24** or **25**, respectively, Figure 5.7). At 60 °C the reactions were complete in 1 h similar to the reaction of dimethyl NNOPt^{II} (**5**). In the product mixture, **24** was observed by ^{1}H NMR spectroscopy with the Pt^{II}-CH_3 at 0.43 ppm and characteristic ^{195}Pt satellites ($^2J_{Pt\text{-}H}$: 78 Hz). The pyrazolyl methyl groups in **24** appear as four singlets (2.21, 2.25, 2.38, 2.39 ppm) consistent with C_1 symmetry. Similar protonolysis reactions with other nitrogen ligated platinum(II) dimethyl complexes have been reported in water and methanol.[8] Complex **25** presented a similar ^{1}H NMR spectrum with the Pt^{II}-CH_3 signal at 0.45 ppm and characteristic ^{195}Pt satellites ($^2J_{Pt\text{-}H}$: 81 Hz). The pyrazolyl methyl groups in **25** appear as four singlets (2.15, 2.19, 2.32, 2.33 ppm) consistent with C_1 symmetry.

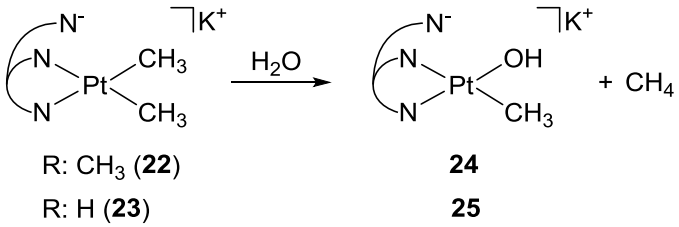

Figure 5.7. Protonolysis of NNNPt^{II}-CH_3 in H_2O.

Oxidation of monomethyl NNNPlatinum(II)

Addition of H_2O_2 to an H_2O solution of **24** or **25** resulted in oxidation to **26** or **27**, respectively (Figure 5.8). By ^{1}H NMR spectroscopy, the Pt^{IV}-CH_3 in **26** was observed as a singlet at 2.48 ppm with characteristic ^{195}Pt satellites ($^2J_{Pt\text{-}H}$: 71 Hz). The pyrazolyl bound methyl groups in **26** appear as four singlets (2.41, 2.42, 2.50, 2.53 ppm) consistent with C_1 symmetry. Complex **27** presented a similar ^{1}H NMR spectrum with the signal for the Pt^{II}- CH_3 at 2.47 ppm with ^{195}Pt satellites ($^2J_{Pt\text{-}H}$: 76 Hz). The pyrazolyl bound methyl groups in **27** appear as four singlets (2.40, 2.41, 2.49, 2.53 ppm) consistent with

C_1 symmetry. In both cases the monomethyl $NNNPt^{II}$ (**24** and **25**) were no longer observed in the ^1H NMR spectrum of the products however the low solubility of the monomethyl $NNNPt^{IV}$ products (**26** and **27**) impeded determination of the yield.

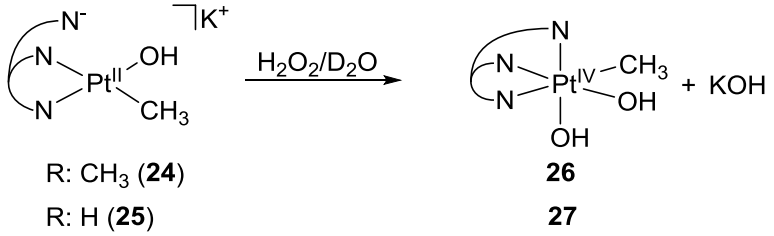

Figure 5.8. Oxidation of aqueous $NNNPt^{II}(CH_3)OH$ with H_2O_2.

Reactivity of aqueous monomethyl NNNPlatinum(II) with O_2

In Chapter 3 the reaction of monomethyl $NNOPt^{II}$ (**6**) with O_2 in neutral/basic resulted in the products of oxidation (**10**) and oxidative methyl transfer (**11** and **7**, Figure 5.9). The ^1H NMR spectrum of the products from the reaction of aqueous **24** or **25** with O_2 was complicated due to poor resolution of the multiple products. However, signals consistent with two Pt-CH_3 groups in a Pt^{IV} dimethyl species were observed from the reaction of **24** with O_2 (1.75, $^2J_{Pt\text{-}H}$: 71.7 Hz and 1.99 $^2J_{Pt\text{-}H}$: 78 Hz) or **25** with O_2 (1.71 $^2J_{Pt\text{-}H}$: 70 Hz and 1.96 $^2J_{Pt\text{-}H}$: 69 Hz) with O_2. These dimethyl $NNNPt^{IV}$ products support that some of the material is undergoing an oxidative methyl transfer reaction similar to that previously described in Chapter 3.

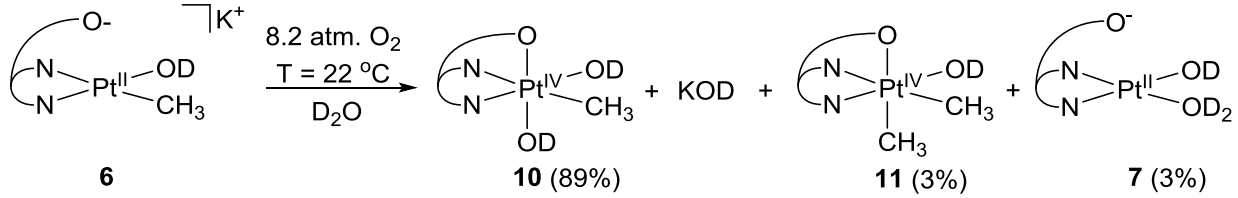

Figure 5.9. Reaction of **6** with dioxygen.

Thermolysis of monomethyl NNNPlatinum(IV)

Heating an H_2O/HBF_4 solution (pH = 1.5) of the monomethyl $NNNPt^{IV}$ species **26** at 150 °C for 3 h resulted in complete disappearance of **26** in the ^1H NMR spectrum and the production of methanol (3.35 ppm) and $NNNPt^{II}(OH)_2$ (**28**, Figure 5.10). The ^1H NMR spectrum of **28** shows only the signals associated with the NNN-CH_3 ligand, shifted from the free ligand (**17**). The NNOPt product possesses a C_s-symmetry (rather than the C_1-symmetry of **26**) supporting its identification as **28**. The product yields could not be determined due to poor solubility of **26** and the NNNPt product possibly due to dimerization of **28**.

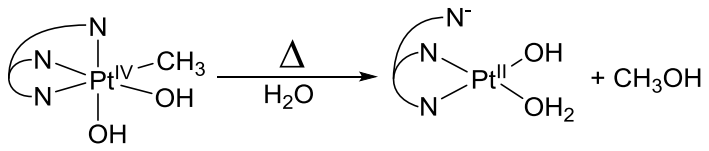

R: CH_3 (**26**) **28**

R: H (**27**) **29**

Figure 5.10. Thermolysis of $NNNPt^{IV}$-CH_3.

Thermolysis of **27** at 150 °C for 16 h in a buffered (KH_2PO_4/K_2HPO_4, pD = 7) D_2O solution resulted in complete conversion of **27** by ^1H NMR spectroscopy and the production of methanol (57%). The low methanol yield may be due to acid catalyzed oxidation of methanol as well as a heterogeneous decomposition of methanol discussed in Appendix A: Low methanol yield in Chapter 4. A NNN containing product with C_1-symmetry was observed which is consistent with dimerization of $NNNPt^{II}(OH)_2$ (**29**) similar to that observed in the NNO system (Figure 5.11). The observed low solubility of the products is also consistent with a dimerized product. In general, the products of thermolysis of **27** and **29** ($NNOPt^{II}(OH)_2$ and methanol) are similar to the products from the

thermolysis monomethyl NNOPt^{IV}(**7** and methanol) discussed in Chapter 4 and from the monomethyl dpmsPt^{IV} in the Vedernikov system[4a].

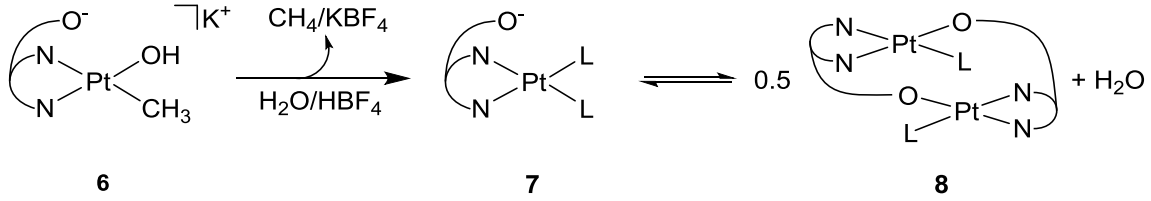

6 **7** **8**

Figure 5.11. Protonolysis of Pt^{II}-CH$_3$ of **6** in the NNO system. A similar dimerization for **28** and/or **29** is suspected in the NNN system.

The presence of a variety of basic regions in the hemilabile arm (lone pairs on O in carbonyl, lone pairs in N of amidate, lone pairs on O of sulfonyl and pi electrons in aromatic ring) make it difficult to determine which group is bound to Pt^{IV} upon coordination of the hemilabile arm. Crystals grown from an air-free ACN/pentane/Et$_2$O solution of **22** resulted in a dimethyl ethyl NNNPt^{IV} (**30**). While the reaction that created **30** is unknown the crystal structure clearly shows coordination of the amidate N to the platinum (IV) center (Figure 5.12).

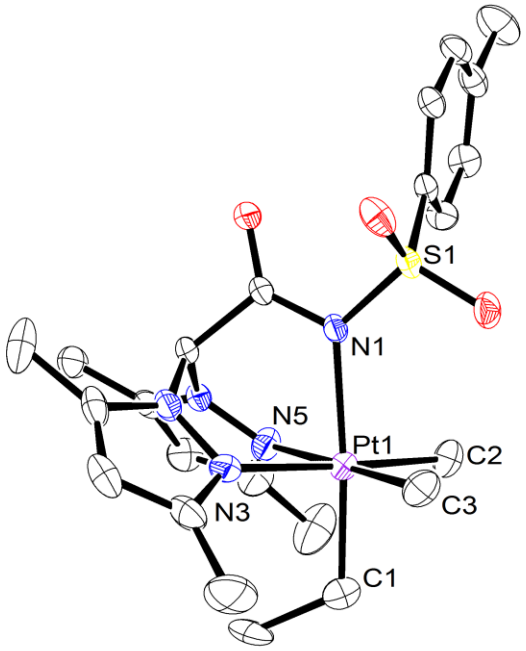

Figure 5.12. ORTEP of **30** ellipsoids at the 50% probability level. Hydrogen atoms are excluded for clarity. Selected bond distances (Å) and angles (°): Pt1-C1 = 2.654(3), Pt1-C2 = 2.034(3), Pt1-C3 = 2.048(3), Pt1-N1 = 2.203(2), Pt1-N3 = 2.168(2), Pt1-N5 = 2.180(2), N3-Pt1-C3 = 93.43(11), C3-Pt1-C2 = 87.62(13), C2-Pt1-N5 = 93.38(11), N5-Pt1-N3 = 85.54(10), N3-Pt1-N1 = 83.67(8), N3-Pt1-C1 = 92.98(11).

Conclusions

The novel NNN ligand coordinated to Pt performed similarly to the NNOPt system as well as Vedernikov's dpmsPt system in terms of protonlysis of a Pt-CH_3, aerobic oxidation of Pt^{II} to Pt^{IV} and reductive elimination of methanol from a monomethyl Pt^{IV}. Addition of the protonated form of the NNN ligand (**18**) to $[Pt(CH_3)_2S(CH_3)_2]_2$ results in a dimethyl hydrido Pt^{IV} species (**21**). When using the potassium salt of the NNN ligand (**17** or **19**) a dimethyl Pt^{II} species (**22** or **23** respectively) is produced. The dimethyl Pt^{II} complexes (**22** and **23**) undergo protonolysis when dissolved in water producing methane and monomethyl $NNNPt^{II}$ (**24** or **25** respectively) which can then be oxidized by H_2O_2 to monomethyl Pt^{IV} (**26** or **27** respectively). While not all of the products from the reaction of **24** or **25**

with O_2 were identified, a methyl transfer reaction occurred consistent to the reactivity of monomethyl NNOPt^{II}. Finally, heating the monomethyl NNNPt^{IV} (**26**) results in the production of methanol and a dihydroxy NNNPt^{II}. The crystal structure of the NNNPt^{IV} **30** shows that the hemilabile arm coordinates through the N in the hemilabile arm.

Similar to the NNO system the NNN architecture appears to be competent for two key steps in Shilov type chemistry: oxidation of monomethyl Pt^{II} to monomethyl Pt^{IV} followed by reductive elimination of methanol. After studies of the NNN ligands had begun we found that the reactivity of the NNO system with O_2 was very slow relative to the Vedernikov dpms system which we attribute to steric congestion around Pt due to the pyrazolyl bound methyl groups in both NNO and NNN.[9] The low solubility of the NNNPt^{IV} complexes may also be due in part to the same methyl groups. The combination of the very slow oxidation of monomethyl NNNPt^{II} by O_2 and low solubility of the oxidized products (NNNPt^{IV}) make mechanistic studies comparing the reactivity of the various substituted NNN ligand very challenging. Due to these constraints this ligand system would likely be better modeled with minimization of aliphatic groups on the NNN ligand and steric congestions near the platinum center. Removing the four methyl substituents from the pyrazolyl rings would likely enhance the reactivity of an NNN ligated platinum(II) center as well as improve solubility. Also, the phenyl linker in the hemilabile arm may not be required to form a stabile anionic N also likely improving the systems solubility in water.

Interestingly, while both our NNO system and Vedernikov's dpms system were capable of performing methyl transfer, reductive elimination of ethane from the dimethyl NNOPt^{IV}, a critical step in methane oligomerization catalysis, was not observed. In the Vedernikov system isomerization of dimethyl NNOPt^{IV} is observed without reductive elimination of ethane. This suggests that

decoordination of weakly coordinating sulfonate group is insufficient to promote reductive elimination of ethane. It has been shown that steric congestion aids in reductive elimination of ethane from trimethyl Pt^{IV}[10] so adding bulky substituents to the hemilabile arm could promote C-C coupling without impeding oxidation of the Pt^{II} center. Adding a bulky substituent such as *tert*-butyl directly to the amidate N, where it is most likely to generate steric interaction with the Pt bound methyl groups, may promote reductive elimination of ethane from dimethyl Pt^{IV} product of oxidative methyl transfer (Figure 5.13). The removal of the electron withdrawing sulfonyl group would destabilize the anionic N but as methyl transfer has been observed in alkaline solutions in both the NNO and dmps systems an anionic amidate N in the hemilabile arm may be accessible at elevated pH without the sulfonyl group.

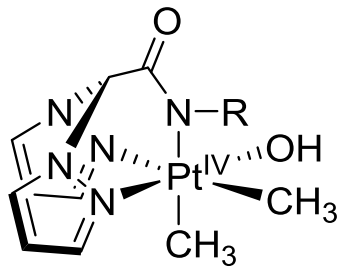

Figure 5.13. Proposed redesign of NNN ligand with an emphasis on reducing steric bulk around Pt center to enhance reactivity with O_2. Adding bulky substituents at R promote reductive elimination of ethane from a dimethyl Pt through steric congestion.

The NNN ligands showed competence for critical reactions associated with functionalization of methane including: oxidation by O_2, reductive elimination of methanol and methyl transfer. The flexibility inherent in its design allowing for alteration of electronic and steric properties make the NNN ligand a promising system to provide information that could be used in the design of a useful methane functionalization catalyst.

Experimental

All air-free manipulations were performed in a N_2 glove box, on a Schlenk line, or on a high vacuum line. Solvents were purified by passage through two columns of activated alumina in the case of THF and diethyl ether, and a column of activated alumina followed by a column of Q5 reactant in the case of benzene, pentane, and toluene. NMR solvents were obtained from Cambridge Isotope Laboratories. Benzene-d_6 and THF-d_8 were dried over Na/benzophenone then vacuum transferred prior to use. Chloroform-d_1 was dried over CaH_2 and vacuum transferred prior to use. NMR spectra were referenced from the residual protiated solvent signal and chemical shifts are reported in parts per million (ppm) from tetramethylsilane (TMS). KH was obtained as a suspension in oil and was purified by washing with pentane. All other chemicals were used as received. pH/pD measurements were obtained using a Hach company ISFET pH Stainless Steel NMR Tube Probe calibrated using phosphate buffered H_2O solutions of pH 4, 7 and 10. Readings from pH meter of D_2O solutions are reported as pD. Elemental analyses were performed by the CENTC Elemental Analysis Facility at the University of Rochester.

Bis(3,5-dimethylpyrazol-1-yl)-N-toluenesulfonylacetamide (16). A 250 mL round bottom flask was charged with bis(3,5-dimethyl-1pyrazolyl)methane (2.2 g, 10.8 mmol) and 100 mL of THF. The solution was cooled to -78 °C in a dry ice/isopropanol bath. 2.5 M *n*-butyl lithium (3.25 g, 11.8 mmol) was added dropwise over 5 min followed by 30 min of stirring. Then p-Toluenesulfonyl isocyanate (96%, 2.34 g, 11.8 mmol) was added dropwise over 15 min. The solution was removed from the dry ice bath and allowed to warm at room temperature for 30 min. H_2O (1 mL) was added dropwise to quench any unreacted *n*-butyl lithium and the solvent was removed under low pressure giving an orange solid. H_2O (40 mL) was added to the orange solid giving a cloudy orange mix. The mixture was separated by

filtration then HCl was added to the filtrate (pH: 1) resulting in precipitation of a faintly orange solid. Dissolution of the slightly soluble orange solid followed by filtration then acidification of the filtrate and collection of the faintly orange precipitate was repeated until no orange solid remained. A total of 300 mL of H_2O was required. The white precipitate was dissolved in THF then dried over $MgSO_4$. The solvent was removed under low pressure giving a faintly orange solid. Adding 2 mL of methanol resulted in a white solid with orange supernatant which was separated by centrifuge then decanted. The white solid was crystallized from THF/pentane then washed with cold methanol. The colorless crystals were dissolved in THF and dried over $MgSO_4$. The solvent was removed under reduced pressure giving a white solid. Yield: 0.64 g (15%). The yield of NNN ligands would likely be greatly improved by drying the isocyanate over molecular sieves before use and allowing more time for its reaction with deprotonated bis(3,5-dimethyl-1-pyrazolyl)methane at room temperature. In the synthesis of **20** the isocyanate was predried and the reaction between the isocyanate with the deprotonated bis(3,5-dimethyl-1-pyrazolyl)methane at room temperature was extended to 12 h giving a final yield of 43% (see below). ^{1}H NMR (300 MHz, $CDCl_3$, 298 K): δ 2.16 (s, 6H, CH_3), 2.18 (s, 6H, CH_3), 2.43 (s, 3H, Tol-CH_3), 3.14 (broad s, C-NH-S), 5.81 (s, 2H, H_{pz}), 6.55 (s, 1H, CH), 7.33 (d, $^3J_{H\text{-}H}$ = 8 Hz, 2H, Tol-H), 8.05 (d, $^3J_{H\text{-}H}$ = 8 Hz, 2H, Tol-H).

Potassium bis(3,5-dimethylpyrazol-1-yl)-N-toluenesulfonylacetamidate (17). A 100 mL round-bottom flask was charged with **16** (640 mg, 1.59 mmol), KH (128 mg, 3.19 mmol) and THF (35 mL). Over 20 m the amount of white solid (**16**) suspended in THF was greatly reduced with vigorous bubbling (H_2). The mixture was separated and the solvent removed under low pressure giving a white solid. Yield: 0.58 g (83%). ^{1}H NMR (500 MHz, $CDCl_3$, 298 K): δ 1.93 (s, 6H, CH_3), 2.15 (s, 6H, CH_3),

2.29 (s, 3H, Tol-CH_3), 5.75 (s, 2H, H_{pz}), 6.44 (s, 1H, CH), 6.97 (d, $^3J_{H\text{-}H}$ = 8 Hz, 2H, Tol-H), 7.76 (d, $^3J_{H\text{-}H}$ = 8 Hz, 2H, Tol-H).

Bis(3,5-dimethylpyrazol-1-yl)-N-benzenesulfonylacetamide (18). A 250 mL round bottom flask was charged with bis(3,5-dimethyl-1-pyrazolyl)methane (1.12 g, 5.46 mmol) then dissolved in 40 mL THF. The solution to was cooled to -78 °C in a dry ice/isopropanol bath then 2.5 M *n*-butyl lithium (1.65 g, 6 mmol) was added drop-wise over 5 min followed by 30 min of stirring. Benzenesulfonyl isocyanate (95%, 1.00 g, 5.46 mmol) was added dropwise over 15 min followed by 30 min of stirring at -78 °C. The orange solution was removed from the dry ice bath and stirred for 12 h at room temperature giving a brown supernatant with a white precipitate. The precipitate was separated and the white solid collected was crystallized from methanol/Et_2O or by evaporation of a methanolic solution. The crystals were dissolved in a minimum amount of H_2O which was acidified to pH 1 by addition of HCl resulting in a white precipitate. The white solid was collected by filtration then dissolved in dichloromethane and dried over $MgSO_4$ with charcoal. The $MgSO_4$ and charcoal were removed by filtration and the solvent was removed under reduced pressure giving a white solid. Yield: 500 g (24%). ^{1}H NMR (300 MHz, $CDCl_3$, 298 K): δ 2.17 (s, 6H, CH_3), 2.18 (s, 6H, CH_3), 5.81 (s, 2H, H_{pz}), 6.55 (s, 1H, CH), 7.55 (t, $^3J_{H\text{-}H}$ = 7 Hz, 2H, Phenyl-H), 7.65 (t, $^3J_{H\text{-}H}$ = 7 Hz, 1H, Phenyl-H), 8.16 (d, $^3J_{H\text{-}H}$ = 7Hz, 2H, Phenyl-H).

Lithium bis(3,5-dimethylpyrazol-1-yl)-N-p-chlorobenzenesulfonylacetamidate (20). A 250 mL round bottom flask was charged with bis(3,5-dimethyl-1-pyrazolyl)methane (3.42 g, 16.74 mmol) and 40 mL THF under an N_2 atmosphere. The solution was cooled to -78 °C in a dry ice/isopropanol bath then 2.5 M *n*-butyl lithium (4.56 g, 5.05 mmol) was added dropwise over 5 m followed by 30 m of stirring. 4-Chlorobenzenesulfonyl isocyanate 97% (3.64 g, 16.74 mmol), dried over 3Å molecular sieves in Et_2O, was added drop-wise over 15 min followed by 30 m of stirring at -78 °C. The brick red mixture

was removed from the dry ice bath and stirred for 12 h at room temperature giving a cloudy orange mixture. A cream colored solid was collected by filtration which was then dissolved in methanol. Slow evaporation of methanol gave colorless crystals. Attempts to protonate the ligand by addition of HCl in H_2O (see next experiment) did not result in a change in the ^1H NMR spectrum. Yield: 3.06 g (43%). ^1H NMR (300 MHz, CD_3OD, 298 K): δ 2.10 (s, 6H, CH_3), 2.11 (s, 6H, CH_3), 5.81 (s, 2H, H_{pz}), 6.66 (s, 1H, CH), 7.44 (d, $^3J_{H\text{-}H}$ = 9 Hz, 2H, Phenyl-H), 7.93 (m, $^3J_{H\text{-}H}$ = 9 Hz, 2H, Phenyl-H).

Attempted synthesis of Bis(3,5-dimethylpyrazol-1-yl)-N-p-chlorobenzenesulfonylacetamide. A 25 mL round bottom flask was charged with **20** (318 mg, 0.743 mmol) and H_2O (8 mL) giving a white mixture. The mixture was acidified with 10 drops of concentrated HCl to a pH of 1 and stirred for 1 h. The white solid was separated however the ^1H NMR spectrum was nearly identical to the spectrum for the lithium salt (**20**). ^1H NMR (300 MHz, CD_3OD, 298 K): δ 2.10 (s, 6H, CH_3), 2.11 (s, 6H, CH_3), 5.81 (s, 2H, H_{pz}), 6.66 (s, 1H, CH), 7.45 (d, $^3J_{H\text{-}H}$ = 9 Hz, 2H, Phenyl-H), 7.93 (m, $^3J_{H\text{-}H}$ = 9 Hz, 2H, Phenyl-H).

κ^3-(NNN-H)$Pt^{IV}(CH_3)_2H$ (21). A Teflon cap sealed NMR tube was charged with $[Pt(CH_3)_2(\mu\text{-}S(CH_3)_2)]_2$ (2 mg, 0.003 mmol), **18** (1.8 mg, 0.005 mmol) and CD_2Cl_2 (0.25 mL). After 1 h at room temperature, a white precipitate formed. When the reaction was observed again 24 h later the ratio of **21_{ax}** : **21_{eq}** had changed from 9 : 1 to 1 : 4. ^1H NMR spectral data for complex **21_{ax}** (500 MHz, CD_2Cl_2, 298 K): δ -21.82 (s, $^1J_{Pt\text{-}H}$ = 1531 Hz, 1H), 1.59 (s, $^2J_{Pt\text{-}H}$ = 70.2 Hz, 6H, Pt-CH_3), 2.33 (s, 6H, CH_3), 2.39 (s, 6H, CH_3), 6.06 (s, 2H, H_{pz}), 6.29 (s, 1H, CH), 7.42 (t, $^3J_{H\text{-}H}$ = 7 Hz, 2H, Phenyl-H), 7.49 (t, $^3J_{H\text{-}H}$ = 7 Hz, 1H, Phenyl-H), 7.88 (d, $^3J_{H\text{-}H}$ = 8 Hz, 2H, Phenyl-H). -21.82 (s, $^1J_{Pt\text{-}H}$ = 1531 Hz, 1H), -21.22 (s, $^1J_{Pt\text{-}H}$ = 1451 Hz, 1H). ^1H NMR spectral data for complex **21_{eq}** due to poor resolution with **21_{ax}** only the

methyl and hydrido groups bound to Pt^{IV} were identifiable. (300 MHz, CD_2Cl_2, 298 K): -21.22 (s, $^1J_{Pt\text{-}H}$ = 1451 Hz, 1H), 1.25 (s, $^2J_{Pt\text{-}H}$ = 71.3 Hz, 3H, Pt-CH_3), 1.53 (s, $^2J_{Pt\text{-}H}$ = 70.8 Hz, 3H, Pt-CH_3).

(Potassium-κ^2-NNN-CH_3)$Pt^{II}(CH_3)_2$ (22). A 100 mL round-bottom flask was charged with $[Pt(CH_3)_2(\mu\text{-}S(CH_3)_2)]_2$[11] (0.379 g, 0.66 mmol), **17** (0.58 g, 1.3 mmol) and THF (25 mL). The faintly cloudy white mixture was stirred overnight giving a thick white mixture. The solvent was removed under reduced pressure leaving a white solid. The solid was extracted with methanol and separated. The filtrate was evaporated under reduced pressure leaving a faintly yellow solid. Yield: 0.35 g (40%). ^{1}H NMR (500 MHz, ACN-d_3, 298 K): δ 0.41 (s, $^2J_{Pt\text{-}H}$ = 87 Hz, 6H, Pt-CH_3), 2.23 (s, 6H, CH_3), 2.28 (s, 6H, CH_3), 2.35 (s, 3H, CH_3), 5.95 (s, 2H, H_{pz}), 6.10 (s, 1H, CH), 7.19 (m, $^3J_{H\text{-}H}$ = 8.0 Hz, 2H, Tol-H), 7.80 (m, $^3J_{H\text{-}H}$ = 8.2 Hz, 2H, Tol-H).

(Potassium-κ^2-NNN-H)$Pt^{II}(CH_3)_2$ (23). A 50 mL round-bottom flask was charged with 0.2 g (0.5 mmol) of **18** and air-free THF (25 mL). Potassium hydride (31 mg, > 0.8 mmol) was then added to the solution. Vigorous bubbling (H_2) was observed. After 20 m the solid was separated by filtration and $[Pt(CH_3)_2(\mu\text{-}S(CH_3)_2)]_2$[11] (0.148 g, 0.258 mmol) was added to the filtrate and left at room temperature for 24 h. The solvent was removed under reduced pressure and the resulting solid was crystallized from THF/pentane. Yield: 0.05 g (7%). ^{1}H NMR (300 MHz, CD_2Cl_2, 298 K): δ 0.39 (s, $^2J_{Pt\text{-}H}$ = 83.4 Hz, 6H, CH_3), 2.18 (s, 6H, CH_3), 2.24 (s, 6H, CH_3), 5.88 (s, 2H, H_{pz}), 6.05 (s, 1H, CH), 7.34 (m, $^3J_{H\text{-}H}$ = 7.6 Hz, 2H, Phenyl-H), 7.44 (m, $^3J_{H\text{-}H}$ = 7.4 Hz, 1H, Phenyl-H), 7.81 (m, $^3J_{H\text{-}H}$ = 8.4 Hz, $^4J_{H\text{-}H}$ = 2.1 Hz , 2H, Phenyl-H).

(Potassium-κ^2-NNN-CH_3)$Pt^{II}(CH_3)$(OH) (24). A sample of **22** (3 mg, 0.005 mmol) was dissolved in N_2-sparged D_2O (0.3 mL) with dioxane (int. std., 0.2 μL) then transferred to Teflon cap sealed NMR tube. The sample was heated at 60 °C for 3 h until complete conversion of **22**. Yield from ^{1}H NMR

spectroscopy: 95%. The reaction was also performed in H_2O allowing for observation of the Pt^{II}-CH_3 in **24** by ^1H NMR spectroscopy. ^1H NMR (300 MHz, D_2O, 298 K): δ 0.43 (s, $^2J_{Pt-H}$ = 78.2 Hz, 6H, Pt-CH_3), 2.21 (s, 3H, CH_3), 2.25 (s, 3H, CH_3), 2.38 (s, 3H, CH_3), 2.39 (s, 3H, CH_3), 2.42 (s, 3H, Tol-CH_3), 6.08 (s, 1H, H_{pz}), 6.06 (s, 1H, H_{pz}), 7.39 (m, $^3J_{H-H}$ = 8.3 Hz, 2H, Tol-H), 7.92 (m, $^3J_{H-H}$ = 8.2 Hz, 2H, Tol-H).

(Potassium-κ^2-NNN-H)Pt^{II}(CH$_3$)(OH) (25). A sample of **23** (5 mg, 0.008 mmol) was dissolved in N_2-sparged H_2O (0.2 mL) then transferred to Teflon cap sealed NMR tube. The sample was heated at 60 °C for 1 h until complete conversion of **23**. ^1H NMR (300 MHz, H_2O, 298 K): δ 0.45 (s, $^2J_{Pt-H}$ = 81.3 Hz, 3H, CH_3), 2.15 (s, 3H, CH_3), 2.19 (s, 3H, CH_3), 2.32 (s, 3H, CH_3), 2.33 (s, 3H, CH_3), 5.98 (s, 1H, H_{pz}), 6.01 (s, 1H, H_{pz}), 6.41 (s, 1H, CH), 7.47 – 7.61 (m, 3H, Phenyl-H), 7.98 (d, $^3J_{H-H}$ = 6.6 Hz, 2H, Phenyl-H).

(κ^3-NNN-CH$_3$)Pt^{IV}(CH$_3$)(OH)$_2$ (26). A Teflon valve sealed NMR tube was charged with **24** (4 mg, 0.006 mmol) and D_2O (0.25 mL) giving a cloudy white mix. 5 drops of 30% H_2O_2/H_2O were added and the sample was left at room temperature for 24 hrs. A significant amount of white solid precipitated over the course of the reaction. ^1H NMR (300 MHz, D_2O, 298 K): δ 2.48 (s, $^2J_{Pt-H}$ = 71.1 Hz, 3H, Pt-CH_3), 2.38 (s, 3H, CH_3), 2.41 (s, 3H, CH_3), 2.42 (s, 3H, CH_3), 2.50 (s, 3H, CH_3), 2.53 (s, 3H, CH_3), 6.25 (s, 1H, H_{pz}), 6.27 (s, 1H, H_{pz}), 7.34(m, $^3J_{H-H}$ = 8.1 Hz, 2H, Tol-H), 7.71 (m, $^3J_{H-H}$ = 8.0 Hz, 2H, Tol-H).

(κ^3-NNN-H)Pt^{IV}(CH$_3$)(OH)$_2$ (27). A Teflon cap sealed NMR tube was charged with **23** (2 mg, 0.003 mmol) and N_2-sparged H_2O (0.15 mL) then heated at 60 °C for 20 m converting **23** to **25**. The solvent was removed under reduced pressure giving a white solid. 0.3 mL of D_2O with 0.5 μL of 30% H_2O_2/H_2O was added. After 2 h all of the ^1H NMR spectrum of **25** was no longer observed and only signals due to **27** were present. The yield could not be calculated as a white solid precipitated over the

course of the reaction. ^{1}H NMR (500 MHz, D_2O, 298 K): δ 2.40 (s, 3H, CH_3), 2.41 (s, 3H, CH_3), 2.47 (s, $^{2}J_{Pt\text{-}H}$ = 75.8 Hz, 3H, CH_3), 2.49 (s, 3H, CH_3), 2.53 (s, 3H, CH_3), 6.24 (s, 1H, H_{pz}), 6.26 (s, 1H, H_{pz}), 6.85 (s, 1H, CH), 7.62 (m, $^{3}J_{H\text{-}H}$ = 7.7 Hz, 2H, Phenyl-H), 7.70 (m, $^{3}J_{H\text{-}H}$ = 7.4 Hz, 1H, Phenyl-H), 7.92 (m, $^{3}J_{H\text{-}H}$ = 7.9 Hz, 2H, Phenyl-H).

Reaction of aqueous (Potassium-κ^2-NNN-CH_3)Pt^{II}(CH_3)(OH) (24) with O_2. A Teflon valve sealed NMR tube was charged with **24** (4 mg, 0.006 mmol) and D_2O (2.5 mL) giving a cloudy white mixture. The solution was degased by successive freeze/pump/thaw cycles then pressurized with O_2 (50 psi) while frozen in a dry ice bath. The frozen solution was rapidly thawed in a 25 °C water bath then placed in a preheated oil bath (60 °C). At timed intervals the NMR tube was removed from the oil bath, rapidly cooled in a 25 °C water bath (10s) then examined by ^{1}H NMR spectroscopy. A significant amount of white solid precipitated over the course of the reaction. While resolution was poor due to multiple species in the product mixture two singlets with what appear to be ^{195}Pt satellites in a 1:1 ratio consistent with a dimethyl Pt^{IV} were observed. ^{1}H NMR (300 MHz, D_2O, 298 K): δ 1.75 (s, $^{2}J_{Pt\text{-}H}$ = 71.7 Hz, 3H, CH_3), 1.99 (s, $^{2}J_{Pt\text{-}H}$ = 77.9 Hz, 3H, CH_3).

Reaction of aqueous (Potassium-κ^2-NNN-H)Pt^{II}(CH_3)(OH) (25) with O_2. A Teflon valve sealed NMR tube was charged with **23** (2 mg, 0.003 mmol) and 0.15 mL H_2O (0.15 mL) then heated at 60 °C for 20 m. The solvent was removed under low pressure giving a white solid which was then dissolved in D_2O (0.3 mL). The solution was degased by successive freeze/pump/thaw cycles then pressurized with O_2 (50 psi) while frozen in a dry ice bath. The frozen sample was rapidly thawed in a 25 °C water bath then placed in a preheated oil bath (60 °C). At timed intervals the NMR tube was removed from the oil bath, rapidly cooled in a 25 °C water bath (10 s) then examined by ^{1}H NMR spectroscopy for 20 h. While resolution was poor due to multiple species in the product mixture a singlet with what appear to

be ^{195}Pt satellites in a 1:1 ratio consistent with a dimethyl Pt^{IV} was observed. ^{1}H NMR (500 MHz, D_2O, 298 K): δ 1.71 (s, $^2J_{Pt\text{-}H}$ = 70.2 Hz, 3H, CH_3), 1.96 (s, $^2J_{Pt\text{-}H}$ = 69.1 Hz, 3H, CH_3).

Thermolysis of (κ^3-NNN-CH_3)Pt^{IV}(CH_3)$(OH)_2$ (26). A Teflon cap sealed NMR tube was charged with **26** (4 mg, 0.006 mmol) and H_2O (0.3 mL) then acidified by addition of 50% HBF_4/H_2O (5 μL, 0.08 mmol, pH = 1.5) giving a white mixture (**26** was the only product detected by ^{1}H NMR spectroscopy). The sample was then placed in 150 °C bath for 3 h until **26** was completely converted by ^{1}H NMR spectroscopy. Methanol was observed in the product mixture (3.35 ppm) but the yield could not be determined due to the use of solvent suppression in the ^{1}H NMR spectrum. ^{1}H NMR (500 MHz, H_2O, 298 K): δ 2.38 (s, 6H, CH_3), 2.42 (s, 6H, CH_3), 2.49 (s, 3H, CH_3), 5.17 (s, 2H, H_{pz}), 6.91 (s, 1H, CH), 7.44 (m, 2H, Tol-H), 7.79 (m, 2H, Tol-H).

Thermolysis of (κ^3-NNN-H)Pt^{IV}(CH_3)$(OH)_2$ (27). A Teflon valve sealed NMR tube was charged with **25** (2 mg, 0.003 mmol) and KH_2PO_4/K_2HPO_4 buffered D_2O (0.3 mL, pD = 7.0) with dioxane (int. std., 0.1 μL). The result was a white mixture but **27** was detected by ^{1}H NMR spectroscopy before heating. The sample was then heated at 150 °C for 16 h until **27** was no longer detected by ^{1}H NMR spectroscopy. Methanol Yield: 57%. ^{1}H NMR (500 MHz, D_2O, 298 K): (methanol) δ 3.34. (**29**) δ 2.07 (s, 3H, pyr-CH_3), 2.42 (s, 6H, pyr-CH_3), 2.47 (s, 3H, pyr-CH_3), 6.12 (s, 1H, pyr-H), 6.19 (s, 1H, pyr-H). 7.15 – 7.3 (m, 5H, S-phenyl).

Crystallization of 30. Under an N_2 atmosphere a 25 mL round bottom flask was charged with **22** (100 mg, 0.15 mmol) which was then dissolved in minimum amount of air free acetonitrile. Air free diethyl ether (10 mL) was added but no precipitation was observed. Air free pentane (5 mL) was added resulting in a cloudy mixture. After 24 h colorless crystals were observed in addition to a significant amount of black solid.

Crystallographic characterization of compound 30

A colorless prism, measuring 0.45 x 0.10 x 0.03 mm^3 was mounted on a glass capillary with oil. Data was collected at -133^oC on a Bruker APEX II single crystal X-ray diffractometer, Mo-radiation. Crystal-to-detector distance was 40 mm and exposure time was 10 seconds per frame for all sets. The scan width was 0.5^o. Data collection was 100% complete to 25^o in ϑ. A total of 60055 (merged) reflections were collected covering the indices, h = -14 to 14, k = -16 to 16, l = -21 to 21. 9462 reflections were symmetry independent and the R_{int} = 0.0456 indicated that the data was good (average quality 0.07). Indexing and unit cell refinement indicated a primitive monoclinic lattice. The space group was found to be P $\bar{1}$ (No.2).

The data was integrated and scaled using SAINT, SADABS within the APEX2 software package by Bruker.[12] Solution by direct methods (SHELXS, SIR97[13]) produced a complete heavy atom phasing model consistent with the proposed structure. The structure was completed by difference Fourier synthesis with SHELXL97.[14,15] Scattering factors are from Waasmair and Kirfel[16]. Hydrogen atoms were placed in geometrically idealized positions and constrained to ride on their parent atoms with C---H distances in the range 0.95-1.00 Angstrom. Isotropic thermal parameters U_{eq} were fixed such that they were 1.2U_{eq} of their parent atom Ueq for CH's and 1.5U_{eq} of their parent atom U_{eq} in case of methyl groups. All non-hydrogen atoms were refined anisotropically by full-matrix least-square. The structure exhibits disorder with a methyl binding to platinum, disordered 1:1 with an ethyl group also binding to platinum. The structure is of high quality and ready for publication. Table 1 summarizes the data collection details. Figure 1 shows an ORTEP[17] of the asymmetric unit.

Table 5.1. Crystallographic data for **30**.

Parameter	**30**
Empirical formula	C45 H64 N10 O6 Pt2 S2
Formula weight	1295.36
Temperature	140(2) K
Wavelength	0.71073 Å
Crystal system	Triclinic
Space group	$P\bar{1}$
Volume	1223.64(11) $Å^3$
Unit cell dimensions	a = 9.2228(5) Å, α= 72.586(3)° b = 10.5619(5) Å, β= 87.949(3)° c = 13.6352(7) Å, γ = 75.123(3)°
Z	1
Density (calculated)	1.758 Mg/m^3
Absorption coefficient	5.852 mm^{-1}
F(000)	640
Crystal size	0.45 x 0.10 x 0.03 mm^3
Theta range for data collection	2.09 to 33.57°.
Index ranges	-14<=h<=14, -16<=k<=16, -21<=l<=21
Reflections collected	60055
Independent reflections	9462 [R(int) = 0.0456]
Completeness to theta = 25.00°	100.0 %
Max. and min. transmission	0.8440 and 0.1782
Refinement method	Full-matrix least-squares on F^2
Data / restraints / parameters	9462 / 0 / 305
Goodness-of-fit on F^2	1.035
Final R indices [I>2sigma(I)]	R1 = 0.0285, wR2 = 0.0654
R indices (all data)	R1 = 0.0366, wR2 = 0.0689
Largest diff. peak and hole	2.047 and -2.422 $e.Å^{-3}$

[1] Shilov, A. E.; Shulpin, G. B. *Russ. Chem.Rev.* **1987**, *56*, 442.
[2] Fettinger, J. C.; Mohr, F.; Vedernikov, A. N. *J. Am. Chem. Soc.* **2004**, 1*26*, 11160.
[3] Binfield, S. A.; Zavalij, P. Y.; Khusnutdinova, J. A.; Vedernikov, A. N. *J. Am. Chem. Soc.* **2006**, *128*, 82.
[4] Based on pK_a (DMSO) significant stabilization of an anionic nitrogen occurs when the nitrogen is bound to a carbonyl (CH_3CONH_2, pK_a: 23.5)) or sulfonyl ($PhSO_2NH_2$, pK_a: 16.1) when compared with NH_3 (pK_a: 41).[5]
[5] Boardwell, F. G. *Acc. Chem. Res.* **1988**, *21*, 456.
[6] (a) Wick, D. D.; Goldberg, K. I. *J. Am. Chem. Soc.* **1997,** *119,* 10235. (b) Vedernikov, A. N.; Fettinger, J. C.; Mohr, F. *J. Am. Chem. Soc.*, **2004**, 126 (36), 11160. (c) Prokopchuk, E. M.; Puddephatt, R. J. *Organometallics* **2003,** *22,* 787. (d) Puddephatt, R. J. *Coor. Chem. Rev.* **2001**, 521.
[7] Holtcamp, M. W.; Henling, L. M.; Day, M. W.; Labinger, J. A.; Bercaw, J.E. *lnorganica Chimica Acta* **1998**, 270, 467.
[8] Lersch, M.; Tilset, M. *Chem. Rev.* **2005**, *105*, 2471. (b) Fettinger, J. C.; Mohr, F.; Vedernikov, A. N. *J. Am. Chem. Soc.* **2004**, 1*26*, 11160. (c) Stahl, S. S.; Labinger, J. A.; Bercaw, J. E. *J. Am. Chem. Soc.* **1996**, *118*, 5961.
[9] Rostovtsev, V. V; Henling, L. M.; Labinger, J. A.; Bercaw, J. E. *Inorg. Chem.* **2002**, *41*, 3608.
[10] Lanci, M. P.; Remy, M. S.; Lao, D. B.; Sanford, M. S.; Mayer, J. M. *Organometallics*, **2011**, *30*, 3704.
[11] Scott, J. D.; Puddephatt, R. J. *Organometallics* **1983**, *2*,1643.
[12] Bruker (**2007**) APEX2 (Version 2.1-4), SAINT (version 7.34A), SADABS (version 2007/4), BrukerAXS Inc, Madison, Wisconsin, USA.
[13] (a) Altomare A, Burla C, Camalli M, Cascarano L, Giacovazzo C, Guagliardi A, Moliterni AGG, Polidori G, Spagna R. **(1999)** SIR97: a new tool for crystal structure determination and refinement *Journal of Applied Cryst*allography, ***32*****,** 115-119. (b) Altomare A, Cascarano G, Giacovazzo C, Guagliardi A. **(1993)** Completion and refinement of crystal structures with SIR 92. *Journal of Applied Cryst*allography, ***26*****,** 343.
[14] Sheldrick GM. **(1997)** SHELXL-97, Program for the Refinement of Crystal Structures. University of Göttingen, Germany.
[15] Mackay, S.; Edwards, C.; Henderson, A.; Gilmore, C.; Stewart, N.; Shankland, K.; Donald, A. **(1997)** *MaXus: a computer program for the solution and refinement of crystal structures from diffraction data*. University of Glasgow, Scotland,.
[16] Waasmaier, D.; Kirfel, A. **(1995)** New Analytical Scattering Factor Functions for Free Atoms and Ions. *Acta Crystallographica* A., ***51***, 416.
[17] Farrugia LJ. **(1997)** Ortep-3 for Windows. *Journal of Applied Cryst*allography, ***30*****,** 565.